TECHNICAL REPORT NO. 3-693

TERRAIN ANALYSIS BY ELECTROMAGNETIC MEANS

Report 2

RADAR RESPONSES TO LABORATORY PREPARED SOIL SAMPLES

by

J. R. Lundien

September 1966

Sponsored by

National Aeronautics and Space Administration
Scientific Experiments Program for Advanced
Orbital Spacecraft Missions (Manned)

Service Agency

U. S. Army Materiel Command

Conducted by

U. S. Army Engineer Waterways Experiment Station
CORPS OF ENGINEERS
Vicksburg, Mississippi

Destroy this report when no longer needed. Do not return it to the originator.

The findings in this report are not to be construed as an official Department of the Army position unless so designated by other authorized documents.

TECHNICAL REPORT NO. 3-693

TERRAIN ANALYSIS BY ELECTROMAGNETIC MEANS

Report 2

RADAR RESPONSES TO LABORATORY PREPARED SOIL SAMPLES

by

J. R. Lundien

September 1966

Sponsored by

National Aeronautics and Space Administration
Scientific Experiments Program for Advanced
Orbital Spacecraft Missions (Manned)
NASA Defense Purchase Request No. R-25-04-001

Service Agency

U. S. Army Materiel Command

Conducted by

U. S. Army Engineer Waterways Experiment Station
CORPS OF ENGINEERS
Vicksburg, Mississippi

ARMY-MRC VICKSBURG, MISS.

FOREWORD

The study reported herein constitutes a portion of the National Aeronautics and Space Administration (NASA) Scientific Experiments Program for Advanced Orbital Spacecraft Missions (Manned). The broad mission of this program is to obtain basic geological-geophysical data for planetary surfaces through the use of remote electromagnetic sensors operating in various portions of the spectrum.

Certain elements of the NASA mission are closely related to the studies being conducted by the U. S. Army Engineer Waterways Experiment Station (WES) for the U. S. Army Materiel Command in furtherance of Department of Army Research Project No. 1-V-0-21701-A-046, "Trafficability and Mobility Research." A cooperative effort was therefore initiated under the preliminary title, "Laboratory and Modeling Studies of Microwave and Radar Responses to Simulated Terrain." Funds were allocated to the WES through NASA Defense Purchase Request No. R-25-04-001. The tests were conducted, with the facilities provided by the Research and Development Directorate of the Army Materiel Command at WES, during the period November 1964 through April 1965. Project coordination under NASA Contract NSR 17-04-003 was provided by Dr. R. K. Moore, University of Kansas, University of Kansas Center for Research, Inc.

The tests were conducted under the general supervision of Mr. W. J. Turnbull, Technical Assistant for Soils and Environmental Engineering; Messrs. W. G. Shockley and S. J. Knight, Chief and Assistant Chief of the Mobility and Environmental Division; and Dr. D. R. Freitag, Chief, Army Mobility Research Branch. Mr. B. R. Davis, Chief, Terrain Analyzer Section, directed the study with the assistance of Dr. H. Nikodem and Messrs. J. R. Lundien and A. N. Williamson, Jr. This report was prepared by Mr. Lundien.

Col. Alex G. Sutton, Jr., CE, and Col. John R. Oswalt, Jr., CE, were Directors of WES during this investigation and the preparation of this report. Mr. J. B. Tiffany was Technical Director.

CONTENTS

CONTENTS

GLOSSARY

A_a	Antenna aperture area, sq m
A_i	Area of illumination, sq m
c	Speed of electromagnetic waves through free space or air, m/sec
CC	Coaxial cable loss, db
d	Diameter of antenna, m
DC	Directional coupler loss, db
E	Electric field intensity of the wave reaching the metal plate, volt/m
E_i	Electric field intensity incident on the sample surface, volt/m
E_m	Electric field intensity of the wave returning to the radar receiver from the subsurface metal plate reflection, volt/m
E_r	Electric field intensity of the wave returning to the radar receiver from the soil surface reflection, volt/m
E_t	Electric field intensity transmitted through the sample surface, volt/m
f	Frequency, cps
FM	Frequency modulation
G	Antenna gain, dimensionless
j	$\sqrt{-1}$
k	Antenna constant for effective antenna area, dimensionless
n	An integer
P	Normalized power, dimensionless

P_R Power received, watts or dbm

PRF Pulse repetition frequency, pulses/sec

P_T Power transmitted, watts or dbm

r^2 Surface power reflectance, db

R Range from radar system to sample, m

RA Receiver attenuator loss, db

T Time, sec

TA Transmitter attenuator loss, db

x Sample depth, m

α Attenuation constant, m^{-1}

β Phase factor, m^{-1}

γ Normalized echo area, dimensionless

γ_{db} Normalized echo area expressed in db

ϵ Dielectric constant, farad/m

ϵ_r Relative dielectric constant or apparent relative dielectric constant, dimensionless

ϵ_v Dielectric constant of free space or air, farad/m

θ Antenna beam width, deg

λ Wavelength, m

μ Electromagnetic permeability, henry/m

σ Conductivity, mho/m

ϕ Phase shift, radian

ω Angular frequency, radian/sec

SUMMARY

Laboratory tests were conducted with radar sensors to detect the presence of and measure the depth to subsurface interfaces when the surface was bare, and to determine the influence of vegetation at various stages of growth on radar responses. A secondary purpose was to continue earlier studies to relate radar returns and the electrical constants they provided to moisture content and density of samples.

Large laboratory samples were prepared at various moisture contents and densities and with various depths to a subsurface metal plate. Standard pulsed radar sensors operating with frequencies of 297, 5870, 9375, and 34,543 megacycles/sec and directed at various angles of incidence to the surface were employed.

The results of this laboratory study indicate that the standard pulsed radar sensors can provide information that will permit an estimate of the moisture content of deep, homogeneous soil samples and the detection of surface vegetation of various heights. Radar signatures of vegetation-covered soil were more significantly altered at Ka-, X-, and C-band frequencies than at P-band frequencies. However, standard pulsed radar sensors used monochromatically cannot provide information for predicting depth to subsurface interfaces or for directly indicating the presence of a subsurface interface.

The systematic manner in which soil depths were varied in this study permitted an analytical solution to the problem of measuring depths of layers and led to the conclusion that properly designed radar systems could measure depths to subsurface interfaces. Three such systems are proposed.

TERRAIN ANALYSIS BY ELECTROMAGNETIC MEANS

RADAR RESPONSES TO LABORATORY PREPARED SOIL SAMPLES

PART I: INTRODUCTION

Background

1. The National Aeronautics and Space Administration (NASA) is currently engaged in planning scientific payloads for orbiting spacecraft for lunar and planetary exploration. Sensors that are being considered as means of exploration include: detectors to measure infrared, microwave, X-ray, and gamma-ray emittance; active radar and infrared systems; multiband photography; and gravity gradient systems. These sensors are expected to play a role in lunar and planetary exploration analogous to aerial surveys for terrestrial exploration objectives; but before they can be used with success in an orbiting spacecraft, they must be thoroughly tested and calibrated on earth.

2. An active radar system has some attractive advantages over other types of sensors for terrain analysis. The principal advantage is that electromagnetic radiation at radio frequencies can penetrate soil surfaces and give indications of subsurface conditions and layering. This information is needed to assist in the evaluation of surface and near-surface conditions for the landing of spacecraft.

Previous WES Investigations

3. The tests reported herein are part of a comprehensive program to correlate the quantity of electromagnetic energy reflected at various frequencies from samples with pertinent soil and vegetation physical parameters. Laboratory investigations have been conducted to determine whether electromagnetic sensors operating in the near- and middle-infrared (0.76 to 12 micron) portions of the spectrum can be used to measure soil parameters

for trafficability purposes. A report[1*] on investigations conducted using active infrared sensors has been published, and a report on tests utilizing a passive infrared sensing device is scheduled for publication soon. Laboratory investigations also have been conducted in the radar region of the spectrum using sensors operating at X-, C-, and P-band frequencies[2] to determine the capabilities of these sensors for detecting the presence of and measuring the depth of surface water and depth to ground water.

Purpose and Scope of Test Program

4. The study reported herein was a continuation of the laboratory investigation of radar sensors, and involved tests utilizing an additional radar band (Ka), different materials (four soils and perlite), and vegetation (wheat). The specific objectives of this study were to determine the ability of standard pulsed radar sensors operating under laboratory conditions in the Ka- (34,543 megacycles/sec), X- (9375 megacycles/sec), C- (5870 megacycles/sec), and P-band (297 megacycles/sec) radar portions of the spectrum to:

a. Detect the presence of sample layers of various moisture contents, densities, and soil types, and measure depth of these layers.

b. Measure the electrical properties of soils of various moisture contents.

c. Measure the effect on a soil radar signature of a stand of wheat at various stages of growth.

Current Investigations

5. In addition to the studies reported herein, studies are being conducted to determine the capabilities of gamma-ray frequencies for delineating soil type and soil moisture content. Also, studies are being conducted to determine the amount of power transmitted through vegetation samples using radar frequencies.

---

* Raised numbers refer to similarly numbered items in Literature Cited following the main text of this report.

Definitions

6. Certain terms used in this report are defined below.

Angle of incidence	The angle between the normal to the surface at the point of incidence and the line of propagation approaching the surface.
Antenna gain	For a directional antenna, the average of the power radiated through the half-power angle of the antenna divided by the power radiated in the direction of maximum radiation by a half-wave dipole.
Attenuator	A device that reduces the amplitude of an electrical signal without introducing appreciable phase or frequency distortion.
Back-to-back	A circuit connection in which a portion of the transmitted radar signal is fed directly into the receiver. This connection is used in calibration of the radar system.
Band	A range of radio frequencies of specific limits designated by a letter; e.g. C-band includes frequencies from 3900 to 6200 megacycles/sec.
Boresight	Alignment of the transmitting and receiving antennas so that their patterns overlap on the sample surface.
Decibel (db)	A means for expressing the intensity of electric or acoustic signal power. The power intensity in decibels is equal to 10 times the common logarithm of the ratio of two amounts of power. The abbreviation db is commonly used.
dbm	Decibel referred to one milliwatt.
Delay line	A real or artificial transmission line or equivalent device designed to delay a signal or wave for a predetermined length of time.
Depth-of-penetration test	A test in which power reflected from the test sample at vertical incidence is measured as layers of the sample are removed.
Dielectric constant	That property of a material that determines the electrostatic energy stored per unit volume for unit potential gradient; synonymous with permittivity.
Directional coupler	A device that splits the input signal into two output signals. Both output signals, one being much larger than the other, are proportional to the input signal.

Lobe	One of the three-dimensional, rounded or elongate portions or sections of the radiation pattern of an antenna.
Magnetron	A transmitting tube that generates microwave energy. A tunable magnetron can be varied in frequency over a limited range.
Microwaves	Radio waves that are so short they exhibit some of the properties of light.
Normalized echo area	A measure of the test sample power gain in the direction of the antennas.
Power received	The amount of power (watts or dbm) that is incident on the receiving antenna. Power returned differs from power received in that returned power refers to the situation at the sample and received power refers to the situation at the radar receiver.
Power reflectance	The ratio of power returned to incident power.
Power returned	The amount of power (watts or dbm) that is reflected by the sample and returned to the receiving antenna. (See definition of "power received" above.)
Pulse	An abrupt change in voltage, either positive or negative with respect to a reference, that conveys information to a circuit. This change is characterized by a rise and decay of a finite duration.
Pulsed radar	A radar system in which the transmitted signal consists of a series of pulses of microwave energy.
Pulse width	The time in seconds of the duration of the pulse measured between the half-power points of the pulse.
Receiver gain	An adjustment in the receiver that allows changes to be made in the amplification of the input signal.
Reflectivity	The ratio of the reflected electric field intensity at the surface divided by the incident electric field intensity; also called reflection factor.
Relative dielectric constant	The ratio of the dielectric constant of a material to that of a vacuum.
Saturation	A circuit condition for which an increase in the driving or input signal no longer produces a change in the output.
Side lobe	A portion of the beam from an antenna other than the main lobe. It is usually much smaller than the main lobe.
Signature test	A test in which reflected power from the test sample is measured as the transmitting and receiving systems

	are moved through a range of incidence angles from 0 to 60 deg.
Surface reflection	The energy coming from a sample due to first-surface phenomena only. Surface reflectance refers to the ratio of first-surface reflection to incident energy.
Trigger	A pulse that activates a circuit or starts action in another circuit which then functions for a certain length of time under its own control.

PART II: TEST FACILITY, RADAR SYSTEM, AND CALIBRATION PROCEDURES

Radar Test Facility

General characteristics

7. The radar sets used in these studies are installed in the test facility shown in fig. 1. The principal parts of the facility are the

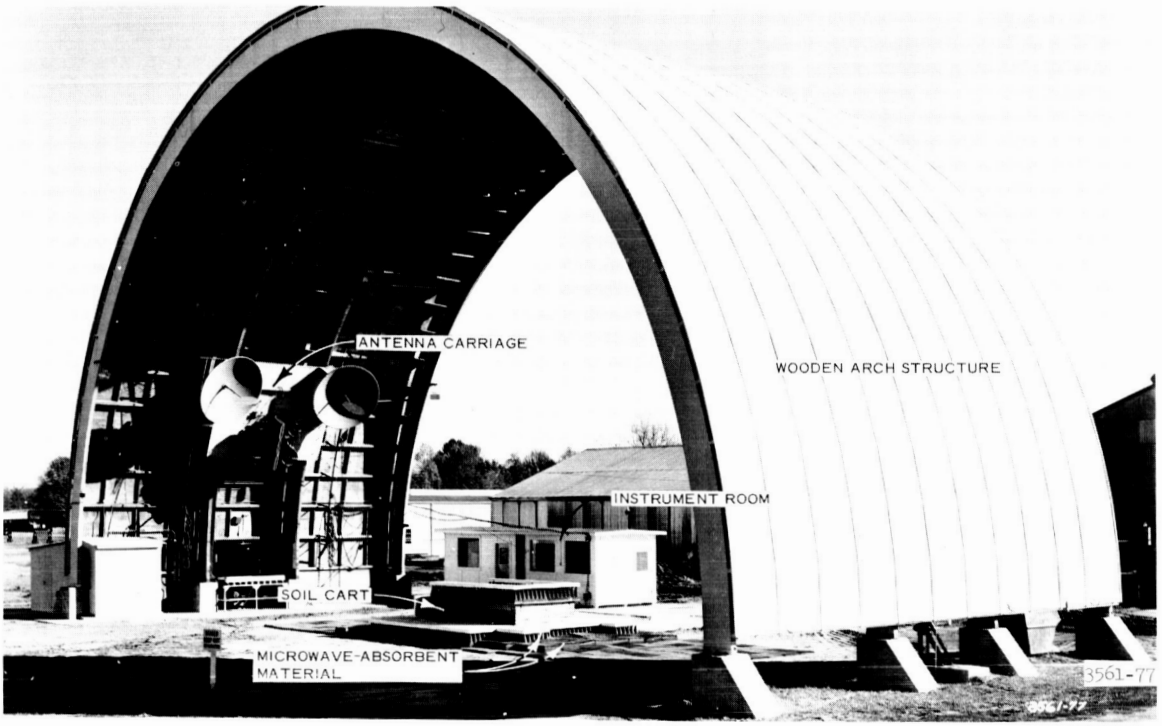

Fig. 1. Radar test facility

wooden arch structure, the antenna carriage, and the instrument room. Fig. 1 also shows the cart that contains a soil sample whose reflectivity characteristics are to be measured, and microwave-absorbent material that is used to reduce extraneous signals from the area surrounding the soil cart. The soil cart is located in the center of the arch and is mounted on a hydraulic lift (not shown) that is used to align the soil cart properly relative to the antennas.

Wooden arch structure

8. A wooden, open-end, 50-ft-radius arch 44 ft in length is the main structure of the test facility. Wood was used in the construction

wherever possible to reduce spurious radar reflections. A track-pulley-cable assembly is attached to the underside of the two center supporting arches to permit movement of the antenna carriage.

Antenna carriage

9. The antenna carriage system is shown in more detail in fig. 2.

Fig. 2. Antenna carriage system

The major portions of each of the radar sets are mounted on this carriage assembly. A transmitting antenna and a receiving antenna for each of the radar bands are mounted on the front of the carriage as shown in fig. 2, while the transmitter and portions of the receiver sections are mounted in an environment-control chamber on the back of the carriage. This chamber eliminates the effects of environmental changes on radar operational characteristics by maintaining a constant temperature and humidity. The carriage system is capable of traversing a 105-deg segment of the arch structure from horizontal to 15 deg past vertical. This arrangement allows the radar systems to collect reflectivity and reradiation data from fixed samples at a number of aspect angles.

Instrument room

10. The instrument room contains (a) the amplifier, video detector,

range gate delay line, boxcar detector, log converter, and recorder portions of each of the radar band's receiver sections (decribed later), (b) power supplies for the radar sets, and (c) the test control console (fig. 3). Using the test control console, the operator can (a) control

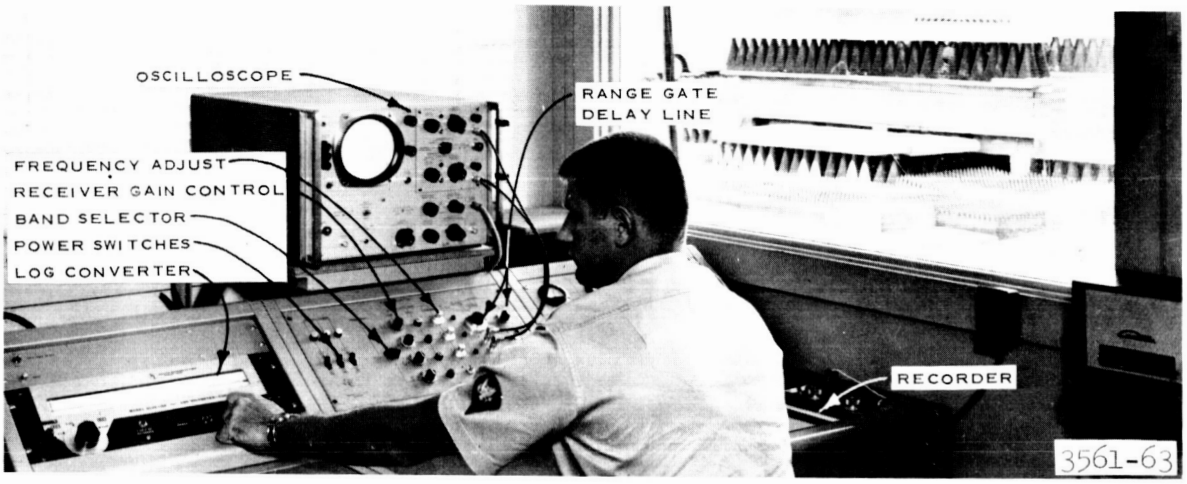

Fig. 3. Test control console

power to all radar sets, (b) select the radar band that he wishes to operate, (c) adjust the gain of the receiver, (d) adjust the frequency of the local oscillator, (e) monitor the video output pulse and range-gating pulse by means of an oscilloscope, (f) adjust the range-gate delay line, and (g) monitor the data results being recorded on an X-Y recorder.

Radar Sets

General characteristics

11. A multifrequency pulsed radar system capable of measuring reflectivity characteristics of terrain specimens at various angles of incidence was used in this study. The system is composed of four radar sets operating independently but not simultaneously at the following frequencies: (a) Ka-band at 34,543 megacycles/sec, (b) X-band at 9375 megacycles/sec, (c) C-band at 5870 megacycles/sec, and (d) P-band at 297 megacycles/sec.

Operational characteristics

12. The principal components of a typical radar set used in these studies are illustrated in the signal flow diagram shown in fig. 4. Each radar set comprises two major subassemblies, i.e. the transmitter and

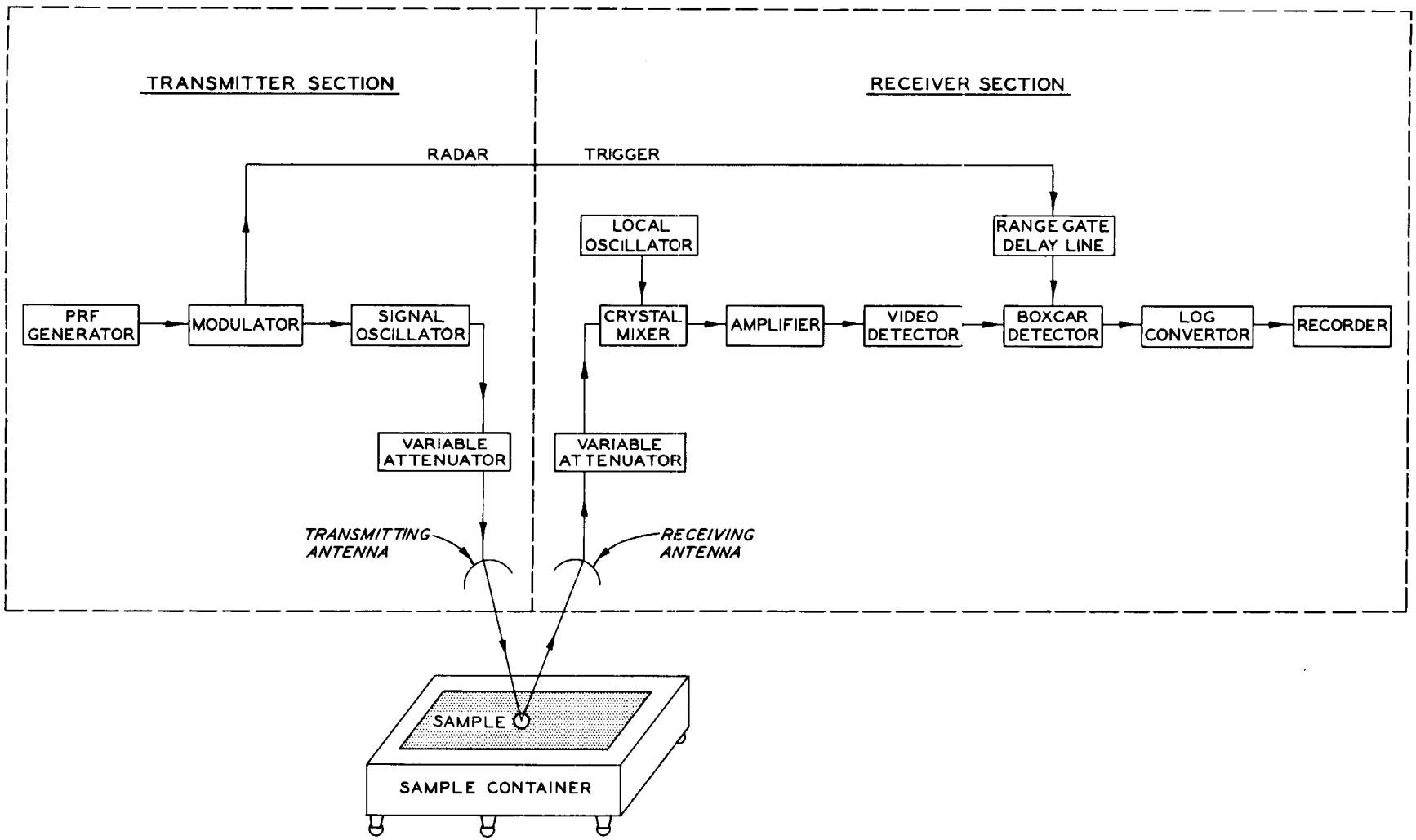

Fig. 4. Typical radar set signal flow diagram

receiver sections. The purpose of the transmitter section is to generate a radar signal that is transmitted toward the sample being investigated. A portion of the radar signal reflected by the sample is received by the receiver section, which processes this signal and displays it in a usable form, such as a graph of the change in radar signal returned versus change in the angle of incidence. Details of how these various functions are performed are presented in the following paragraphs.

13. Pulse repetition frequency (PRF) generator. When an area is being scanned by a pulsed radar system, a sufficient number of pulses of radar energy must be transmitted by the system for each small increment of distance traveled by the antennas to ensure continuous monitoring of the reflectivity characteristics of the terrain. The PRF generator is the component in a pulsed radar system that controls this rate of transmission. In laboratory radar systems, the PRF is not a critical factor since the antennas move slowly. For these studies, the PRF generator was arbitrarily adjusted for approximately 1800 pulses per sec. The output of this generator, which is a 200-volt positive pulse produced at a rate of 1800 pulses per sec, is used to trigger the modulator portion of the radar transmitter.

14. Modulator. For each 200-volt positive pulse received from the PRF generator, the modulator produces two output voltages. One output is a radar trigger pulse used in the receiver section's boxcar detector to sample specific time increments of the received pulse (see paragraph 23 for details). The other output is a 10,000-volt negative pulse with a pulse width for each of the radar bands as follows:

Radar Band	Pulse Width, microsec
Ka	0.31
X	0.54
C	0.50
P	0.82

15. Signal oscillator. The 10,000-volt negative pulse triggers the signal oscillator which in turn generates a pulse of microwave energy at a fixed tuned frequency (paragraph 11). The Ka-, X-, and C-band radar sets

utilize nontunable magnetrons as signal oscillators, whereas the P-band radar set uses a ceramic triode tube oscillator. The signal oscillator emits microwave energy for a period of time equivalent to the pulse width of the modulator output. The power level of the output microwave energy, which is determined by the design of the signal oscillator, is as follows for each of the bands used:

Radar Band	Average Pulse Power, watts	Average Pulse Power, dbm
Ka	10,000	70.0
X	6,026	67.8
C	72	48.6
P	52	47.2

16. Transmitter variable attenuator. The microwave energy pulse emitted by the signal oscillator is introduced into the transmitting antenna through a variable attenuator. This attenuator is adjusted to reduce the transmitted power level in such a way that the level of energy received by the receiver section can be processed in a usable form.

17. Transmitting antenna. After passing through the variable attenuator, the pulse of microwave energy is propagated into space by means of a parabolic antenna that is boresighted toward the center of the top surface of the sample. When the transmitted wave strikes the sample, a portion of the microwave energy is reflected toward the receiving antenna.

18. Receiving antenna. The parabolic receiving antenna, which is also boresighted toward the center of the top surface of the sample, collects a portion of the reflected microwave energy and passes it through a variable attenuator in the receiver section.

19. Receiver variable attenuator. The function of this variable attenuator is identical with that of the attenuator used in the transmitter section (paragraph 16), except that here the received microwave energy is reduced to a level that will not saturate the receiver section. In normal practice the attenuator in the transmitter section is adjusted so that the maximum amount of power permissible is transmitted toward the sample with the receiver attenuator range available. This maximum level is determined by the reflectivity of the sample and the attentuation range of the receiver section attenuator.

20. Crystal mixer. Frequencies as high as those used in radar transmission (i.e. 9375 megacycles per sec for X-band) cannot be processed through standard electronic wiring and amplifier tubes. Wave guides must be used to route the high-frequency signals efficiently from one point to another. To simplify the processing of these radar signals, the crystal mixer reduces the frequency of the received radar energy. It does this by mixing the frequency of the received signal with the output of the local oscillator, which is tuned to produce a signal having a frequency 60 megacycles per sec higher than that of the received signal. The output frequency of the crystal mixer is the difference between the frequency of the received signal and the frequency of the local oscillator. The following tabulation gives the input and output frequencies of the crystal mixers for each of the radar bands used:

Radar Band	Frequency of Received Signal megacycles/sec	Frequency of Local Oscillator Signal megacycles/sec	Output of Crystal Mixer megacycles/sec
Ka	34,543	34,603	60
X	9,375	9,435	60
C	5,870	5,930	60
P	297	357	60

21. Amplifier. The input from the crystal mixer to the amplifier is a pulse having a frequency of 60 megacycles per sec, an amplitude proportional to that of the energy received, and a time duration proportional to that of the transmitted signal. The amplifier, which is tuned to receive signals having a frequency of approximately 50 to 70 megacycles per sec, amplifies the 60-megacycle-per-sec signal input and passes it on to the video detector portion of the receiver.

22. Video detector. The video detector rectifies the 60-megacycle-per-sec frequency signal input into a d-c pulse proportional to the amplitude of the input signal and applies this pulse to the boxcar detector.

23. Boxcar detector. The boxcar detector has two inputs as follows: (a) the signal from the video detector, and (b) a range gate that is produced by passing the radar trigger through a delay line. Unless both of these inputs are present at the same time, the boxcar detector has no

output. When both inputs are present at the same time, the output of the boxcar detector is a d-c voltage proportional to the amplitude of the detected video pulse that is coincident with the range gate (see fig. 5).

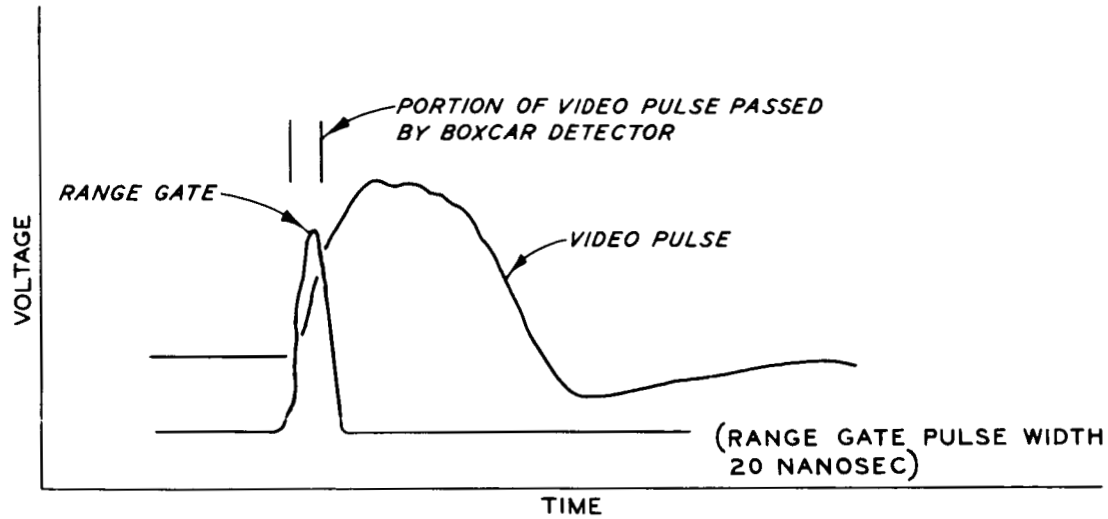

Fig. 5. Boxcar detector inputs; voltage versus time

The range gate can be adjusted to coincide with any portion of the video pulse. The trigger that produces the range gate is generated by the modulator portion of the transmitter section at the same time that the signal oscillator is triggered to transmit a signal toward the sample. In order to pass the detected video signal from the sample through the boxcar detector, the range gate must be delayed by a period of time equivalent to the time that it takes the transmitted signal to travel from the transmitting antenna through space to the sample, and back through space to the receiving antenna. The time required for the transmitted pulse to travel through space to and from the sample is computed as follows:

$$T = \frac{2R}{c} \tag{1}$$

where

T = time required, sec

R = distance from antenna to sample, m

c = speed of electromagnetic waves through air, m/sec

With the test facility used in these studies, R equals 13.7 m and T is computed as follows:

$$T = \frac{2(13.7\ \text{m})}{3 \times 10^{8}\ \text{m/sec}}$$

$$T = 9 \times 10^{-8}\ \text{sec}$$

$$T = 0.09\ \text{microsec}$$

The range gate is adjusted so that it is coincident with the portion of the video pulse that represents a time delay of 0.09 microsec from the time the radar signal is propagated by the transmitting antenna. All of the remainder of the video pulse shown in fig. 5 is a combination of (a) reflections from objects other than the sample and (b) reflections from the sample due to the trailing edge of the transmitted pulse.

24. Log converter. The log converter receives the d-c signal from the boxcar detector and converts it to a logarithmic output voltage. This permits compression of the high-energy-level signals received at vertical incidence and expansion of the low-energy signals received off vertical incidence. This is necessary because the return signal off vertical incidence is of such a low level that any changes in the quantity of reflected energy due to changes in sample parameters will be only slight, and these changes must be amplified if the data are to be of any value.

25. Recorder. The output of the log converter is recorded by the X-Y recorder as a function of the radar energy reflected from the sample versus the angle of incidence.

System Calibration

Calibration of X-Y recorder

26. As stated in paragraph 25, variations in the quantity of radar energy reflected by the samples were recorded on an X-Y recorder. To interpret the recorder deflections in terms of actual power received, the recorder had to be calibrated for each of the radar bands by inserting known amounts of radar power into the receiving system and measuring the resulting

voltage output on the X-Y recorder. To accomplish this, the transmitted power (average pulse power) of each radar transmitter was calculated by dividing the measurement obtained with a standard power meter (average power) by the product of the pulse width taken at half-power points and the pulse-repetition frequency. Next, the transmitter and receiver were coupled back-to-back as shown in fig. 6. With the equipment connected in this manner, the energy being received by the receiver section came

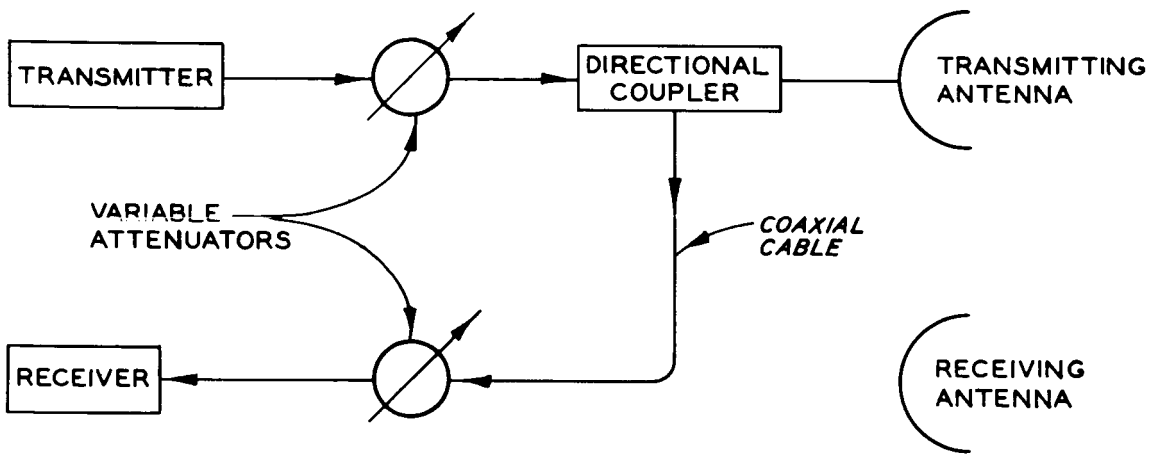

Fig. 6. Radar sets connected back-to-back

directly from the transmitter through a directional coupler instead of being received through the receiving antenna. Attenuation was then added between the transmitter and receiver by means of the variable attenuators (paragraphs 16 and 19) until the power level being received resulted in a minimum reading on the recorder. Next, the attenuation was removed in carefully measured increments until the receiver became saturated and further increases in power did not result in an increase in recorder deflection. Throughout this calibration procedure, the attenuation value of each of the variable attenuators was recorded along with the corresponding recorder deflection. To ensure accuracy, it was necessary to go through the calibration procedure periodically (paragraph 28). Typical calibration recordings are given for each of the radar sets in the first three columns of table 1.

27. The power received P_R that corresponded to each of the recorder deflection values was calculated and plotted versus recorder deflection to

provide a receiver calibration curve. P_R for each recorder deflection was found by subtracting all power losses between the transmitter and receiver from the transmitted power. These losses were due to the fixed losses of the directional coupler and the coaxial cable and to the losses due to the variable attenuators. Therefore, P_R for a given recorder deflection was calculated using the following equation:

$$P_R = P_T - (DC + CC + TA + RA) \qquad (2)$$

where

P_R = power received, dbm
P_T = power transmitted, dbm
DC = loss in directional coupler, db
CC = loss in coaxial cable and wave guide, db
TA = loss due to the transmitter attenuator, db
RA = loss due to the receiver attenuator, db

The loss for each item was defined as: loss = 10 log (power in/power out). The fixed losses are given below.

Radar band	DC, db	CC, db
Ka	20.0	0.0
X	9.2	4.0
C	20.0	3.8
P	20.0	1.7

Calculated values for P_R are given in the last column of table 1, and plots of the resulting calibration curves are illustrated in plate 1 for each of the radar sets used.

Daily calibration checks

28. To maintain system accuracy, a regular calibration check was performed. Twice each day, once in the morning at the beginning of operation and again in the evening at the end of operation, each of the radar receivers was coupled back-to-back with its respective transmitter. A standard amount of attenuation was inserted, using the variable attenuators between the transmitting and receiving units, and the transmitter was

turned on. The output voltage of the receiver resulting from the input power of the transmitter was monitored on the X-Y recorder. By measuring the output power of the transmitter and subtracting all subsequent power losses between the transmitter and receiver, the amount of power reaching the receiver could be calculated. This value was compared with the one obtained by converting the output voltage of the receiver to power by use of the receiver calibration curve shown in plate 1. In this way, any changes in the system were detected and corrected.

29. It was realized that in setting up the system each day there would be a certain amount of human error. Also, a certain amount of inherent fluctuation in the radar systems was to be expected. Therefore, as soon as a sufficient number of data points were available, the mean deviation of the daily readings from the values obtained during the calibration of the X-Y recorder was calculated and confidence limits were established for the calibration check. These confidence limits were used to ascertain if the system was functioning properly. If the value obtained from the daily check was between these confidence limits, the system was considered to be functioning satisfactorily. If the value fell outside these limits, the operator first checked to ascertain if the system was set up properly, and second, checked for system malfunctions. If both checks were positive, the system was assumed to have drifted due to aging of components and it was recalibrated. In this way, the daily calibration check not only monitored system accuracy, but also gave a convenient indication of the proper time to recalibrate each of the radar systems.

30. The daily checks revealed that the mean deviations of the measured values of P_R, using all data points, of the Ka-, X-, C-, and P-bands were ± 2.6 dbm, ± 0.7 dbm, ± 1.8 dbm, and ± 1.0 dbm, respectively. The average differences between the two daily readings, again using all data points, were 0.4 dbm for Ka-band, 0.2 dbm for X-band, 0.1 dbm for C-band, and 0.2 dbm for P-band.

PART III: TEST PROGRAM

Types of Tests

31. The test program consisted of using a multifrequency pulsed radar system operating in the Ka-, X-, C-, and P-band regions of the spectrum to measure and record the proportion of transmitted radar energy that was reflected from samples prepared in the laboratory. Tests in which incidence angle was varied (signature tests) were used to determine the feasibility of measuring sample moisture content of bare and vegetation-covered soil. Tests in which the sample depth was varied (depth-of-penetration tests) were used to measure sample moisture content and density, and the penetration capabilities of the various frequencies.

Materials Tested

32. Five materials were used in this test program, i.e. four soils (Sharkey clay, Richfield silt loam, Putnam silt loam, and Putnam clay) and perlite. The source, classification under the Unified Soil Classification System (USCS) and U. S. Department of Agriculture (USDA) classification systems, specific gravity G_s, average Atterberg limits, and gradation for all four soils are shown in plate 2. A detailed description of each material is contained in Appendix A. In addition to these materials, a stand of wheat was tested at various stages of growth.

Preparation of Samples

Sample container

33. A cross section of the test cart in which the samples were prepared is shown in fig. 7. The cart was constructed of wood and was 12 ft long, 6 ft wide, and 2 ft deep. The walls of the cart were constructed in 4-in. vertical segments to facilitate removal of layers of the sample during the depth-of-penetration tests.

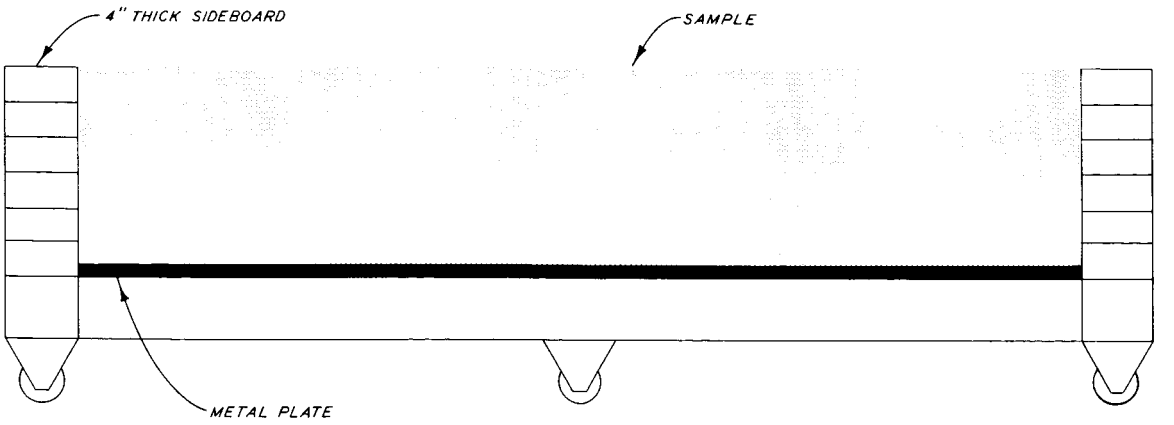

Fig. 7. Cross section of test cart

Soil samples

34. In the construction of the soil samples, a conductive metal plate of the inside areal dimensions of the cart was placed on the bottom of the test cart (see fig. 7). The sides of the test cart were then built up to the height of 2 ft, using the 4-in. sideboards. The cart was filled with soil in at least two lifts, and the soil was compacted with a pneumatic-tired roller after each lift was placed. Sometimes as many as five lifts were used so that the dry density and moisture content could be kept uniform throughout the sample. Moisture content and dry density were measured at intervals during the construction of the sample to ensure uniformity. No attempt was made to obtain a specific density, but the moisture content was varied from sample to sample over a range of values for each soil type.

35. Usually each soil sample consisted of one type of soil; however, a slightly different procedure was used to construct samples of Putnam silt overlying Putnam clay. In nature, a surface layer of Putnam silt loam normally covers a subsurface layer of Putnam clay, and the test samples were constructed to simulate this condition. After the metal plate was positioned on the bottom of an empty cart, a layer of Putnam clay 13.5 in. deep at a moisture content of approximately 45 percent was placed in the cart. An 11.5-in. layer of Putnam silt loam at the desired test moisture content was placed on top of the clay. This brought the total thickness of the soil in the cart to 25 in.

Perlite samples

36. The process used for construction of perlite samples was much the same as that for the soil samples except that no water was added to the samples, nor were they compacted. A metal plate was placed on the bottom of the test cart, the sides were built up to the height of 2 ft, and the cart then was filled with perlite. The desired density was obtained by mixing a volume of unexpanded perlite (at 61 pcf) with a volume of expanded perlite (at 10 pcf). The following proportions were used:

Sample Density pcf	Expanded Perlite %	Unexpanded Perlite %
10	100	--
20	80.4	19.6
30	60.8	39.2
40	41.1	58.9

Wheat-covered sample

37. A sample of Richfield silt loam at 20.0 percent moisture content was constructed as described in paragraph 34 and was seeded with wheat. During the next six months, a thick growth was produced on the sample by periodic watering and by exposure to the weather. This, of course, was necessary to ensure the growth of the wheat, but unfortunately it also produced fluctuations in the moisture content of both the wheat and the soil. The soil moisture content ranged from 15.2 to 27.7 percent, and the vegetation moisture content ranged from 272.8 to 346.5 percent over the period of a few months.

Measurement of Reflectivity

Signature tests

38. Once it was established that the radar sets were functioning properly, the test cart containing the sample was moved into position under the wooden arch structure and placed on a hydraulic-lift system located in the center of the arch. The surface of the sample was elevated to 50.7 in. above the ground, which was the height of the point in space at which the

transmitting and receiving antennas for all four radar bands had been boresighted. The sample then was surrounded with microwave-absorbent material, as shown in fig. 8, to reduce reflections from areas other than the sample.

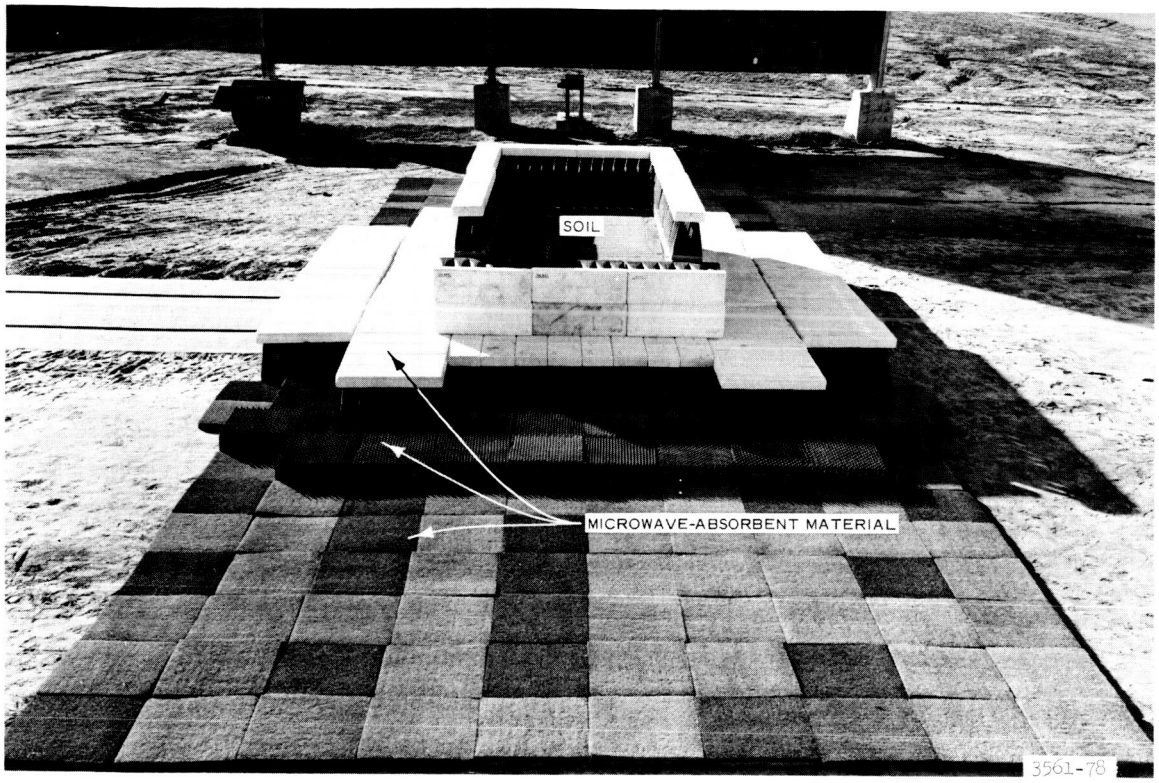

Fig. 8. Microwave-absorbent material layout

39. Signatures from bare soils, perlite, and the wheat-covered soil were determined by measuring and recording the quantity of radar energy reflected by the sample as the radar antenna carriage moved from vertical incidence through an angle of incidence of 60 deg. A typical soil sample signature is shown in fig. 9. Radar signatures of the wheat-covered soil were taken after one month of growth when the wheat was approximately 3-1/2 in. tall, after four months of growth when the wheat was approximately 14 in. tall, and after six months of growth when the wheat was approximately 29 in. tall. The quantity of energy reflected was a measure of the sample's normalized echo area[3] γ_{db} expressed in db . The quantity γ_{db} is used as the radar return parameter because it is not dependent on radar system constants and is a measure of the sample properties

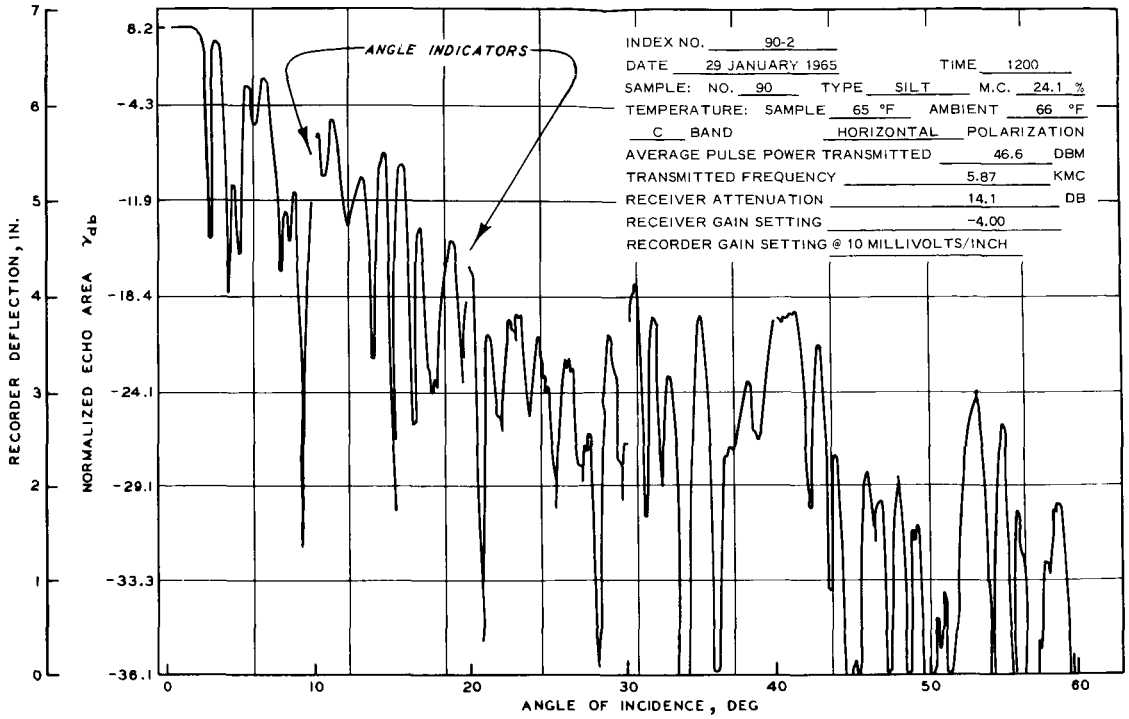

Fig. 9. Typical soil sample signature

only. The method of computing γ_{db} is discussed in Appendix B. Since the antenna carriage did not move at a constant speed, it was necessary to record the position of the carriage at certain increments. This was accomplished by devices on the antenna carriage that were actuated every 10 deg by spacers mounted on the track of the arch. These devices broke the recorder circuit and caused an event mark to appear on the signature.

Depth-of-penetration tests

40. The final phase of a sample test was to determine the depth-of-penetration capabilities of the radar waves for the four radar bands, and to determine changes in the depth of penetration due to variations in pertinent sample parameters, such as soil-moisture content and soil composition, or perlite density. With the sample in position under the arch and surrounded by microwave-absorbent material, measurements were taken with the antenna carriage at vertical incidence. The quantity of microwave energy reflected by the sample at vertical incidence was recorded for each of the radar bands. A 1/2-in. layer of the sample was then removed, the sample surface was raised to the original height of 50.7 in., and another

recording was taken of the radar return energy with each of the radar sets at vertical incidence. This process of removing thin layers and recording the microwave energy returned was repeated until the metal plate at the bottom of the sample was exposed.

41. A similar procedure was followed in running the depth-of-penetration tests on samples of Putnam silt overlying Putnam clay. This kind of sample was tested in the normal manner until, in the process of removing soil layers, all the surface soil (silt loam) was removed and the clay was exposed. The testing was then halted and the soil level was brought back to the original 25-in. depth by filling the cart with Putnam silt loam at another moisture content. However, in the final test the removal of layers was continued after the clay was reached until the metal plate on the bottom of the cart was exposed.

PART IV: DATA ANALYSIS

Basis of Analysis

42. Radio waves transmitted in a completely homogeneous medium will be propagated with a constant rate of attenuation until they disappear, having been consumed as heat. When the waves strike a sudden discontinuity in the medium, such as the boundary between two materials with differing electrical properties, some of the waves are reflected, while the remainder continue at a modified rate of attenuation and velocity. In this program, the attenuation occurring in air in the 50-ft distance between the test medium and the antennas was assumed to be zero and the velocity of the waves was assumed to be equal to that of light in free space. Thus, the first and most important reflection-causing discontinuity was the surface of the test medium itself. The remainder of the waves traveled through the surface into the sample until they encountered another discontinuity and a second reflection of the waves was produced. The phase shift between the first and second reflections varied with sample depth due to the longer path length for the second reflection. The analysis of the data collected in the program from the depth-of-penetration tests and the signature tests was based on the measurement of the proportion of emitted energy which was reflected upon contact with the various discontinuities, the phase shifts which occurred between reflections of radar waves from the various discontinuities, and the change in wavelength that occurred in different media.

Analysis of Depth-of-Penetration Test Data

43. The radar returns from the surface of a sample, the subsurface sample-metal plate interface, and the area surrounding the sample can be thought of as three separate vectors. The phase of each vector depends on the distance the wave travels, and its magnitude depends on the reflectivity of the area, the distance the wave travels, and the electrical properties of the material through which the wave travels. These three vectors combine to form a vector sum whose phase and magnitude are influenced by the

depth to the sample-metal plate interface (fig. 10). As this depth is decreased, the phase of the subsurface sample-metal plate interface vector advances in a counterclockwise direction and its magnitude steadily

a. REINFORCEMENT

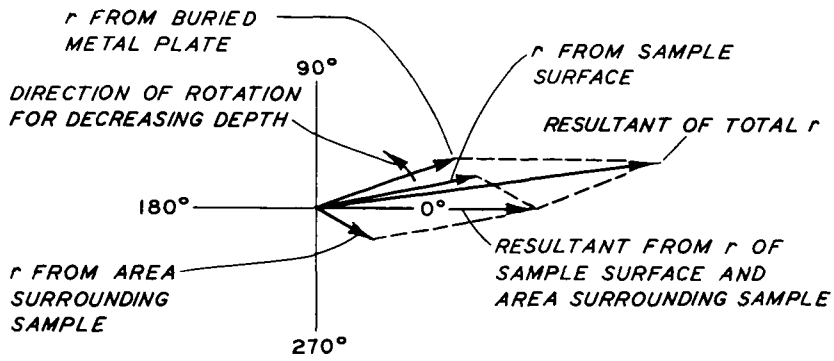

NOTE: r = ELECTRIC WAVE REFLECTANCE.

b. DESTRUCTION

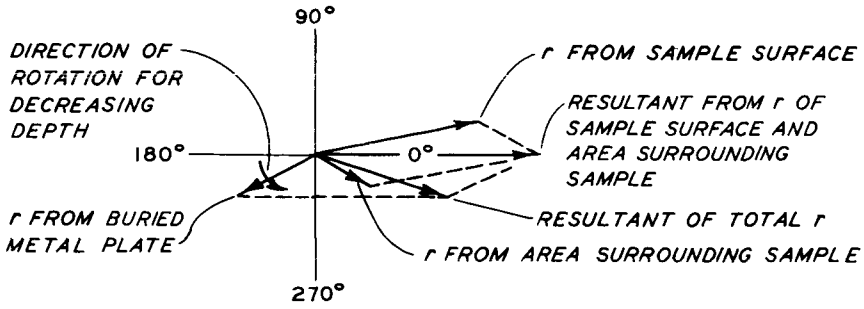

Fig. 10. Radar return phasor diagrams

increases. The phase and magnitude of the surface-reflection vector and the vector from the area surrounding the sample remain constant during the test. A maximum power return or reinforcement is produced when the rotating vector is in phase with the resultant of the constant vectors, and a minimum power return or destruction is produced when the rotating vector is out of phase with the resultant of the constant vectors. Thus there will be a reinforcement and a destruction for every 360-deg rotation of the rotating vector. The pulsed radar systems used in these tests, however,

are sensitive only to the magnitude of the total radar return, and individual pulse returns cannot be analyzed directly to determine the contribution being made by each reflecting surface. However, it was possible to make this type of analysis indirectly because the depth of the sample was controlled in the test program. In the following paragraphs, the procedures will be discussed for the determination of the existence of subsurface interface reflections, calculation of electrical constants of soils from interference patterns, and calculation of electrical soil constants from surface radar return.

Determination of existence of subsurface interface reflections

44. As the sample thickness was reduced in the depth-of-penetration tests (paragraph 40), the phase of the subsurface interface reflection advanced, thereby producing oscillations in the total radar return. This situation is illustrated in fig. 11a for a sample composed of Yuma sand overlying a metal plate. Obviously, a plot of this type by itself is of very limited use as a calibration or reference chart for measuring depth to an interface. The appearance of this uniform cyclic pattern together with the fact that the in-soil wavelength is shorter than the in-air wavelength of the radar used is, however, proof that the radar wave is penetrating through the upper material in the sample, reflecting from the interface, and returning to the radar receiver. For the example in fig. 11a, the oscillations indicate that a wave at P-band frequencies penetrated through the entire 0.56-m sample. In this example and in all tests, the actual depth to the metal plate could not be measured directly with any one band of the type of radar system used. The depth at which the oscillations first appear indicates the probable limit of a depth-measuring system that uses that particular wavelength.

Calculation of electrical properties from interference patterns

45. Phase-shift method of calculating electrical constants of samples. The radar return that produced the type of oscillations illustrated in fig. 11a can be separated into two components as follows: a constant surface reflection that included a small amount of background

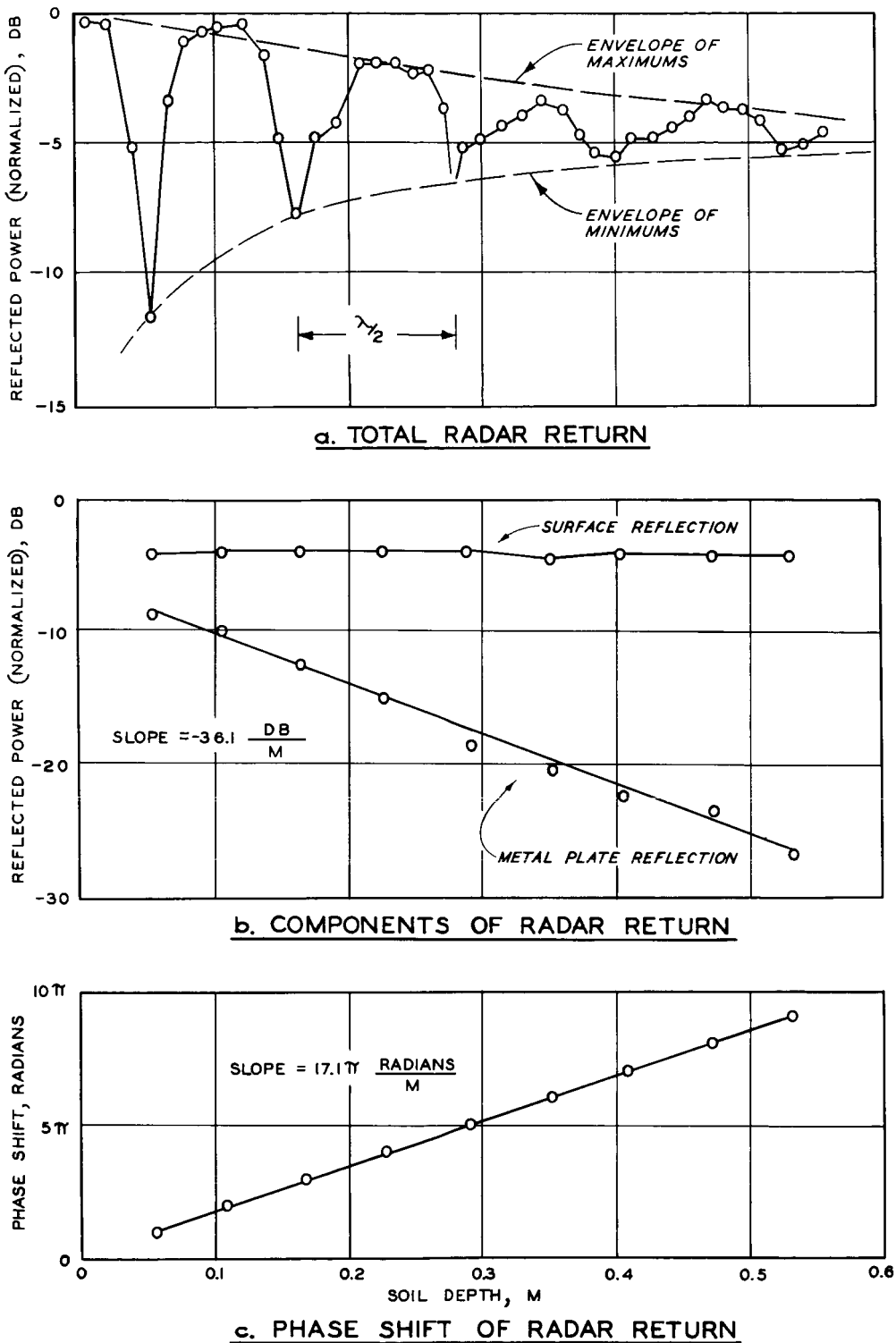

Fig. 11. P-band depth of penetration test results for Yuma sand. Moisture content = 19.2%

reflection (fig. 11b), and a metal plate reflection that varied in magnitude (fig. 11b) and in phase (fig. 11c) with depth of overlying soil. The wave that reaches the metal plate in the bottom of the sample has a phase and magnitude which are functions of depth. The equation for the intensity of this wave at an instant in time is:[4,5]

$$E = E_t e^{-\alpha x} e^{-j\beta x} \tag{9}$$

where

E = electric field intensity of the wave reaching the metal plate, volt/m

E_t = electric field intensity of the wave transmitted through the air-sample surface boundary, volt/m

α = attenuation factor of the sample, m^{-1}

β = phase factor of the wave, m^{-1}

x = sample depth, m

$j = \sqrt{-1}$

In these tests the radar wave traveled twice the sample depth as it penetrated through the surface boundary to the metal plate and was reflected back through the surface of the sample. When equation 3 is adjusted by this factor, added to the surface reflection, and written in terms of power, it becomes:

$$P = \left| \frac{E_r}{E_i} + \frac{E_m}{E_i} \left(\frac{R}{R + x} \right)^2 e^{-2\alpha x} e^{-j2\beta x} \right|^2 \tag{10}$$

where

P = normalized power of the wave returning to the radar receiver from the sample, dimensionless

E_r = electric field intensity of the wave returning to the radar receiver from the sample surface reflection, volt/m

E_i = electric field intensity of the incident wave striking the surface of the sample, volt/m

E_m = electric field intensity of the wave returning to the radar receiver from the subsurface metal plate reflection, volt/m

R = range from radar system to sample, m

The constant surface-reflectance term in this equation is E_r/E_i ; the magnitude of the metal plate reflection, which varies with sample depth, is $\frac{E_m}{E_i}\left(\frac{R}{R+x}\right)^2 e^{-2\alpha x}$; and the phase shift of the metal plate reflection, which also varies with sample depth, is $e^{-j2\beta x}$. By using each data point obtained in the depth-of-penetration test (fig. 11a) as a solution to equation 10 and solving the equations simultaneously, α , β , E_r/E_i , and E_m/E_i can be evaluated. This method requires many calculations and is best suited for use with a digital computer. A much simpler method can be used to demonstrate the procedure and evaluate the unknown quantities in equation 10 by using the maximum and minimum points from the cyclic depth-of-penetration curve as solutions to the equation. The maximum points are given by the equation

$$P_{max} = \left[\frac{E_r}{E_i} + \frac{E_m}{E_i}\left(\frac{R}{R+x}\right)^2 e^{-2\alpha x}\right]^2 \tag{11}$$

and the minimum points are given by the equation

$$P_{min} = \left[\frac{E_r}{E_i} - \frac{E_m}{E_i}\left(\frac{R}{R+x}\right)^2 e^{-2\alpha x}\right]^2 \tag{12}$$

Equations 11 and 12 describe the envelopes of the maximum and minimum points, respectively, as shown in fig. 11a and are obtained by setting $e^{-j2\beta x}$ in equation 10 equal to +1 to obtain equation 11 and -1 to obtain equation 12. As an example of the calculations used to separate the components of the total radar return, consider the point at a sample depth x of 0.165 m in fig. 11. The minimum point as shown in fig. 11a is -7.7 db or a power ratio P of 0.17 (db = 10 log P), and by interpolation of the maximum point envelope, a maximum point at this sample depth would be approximately -1.3 db or a power ratio of 0.74. Substituting these values in equations 11 and 12 gives:

$$0.74 = \left[\frac{E_r}{E_i} + \frac{E_m}{E_i}\left(\frac{R}{R+x}\right)^2 e^{-2\alpha x}\right]^2$$

and

$$0.17 = \left[\frac{E_r}{E_i} - \frac{E_m}{E_i}\left(\frac{R}{R+x}\right)^2 e^{-2\alpha x}\right]^2$$

Taking the square root of both sides and solving two simultaneous equations, the reflections in terms of voltage ratios are

$$\frac{E_r}{E_i} = 0.64$$

and

$$\frac{E_m}{E_i}\left(\frac{R}{R+x}\right)^2 e^{-2\alpha x} = 0.23$$

or in terms of power ratios

$$10 \log (E_r/E_i)^2 = 10 \log (0.64)^2 = -3.9 \text{ db} = \text{surface power reflection}$$

$$10 \log \left[E_m/E_i \left(\frac{R}{R+x}\right)^2 e^{-2\alpha x}\right]^2$$

$$= 10 \log (0.23)^2 = -12.8 \text{ db} = \text{metal plate power reflection}$$

The above solutions for the metal-plate reflections and the surface reflections along with the solutions from other maximum and minimum points are plotted in fig. 11b. Although not used in any calculations, the value for $(E_m/E_i)^2$ can be found by extrapolation and is the point where sample depth x is zero. In fig. 11b, this value is the point where an extension of the metal-plate reflection curve (straight line) crosses the vertical axis at zero sample depth.

46. The attenuation factor α varies with sample composition, moisture content, density, etc., and is computed using the term in equation 10 involving the magnitude of the metal plate reflection as follows:

$$\text{Return signal from the metal plate} = \left[\frac{E_m}{E_i}\left(\frac{R}{R+x}\right)^2 e^{-2\alpha x}\right]^2 \qquad (13)$$

or, expressed in db:

Return signal from the metal plate, db = 10 log $\left[\frac{E_m}{E_i}\left(\frac{R}{R+x}\right)^2 e^{-2\alpha x}\right]^2$

$$= 20 \log \frac{E_m}{E_i} + 40 \log R - 40 \log (R + x) + 20 (\log e)(-2\alpha x) \quad (14)$$

The slope of the metal plate reflection versus depth relation is the derivative with respect to x of equation 14. Thus,

$$\text{slope, db/m} = -40 \left(\frac{1}{R+x}\right) \log e + 20 (\log e)(-2\alpha)$$

$$= -(17.372) \left(\frac{1}{R+x}\right) - (17.372)(\alpha) \quad (15)$$

The value of x varies between 0 and 0.5 m, and when compared with the range R of 13.7 m, it is negligible. Thus, the expression $\frac{1}{R+x}$ can be approximated by $1/R$, and the expression $(17.372)\left(\frac{1}{R+x}\right)$ becomes 1.3 db/m. Equation 15 then reduces to

$$\text{Slope, db/m} + 1.3 \text{ db/m} = -17.372\alpha \quad (16)$$

Using the example in fig. 11 for illustration purposes, α can be calculated by inserting -36.1 db/m, the measured slope of the metal plate reflection curve (fig. 11b), into equation 10 as follows:

$$-36.1 \text{ db/m} + 1.3 \text{ db/m} = -17.372\alpha \text{ , or } \alpha = 2.0 \text{ m}^{-1}$$

47. The phase shift of the radar return (fig. 11c) is shown in equation 10 by the term $e^{-j2\beta x}$. It is found by inspection of the oscillations in fig. 11a and the prior knowledge that there are π radians of phase shift between a maximum and a minimum, or 2π radians between successive minimums and maximums. The phase factor β can then be obtained from the cycling effect (fig. 11a) or phase shift shown in fig. 11c as follows:

$$\beta = (1/2)(\text{phase-shift slope, radian per m}) \quad (17)$$

where phase-shift slope is equal to the number of oscillations occuring over a change in depth of 1 m multiplied by 2π . Using the example in fig. 11, β can be calculated by inserting 17.1π radians/m (the measured value of the slope of the phase-shift curve, fig. 11c) into equation 11.

$$\beta = (1/2)(17.1\pi \text{ radians/m})$$

or

$$\beta = 26.8 \text{ m}^{-1}$$

48. Of the factors influencing the normalized power, the relative dielectric constant is of primary interest because it can be shown to be related to the moisture content of the sample. The equations[5] for determining relative dielectric constant ϵ_r and conductivity σ for nonmagnetic samples are as follows:

$$\alpha = \omega \sqrt{\frac{\mu\epsilon}{2}\left(\sqrt{1 + \frac{\sigma^2}{\omega^2\epsilon^2}} - 1\right)} \tag{18}$$

$$\beta = \omega \sqrt{\frac{\mu\epsilon}{2}\left(\sqrt{1 + \frac{\sigma^2}{\omega^2\epsilon^2}} + 1\right)} \tag{19}$$

Solving equations 18 and 19 simultaneously yields:

$$\epsilon_r = \frac{c^2}{\omega^2}(\beta^2 - \alpha^2) \tag{20}$$

$$\sigma = \frac{2\alpha\beta}{\omega\mu} \tag{21}$$

where

α = attenuation factor, m^{-1}

ω = angular frequency, radian/sec

μ = electromagnetic permeability of the sample (assumed to be equal to that of free space), $4\pi \times 10^{-7}$ henry/m

ϵ = dielectric constant ($\epsilon/\epsilon_v = \epsilon_r$), farad/m

σ = conductivity, mho/m

β = phase factor, m^{-1}

ϵ_r = relative dielectric constant, dimensionless

ϵ_v = dielectric constant of free space, $1/(36\pi \times 10^9)$ farad/m

c = speed of light in free space, 3×10^8 m/sec

The assumption that the electromagnetic permeability μ of the samples is equal to that of free space is valid because the samples tested are known to be nonmagnetic. Only traces of magnetic materials have been found in these samples.

49. Again using the example in fig. 11 for illustration purposes, the following calculations can be made. Substituting the previously calculated values for α and β into equations 20 and 21 yields values for ϵ_r and σ. The angular frequency ω is equal to $2\pi \times 297 \times 10^6$ radians per sec, where 297×10^6 is the frequency in cycles per sec of the P-band radar system.

$$\epsilon_r = \frac{(3 \times 10^8 \text{ m/sec})^2 \left[(26.8 \text{ m}^{-1})^2 - (2.0 \text{ m}^{-1})^2\right]}{(2\pi \times 297 \times 10^6 \text{ radians/sec})^2}$$

$$\epsilon_r = 18.5$$

$$\sigma = \frac{(2)(26.8 \text{ m}^{-1})(2.0 \text{ m}^{-1})}{(2\pi \times 297 \times 10^6 \text{ radians/sec})\ (4\pi \times 10^{-7} \text{ henry/m})}$$

$$\sigma = 45.8 \times 10^{-3} \text{ mhos/m}$$

50. Wavelength method for computing electrical constants of samples. The relative dielectric constant of a sample also can be calculated from the wavelength of the radar wave in the material. Examination of the radar return phasor diagram shown in fig. 10 indicates that a maximum and minimum will occur in the oscillations of the reflected power from a sample every 360 deg. Since the wave travels through two sample depths (down and back) to produce the oscillations, it is necessary only to measure the distance between two successive minimums or maximums of the depth-of-penetration test results and double the value obtained to determine the wavelength of a radar wave in a medium. In the sand sample used for illustration of these oscillations (fig. 11a), P-band frequencies had a wavelength of 0.234 m as compared to 1.01 m in air. A numerical value for the

attenuation constant α is not always attainable from the sample data since this determination requires that very little system drift occur during the entire depth-of-penetration test. The phase factor β is not as readily obscured because the minimums and maximums are usually available even under the most undesirable conditions. From prior tests, the dissipation factor $\sigma/\omega\epsilon$ (equations 18 and 19) has been found to be small at P-band frequencies and can be neglected when calculating the relative dielectric constant without causing much error. Equations 18 and 19 then reduce to the following expressions:

$$\alpha = \omega \sqrt{\frac{\mu\epsilon}{2} \left(\sqrt{1 + 0} - 1\right)}$$

$$\alpha = 0$$

$$\beta = \omega \sqrt{\frac{\mu\epsilon}{2} \left(\sqrt{1 + 0} + 1\right)}$$

$$\beta = \omega \sqrt{\mu\epsilon} \tag{22}$$

Since $\beta = 2\pi/\lambda$, $\epsilon = \epsilon_v \epsilon_r$, $c^2 = \frac{1}{\mu\epsilon_v}$, and $\omega = 2\pi f$, substituting in equation 22 gives:

$$\epsilon_r = c^2/f^2\lambda^2 \tag{23}$$

where

ϵ_r = apparent relative dielectric constant (terminology changed to "apparent" since dissipation factor is being neglected)

c = speed of light in free space, 3×10^8 m/sec

f = frequency, cps

λ = wavelength in the medium, m

Using the wavelength value determined from the oscillations (fig. 11a), the apparent relative dielectric constant for Yuma sand at a moisture content of 19.2 percent was calculated as follows:

$$\epsilon_r = \frac{(3 \times 10^8)^2}{(297 \times 10^6)^2 \ (0.234)^2}$$

$$\epsilon_r = 18.7$$

When the above value for apparent relative dielectric constant is compared with the relative dielectric constant calculated previously ($\epsilon_r = 18.5$) in equation 20, it differs by only 0.2. Similar differences were noted for other samples (table 2).

Calculation of electrical properties from surface reflection

51. If radar waves are not reflected from a subsurface layer such as a metal plate, the total energy reflected by a sample will be due to surface reflections and can be expressed as follows for vertical incidence.[5]

$$r = \frac{E_r}{E_i} = \frac{\sqrt{\epsilon_r}\left(1 - j\frac{\sigma}{\omega\epsilon}\right)^{1/2} - 1}{\sqrt{\epsilon_r}\left(1 - j\frac{\sigma}{\omega\epsilon}\right)^{1/2} + 1} \qquad (24)$$

If the dissipation factor $\frac{\sigma}{\omega\epsilon}$ is considered to be very small as assumed before:

$$r = \frac{\sqrt{\epsilon_r} - 1}{\sqrt{\epsilon_r} + 1}, \text{ or the power reflectance is } r^2 = \left(\frac{\sqrt{\epsilon_r} - 1}{\sqrt{\epsilon_r} + 1}\right)^{2*} \qquad (25)$$

A graphical illustration of the relation between the power reflectance and the apparent relative dielectric constant is shown in fig. 12. For example, water is known to have a high relative dielectric constant of approximately 81. When this value is inserted in equation 25, the power reflectance is found to be 0.64, or -1.94 db, a high value compared with that of soil (see table 2). In the case of actual sample measurements, the power reflectance r^2 was taken to be the average soil surface power reflection in watts divided by an average bare metal plate power reflection in watts. The power reflectance r^2 taken from the depth-of-penetration data (table 2) was inserted in equation 25 so that a solution for apparent relative dielectric constant ϵ_r could be obtained.

* Equation must be squared because power as measured with the radar sets is in terms of watts while equation 24 is in terms of volts.

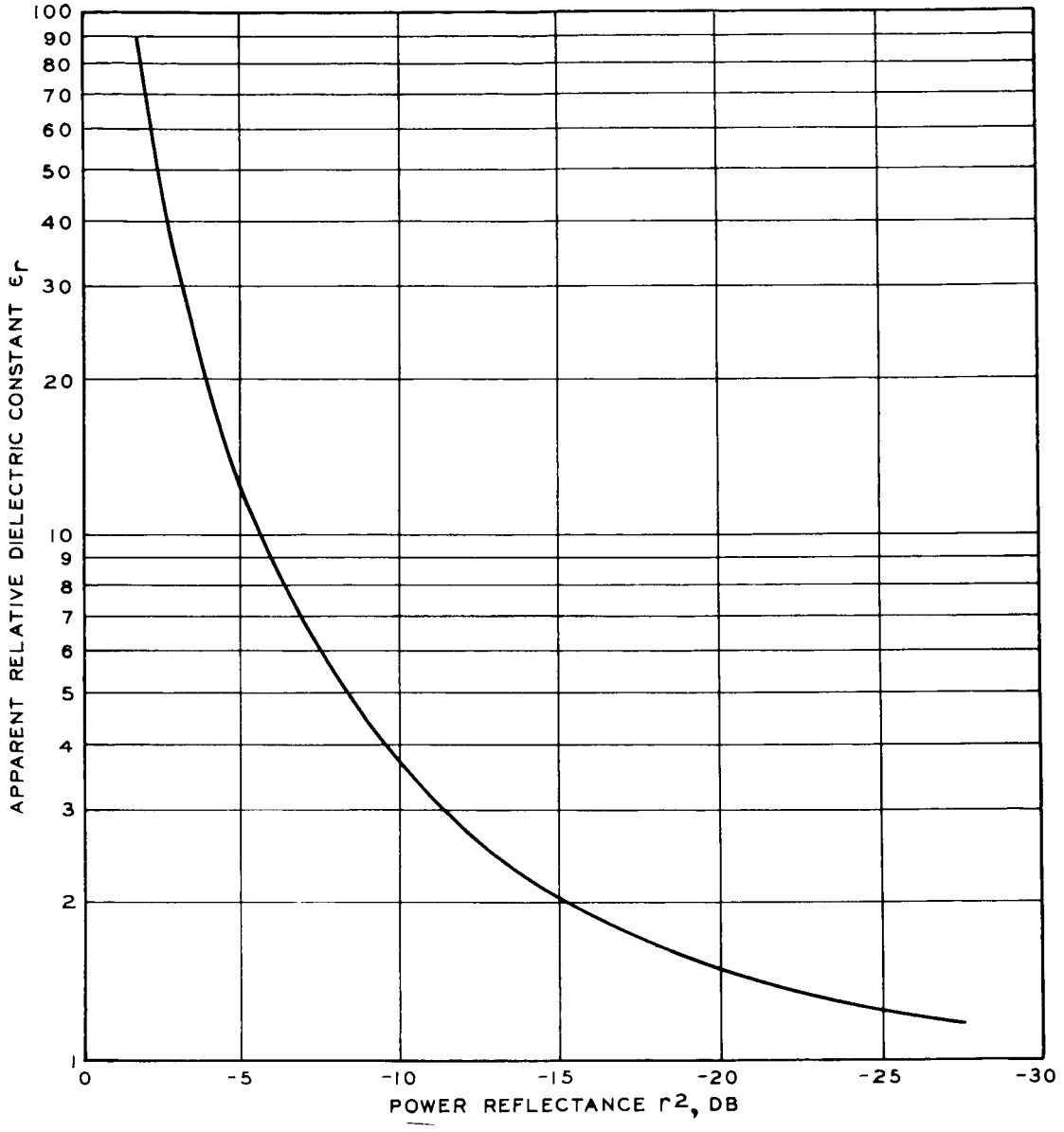

Fig. 12. Power reflectance versus apparent relative dielectric constant as determined from $r^2 = \left(\frac{\sqrt{\epsilon_r} - 1}{\sqrt{\epsilon_r} + 1} \right)^2$

Analysis of Signature Test Data

Soils and perlite

52. Signature tests were run to determine the feasibility of predicting soil electrical constants which could be related to soil properties. It is possible to calculate one electrical constant, the apparent relative dielectric constant, from the signature tests at angles of incidence near 0 deg (± 10 deg). This requires modification of the surface-reflection method for computing soil electrical constants described in paragraph 51 to include changes in incidence angle. In the tests of the soils and perlite, the surface of the samples appeared specular to the waves that were transmitted by each of the four radar bands, and the amplitude of the radar return from the sample at angles of incidence greater than 10 deg often was less than the noise level of the system. This noise level was made up primarily of (a) return from the microwave-absorbent material surrounding the soil sample, (b) return produced by the antenna-beam side lobes which struck areas outside the immediate test area, and (c) electronic noise in the electrical circuits. It should be noted that these radar sets were being used inside a test facility that would contribute to the noise of the system because of multiple reflections within the arch. Efforts thus far to develop valid techniques for analyzing the signature test data have been unsuccessful because of the noise and because the shapes of the signature curves change drastically with changes in surface texture of the soil.[6] Although care was taken to smooth the surface of the test specimen prior to the signature test, pits and scratches were unavoidably left on the surface. It was found that even these slight changes in the surface texture altered the signature curves more than large changes in sample constants. For these reasons, results of the signature tests for soils and perlite are not discussed herein.

Vegetation

53. Analysis of the data from samples of wheat-covered soil was difficult because the vegetation presented a complex surface to the radar wave. Unfortunately, the nature of this surface was not even constant

with time. A slight breeze produced large fluctuations in the radar return from the wheat-covered soil even when the transmitting and receiving antennas were not moving. This fluctuation was more apparent with the higher frequency bands (Ka, X, and C) than it was for P-band. However, these vegetation samples did not appear specular to the radar waves at incidence angles other than vertical, and the level of return signal obtained was well above the noise level of the system. The return signals were subject to interference patterns (radar return reinforcement and destruction) from the large number of reflecting surfaces in the wheat samples as the angle of incidence was varied. To minimize these random fluctuations, the signature curves were reduced by taking an average of the peaks (radar return reinforcement) over a 10-deg angle of incidence interval; e.g. a value shown at 20 deg on the data plots is the average of peaks between 15 and 25 deg. The resulting curves were then compared for the different heights of wheat.

Discussion of Test Results

Depth-of-penetration tests

54. The ability of radar waves to penetrate a material is determined not only by their frequencies but also by the electrical properties of the media through which the waves travel after entering the sample. Results of the tests for each of the materials used are summarized in tables 3-6 and are shown graphically in plates 3-16, as plots of normalized echo area γ_{db} versus sample depth above the metal plate.

55. Homogeneous soils (Sharkey clay and Richfield loam). Plates 3-10 illustrate the results obtained with Sharkey clay (fig. 13) and Richfield silt loam (fig. 14) at four moisture contents each. A fairly well defined pattern for Sharkey clay at a moisture content of 9.7 percent and for Richfield silt loam at 8.3 percent resulted with P-band frequencies (plates 3 and 7) and indicated a depth of penetration of 2 ft. At higher moisture contents, the pattern of oscillations was less well defined and the following depths of penetration were suggested:

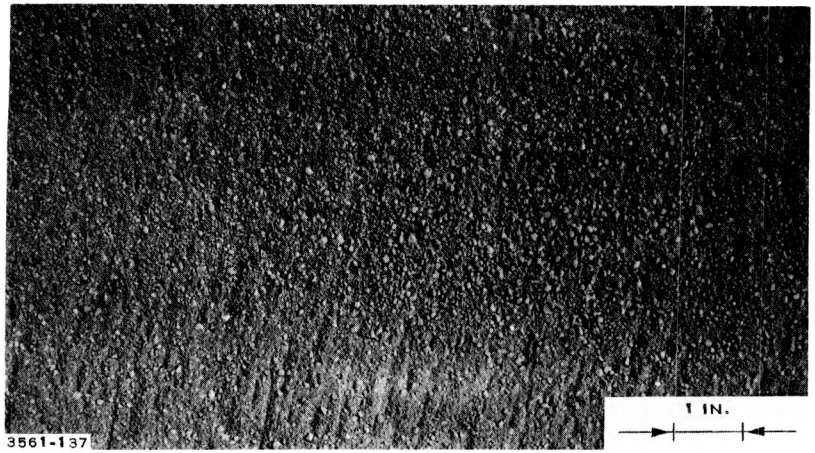

a. Moisture content 9.7%

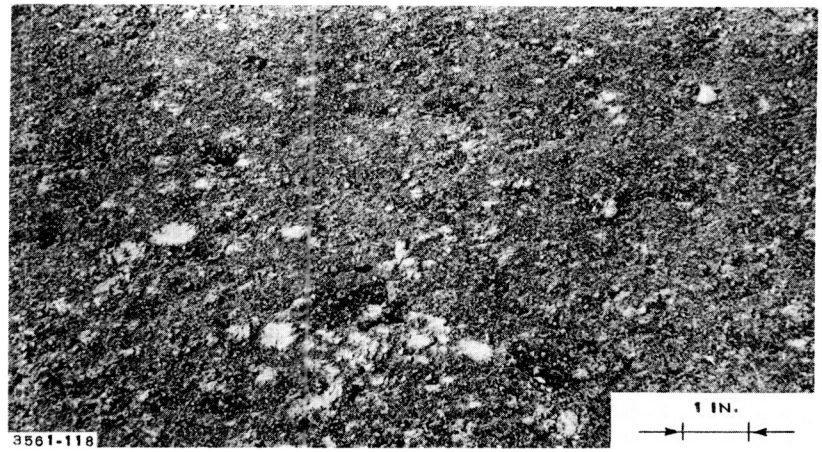

b. Moisture content 20.8%

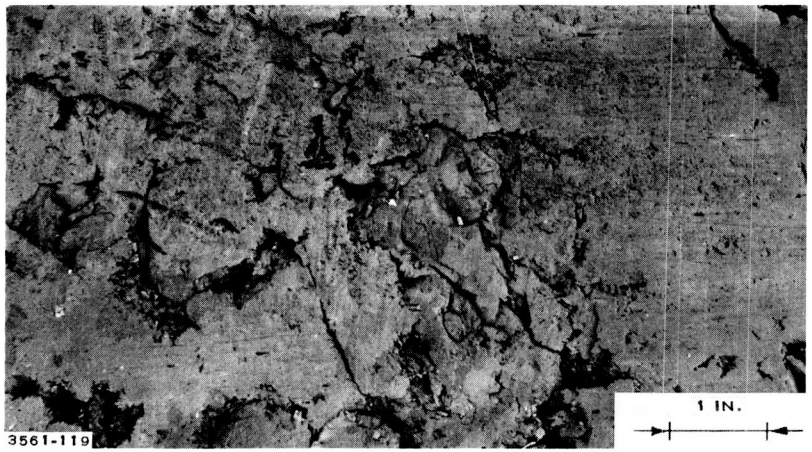

c. Moisture content 36.5%

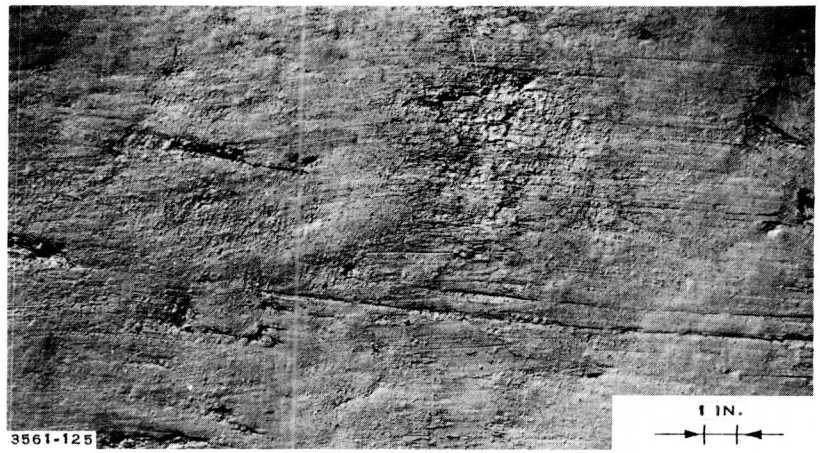

d. Moisture content 51.4%

Fig. 13. Sharkey clay at four moisture contents

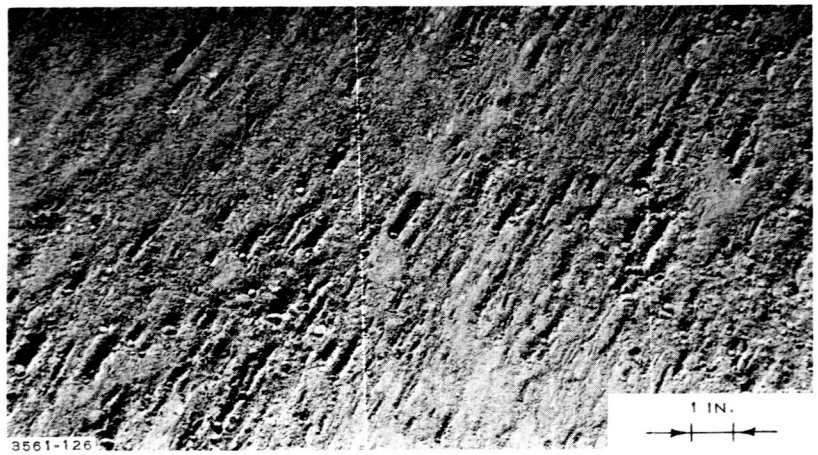

a. Moisture content 8.3%

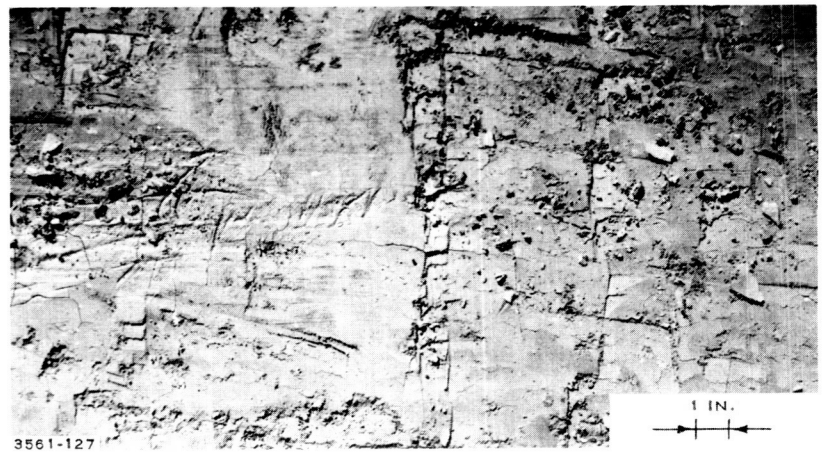

b. Moisture content 24.1%

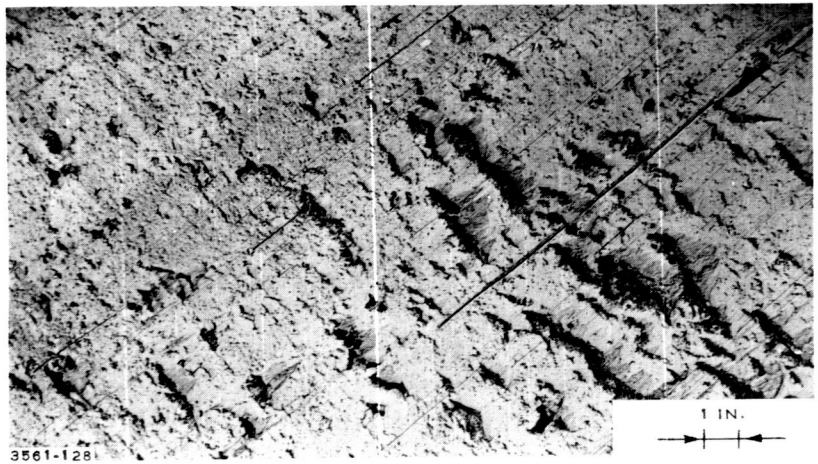

c. Moisture content 27.9%

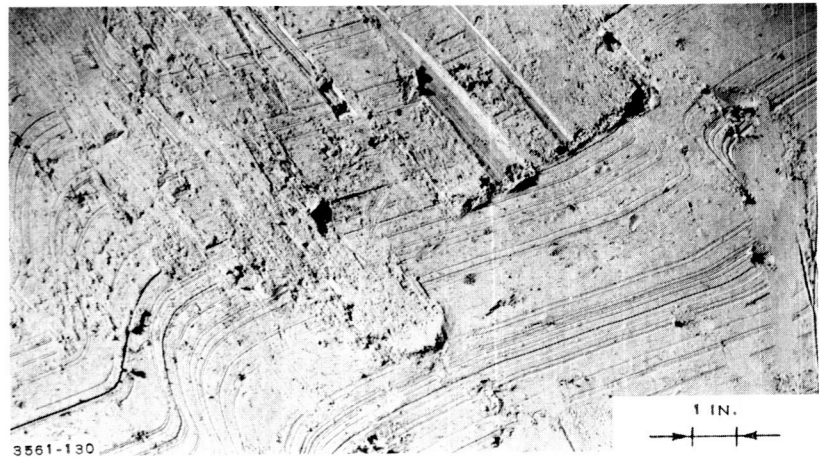

d. Moisture content 35.8%

Fig. 14. Richfield silt loam at four moisture contents

Sharkey Clay		Richfield Silt Loam	
Moisture Content %	Depth of Penetration in.	Moisture Content %	Depth of Penetration in.
20.8	12-24	24.1	24
36.5	8	27.9	10
51.4	8	35.8	8

It should be emphasized that the power measured by the radar receiver was in terms of relative power and was expressed in db; therefore, variations that appear to be only minor were actually produced by rather large changes in the quantity of radar energy being reflected from the sample. For example, an increase of 3 db means that the return power, when expressed in watts, had doubled. Penetration tests conducted using C-, X-, and Ka-band frequencies (plates 4-6, 8-10) resulted in distinct fluctuations in the relative quantities of power received as the depth of the soil material overlying the metal plate was reduced, but no well-defined pattern of oscillations compatible with the wavelength to be expected in soils for these frequencies could be established. This probably can be attributed to the relatively short wavelengths of C-, X-, and Ka-bands.

56. Consider the pattern of oscillations produced by P-band in the Sharkey clay sample having a moisture content of 9.7 percent. Plate 3a indicates that there were approximately four oscillations produced at this frequency (297 megacycles/sec) for the depth range of 0 to 2 ft. The number of oscillations is roughly proportional to frequency, and therefore for C-band (5870 megacycles/sec), X-band (9375 megacycles/sec), and Ka-band (34,543 megacycles/sec) frequencies, a total of approximately 78, 126, and 465 oscillations, respectively, would appear for the same change in depth if penetration were achieved. With so many oscillations present, measurements made at 1/2-in. increments of sample depth would not produce enough data points to define the pattern.

57. Assuming at least four data points per cycle for good definition of the pattern, the sample would have had to be cut in layers as thin as 0.1 in. or less to define the pattern of oscillations for C-band,

and even less than this for X- and Ka-bands. For wet samples, the number of cycles would be further increased, requiring the removal of even thinner layers. Cutting such thin layers of soil was found to be impracticable because of the rough, uneven surfaces that often resulted (fig. 13). Deviations in elevation of points on the soil surface in excess of 0.1 wavelength cause serious fluctuations in the return energy and are most pronounced when short wavelengths such as those at C-, X-, and Ka-band frequencies are used. Greater deviations probably would obscure any pattern of oscillation that might be present. In actual testing, deviations as large as 0.3 wavelength for C band, 0.5 wavelength for X band, and 2 wavelengths for Ka band were not uncommon. Therefore, data from the C-, X-, and Ka-band depth-of-penetration tests were considered inadequate for determining the depth of penetration actually achieved.

58. Perlite. Results of tests using air-dry perlite (fig. 15) at various densities are shown in plates 11-14. Plate 11 shows the radar return pattern achieved by P-band frequencies in perlite having densities of 10, 20, 30, and 40 pcf. Cyclic patterns are present on all four samples, which indicates that P-band frequencies can penetrate at least 2 ft of perlite at any of the four densities tested. Analysis of the data from these samples showed that the subsurface metal-plate reflection was larger at all depths than was the surface reflection. Plates 12-14 present the results of the C-, X-, and Ka-band tests on the perlite samples.

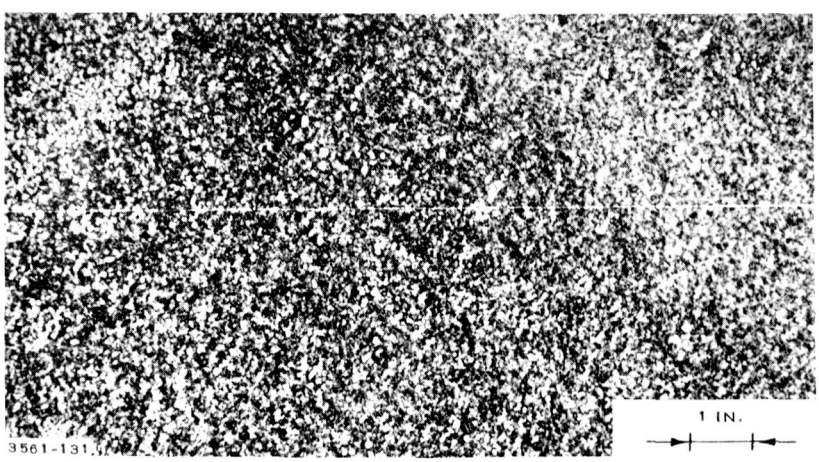

Fig. 15. Perlite

Fluctuation in the return signal was noted as the sample thickness was decreased, but no pattern of oscillation compatible with the wavelengths to be expected could be defined. The data from tests using the C-, X-, and Ka-bands must therefore be considered inadequate to determine penetration to the metal plate on the basis of a cyclic pattern.

59. The unusually high return power when the depth to the metal plate was small indicates another manner by which penetration of radar waves can be determined. Inspection of the radar return phasor diagram (fig. 10, page 25) shows that if, as normally is the case, the subsurface (metal plate) return is smaller than the surface return, the subsurface vector rotates around the surface vector. The average of measurements under this condition would be the magnitude of the surface return. In the case of perlite, the subsurface return appears larger than the surface return, and for shallow depths, a straight line drawn through the test points gives the magnitude of the subsurface metal-plate return at any depth. As an example, consider the X-band test in plate 13a for perlite at a dry density of 10 pcf. The data obtained when the sample depth ranged from 0 to approximately 19 in. show an unusually high return that decreases with increasing depth. The return from 19 to 24 in. depths fluctuates, but the average return is of the correct magnitude for a surface reflection from the sample as indicated by the low relative dielectric constant measured with the P-band system cyclic pattern. It is therefore assumed that the 19-in. depth is the point where the surface and the subsurface returns are equal. The perlite penetration results in the tabulation below show the maximum depths of perlite at which the subsurface metal-plate reflection is considered to be larger than the surface reflection. At lesser depths, the subsurface metal-plate reflection is larger than the surface reflection.

Radar Band	Depth to Which the Subsurface Return is Larger than the Surface Return, in.			
	Density 10 pcf	Density 20 pcf	Density 30 pcf	Density 40 pcf
P	24*	24*	24*	24*
C	24*	24*	24*	20
X	19	18	15	10
Ka	7	2	2	1

* Maximum depth of sample.

60. Putnam silt loam overlying Putnam clay. Results of tests conducted using Putnam silt loam (fig. 16) overlying Putnam clay are shown in plates 15 and 16. The data in plate 15 were obtained with the silt at 7 percent moisture content, and the data in plate 16 with the silt at 35.7 percent moisture content. The clay was at the same moisture content (45.5 percent) for both sets of tests. Plates 15a and 16a show the penetration achieved by P-band frequencies for these samples. The test data from the 7 percent moisture content silt loam sample show a well-defined cyclic pattern which indicates that the waves penetrated the entire 11.5 in. of silt loam and were strongly reflected by the silt loam-clay

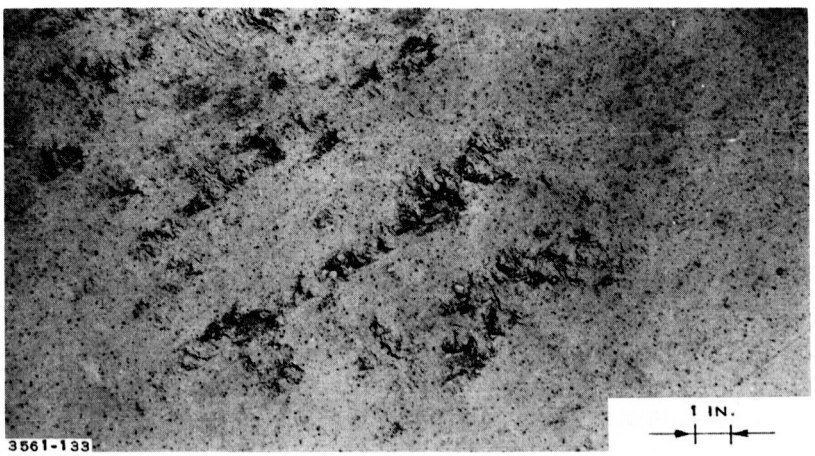

a. Moisture content 7%

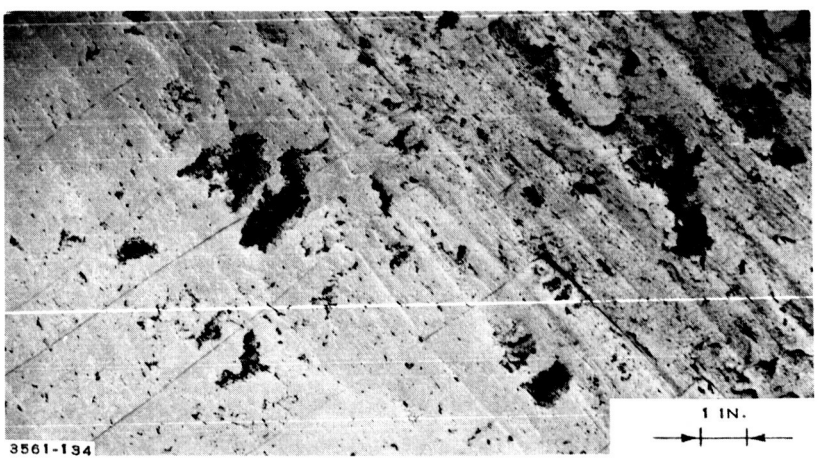

b. Moisture content 35.7%

Fig. 16. Putnam silt loam at two moisture contents

interface. The data from the 35.7 percent moisture content silt loam sample do not show a well-defined cyclic pattern, probably because there is little difference in the dielectric constants of the wet silt and wet clay (see table 2). The P-band energy probably penetrated the wet silt to the clay-silt interface, but the reflection from this interface was not great enough to produce a good cyclic pattern. P-band results show a penetration of about 1 ft through the Putnam clay.

61. The remainder of the data in plates 15 and 16 represents the results of C-, X-, and Ka-band tests. Fluctuations in the return signal were noted as the sample thickness was decreased, and in plate 15 the C-, X-, and Ka-band data show a definite increase at the silt-clay boundary, but no pattern of oscillation could be defined compatible with the wavelengths to be expected. Therefore, the results of C-, X-, and Ka-band tests must be considered inadequate to determine penetration.

Determination of soil parameters

62. Using the methods described in paragraph 51, the data obtained from the depth-of-penetration tests were examined for correlations between the moisture content of soils, or dry density in the case of perlite, and certain electrical properties of these materials. These electrical properties, apparent relative dielectric constant and conductivity, are summarized in table 2. Plots of apparent relative dielectric constant versus moisture content for soils and apparent relative dielectric constant versus density for perlite are shown in plates 17-19. Plate 20 shows conductivity versus moisture content or density for the P-band depth-of-penetration tests.

63. The apparent relative dielectric constant values calculated from the Ka-, X-, and C-band data were obtained from the analysis of surface power reflection at normal incidence and are representative of only a relatively thin surface layer. Prior to the time a sample was tested, the sample surface was exposed to the weather for a few minutes while the test equipment was assembled; therefore, the results may have been influenced by surface drying and temperature fluctuations. Minor variations in surface roughness also caused fluctuations in the results at Ka-, X-, and C-band frequencies.

64. Electrical properties calculated from the P-band data represent the average properties of the sample mass since the calculations were based on the cyclic pattern from a depth-of-penetration test. The cyclic pattern is not as sensitive to variations in the surface conditions as the surface power reflection. The moisture content and density measurements also represent average internal conditions of the sample mass; therefore, the best correlations can be expected with the P-band frequency data.

65. Changes in apparent relative dielectric constant and conductivity are primarily due to the amount of water in the soil, and these two electrical properties increase with increasing moisture content for all frequencies (plates 17, 18, and 20a and b). The apparent relative dielectric constant for each value of soil moisture content is not the same at all frequencies. Some frequency dependence has been noted for the relative dielectric constant of water,[7] and values obtained at frequencies above 15 to 20 kilomegacycles/sec have been found to be less than half those at frequencies less than 1 kilomegacycle/sec. In all of the 11 soil samples, the apparent relative dielectric constant measured for the Ka-band is less than that measured for P-band, and in 9 of these samples the values for the C- and X-bands fall between those for the Ka- and P-bands.

66. The apparent relative dielectric constant and conductivity increase with increasing dry density of perlite (plates 19 and 20c). The P-band values for apparent relative dielectric constant range from 1.29 to 2.34 for a dry density range of 10 to 40 pcf and the C-, X-, and Ka-band values are in general agreement with these values.

67. The relation between the relative dielectric constant as obtained from P-band depth-of-penetration test data and soil moisture content in pounds per cubic foot is shown in plate 21. Data for Sharkey clay and Richfield silt loam from the tests reported herein and for Yuma sand from a previous study[2] are included on the plot. The data indicate that the dielectric constant of the soil depends only on the quantity of water, and the effect of the soil type is minor. The curve starts at approximately 1 on the ordinate (the relative dielectric constant for

free space) at zero moisture content and rises toward 81 (the relative dielectric constant for water). This dielectric constant-moisture content correlation may provide an important relation for remote terrain investigations.

Vegetation samples

68. Faired signature curves from tests on the stand of wheat at three stages of growth are shown in plates 22 and 23. The appearance of the wheat at these stages of growth is shown in fig. 17. The general

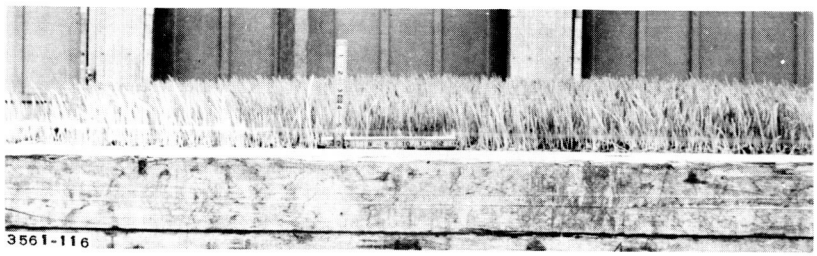

a. Wheat, 3-1/2 in. high, 20 Nov 64

b. Wheat, 14 in. high, 22 Mar 65

c. Wheat, 29 in. high, 20 Apr 65

Fig. 17. Wheat stand at three ages

patterns revealed are similar for all radar bands tested. At a 0-deg angle of incidence, the reflection was less for the wheat-covered samples than for corresponding bare samples; but at a degree of incidence greater than 10 to 20 deg, the normalized echo area of the bare soil was less than for the stand of wheat. The normalized echo area from the wheat-covered samples dropped abruptly during the first 15 deg of antenna movement from vertical. The drop was greater when the wheat was short than when it was tall. The normalized echo area then stabilized at a relatively constant value as the antenna moved from 15 to 60 deg. The fluctuation around an average in the region of 15- to 60-deg angle of incidence was about $\pm$ 10 db.

69. From plate 23 it can be seen that the P-band normalized echo area values do not fluctuate with changes in vegetation height as much as do the Ka-, X-, and C-band normalized echo area values. This suggests that the Ka-, X-, and C-band results could be used to measure vegetation parameters (height, thickness, moisture content, etc.) and that P-band frequencies may still be used for soil interrogation either directly or with simple correction factors.

PART V: DISCUSSION OF VARIOUS RADAR SYSTEMS FOR DEPTH MEASUREMENT

70. The time delay between reflections from layered media at vertical incidence can be used to determine depth of layers if an estimate of wave velocity in the material (i.e. the relative dielectric constant) is available. The necessary reflections are present for a single-frequency radar system of the type used to obtain data in this study, but the depth cannot be calculated directly because the time delay between the various reflections cannot be measured. Three systems which may give satisfactory results are: (a) a monopulse radar system, (b) an FM radar system, and (c) a variable-frequency radar system.

Monopulse Radar System

71. The monopulse system is the simplest to operate. A single pulse of electromagnetic energy with a very short pulse width is transmitted. The surface radar reflection is the first to return, and the subsurface reflection is delayed because of the longer distance traveled. The time delay between the two reflections is measured, and the depth is calculated using the relative dielectric constant. A monopulse-type system has been used successfully to measure ice thickness.[8]

FM Radar System

72. In an FM radar system, a long pulse of constant-amplitude is transmitted. The pulse is linearly frequency-modulated from an initial frequency f_1 at the beginning of the pulse to a final frequency f_2 at the end. The radar return, sampled at one instant in time, is made up of individual frequencies of various amplitudes. The frequency difference between the surface and subsurface reflections returning to the receiver can be interpreted as time delay and converted to a measure of depth. The amplitudes at each frequency can be used as a base for estimates of relative dielectric constant values.

Variable-Frequency Radar System

73. A variable-frequency radar system probably would give good results with relatively simple radar equipment. The system would consist of an ordinary radar receiver and a transmitter with a variable-frequency output. This system could operate with either a pulsed or a continuous wave transmitter output. The speed of the frequency variation is not critical, but must be slow enough so that the frequencies of the returns from the surface and the subsurface layers are essentially the same. In operation, the transmitter and receiver are positioned at vertical incidence to the soil, and the frequency is varied from lowest to highest. The return received will decrease with frequency to a minimum, increase to a maximum, and then repeat the cycle over and over. The only measurement required is the frequency difference between either two adjacent maximums or two adjacent minimums. A block diagram of the variable-frequency radar system is shown in fig. 18 and the derivation of the depth-determination formula is shown below. For the geometry

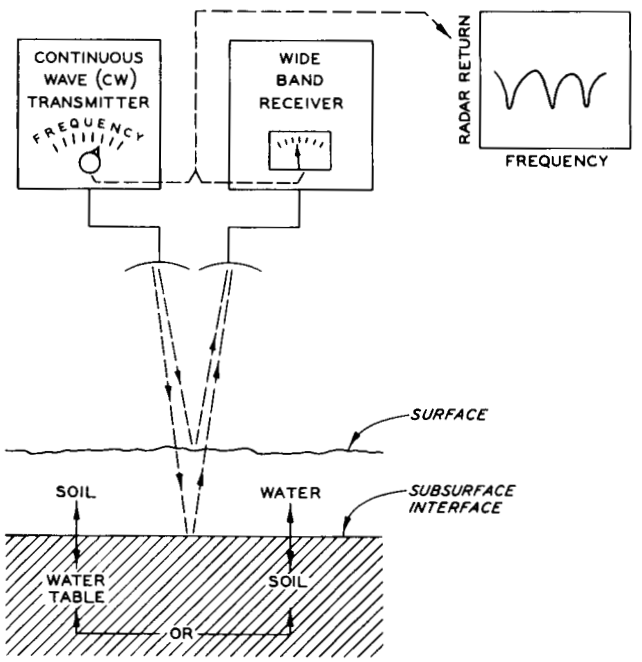

Fig. 18. Variable-frequency radar system block diagram

shown in fig. 19, the return to the receiver will be a minimum. The

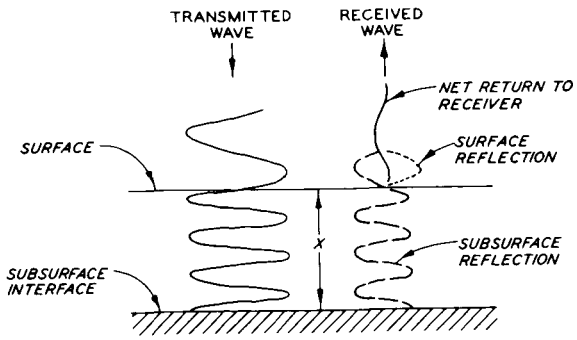

Fig. 19. Wave phase change in soils

phase shift between the surface and subsurface reflections is given by:

$$\phi = \frac{2x}{\lambda}(2\pi) = \frac{4\pi x}{\lambda} \tag{26}$$

and

$$\lambda = \frac{c}{\sqrt{\epsilon_r}}\left(\frac{1}{f}\right) = \frac{c}{\sqrt{\epsilon_r}\, f} \tag{27}$$

where

ϕ = phase shift, radian
x = depth of the medium, m
λ = wavelength of wave in the medium, m
c = speed of light, 300×10^6 m per sec
ϵ_r = relative dielectric constant
f = frequency of radar wave, cps

The term $\frac{c}{\sqrt{\epsilon_r}}$ gives the speed of an electromagnetic wave in a medium with the conductivity term neglected (the conductivity term has little effect on wave velocity at frequencies above 200 megacycles/sec for the samples thus far tested). From equations 26 and 27

$$\phi = \frac{4\pi x f \sqrt{\epsilon_r}}{c} \tag{28}$$

For a minimum, ϕ must be some odd multiple of π such as π, 3π, 5π, etc. This can be shown by $\phi = 2\pi n - \pi$, where n is an integer. There will be two adjacent minimums as the frequency is increased from f_1 to f_2 when n is increased by one unit.

$$\phi_1 = 2\pi n - \pi = \frac{(4\pi x)\left(\sqrt{\epsilon_r}\right)(f_1)}{c} \tag{29}$$

$$\phi_2 = 2\pi(n + 1) - \pi = \frac{(4\pi x)\left(\sqrt{\epsilon_r}\right)(f_2)}{c} \tag{30}$$

Subtracting equation 29 from equation 30 yields

$$\phi_2 - \phi_1 = 2\pi = \frac{(4\pi x)\sqrt{\epsilon_r}\,(f_2 - f_1)}{c} \tag{31}$$

or

$$x = \frac{1}{2\sqrt{\epsilon_r}}\left(\frac{300 \times 10^6}{f_2 - f_1}\right) \tag{32}$$

This derivation is good for either a pair of minimums at f_1 and f_2 or a pair of maximums at f_1 and f_2 because only the frequency difference is used in the calculation for depth. From the formula, the only other variable besides the frequencies is that of relative dielectric constant ϵ_r. The relative dielectric constant can be calculated from the average power reflectance of this variable-frequency radar system. From the limited number of studies conducted, the relative dielectric constant of soils appears to vary between 3 and 50. If, for purposes of illustration, it is assumed that (a) the dielectric constant is 9, (b) f_1 is 300 megacycles/sec, and (c) f_2 is 350 megacycles/sec, the predicted depth to a subsurface discontinuity from equation 32 would be 1 m. If f_1 were 300 megacycles/sec and f_2 305 megacycles/sec, for the same dielectric constant the indicated depth would be 10 m.

74. An advantage of a system of this type is that no calibration of the radar system is needed if the relative dielectric constant of the medium being tested is known. All measurements are relative. The accuracy of such a system would depend mainly on the ability to measure the transmitter frequencies.

PART VI: CONCLUSIONS AND RECOMMENDATIONS

Conclusions

75. The following conclusions are based on the data from the tests reported and the measurement techniques described herein:

a. Standard pulsed radar systems such as those used in this study are amplitude-sensitive only, and an individual return signal obtained using this type of system cannot be separated into the components resulting from surface and subsurface reflections. Therefore, this type of radar system cannot be used directly to detect the presence of a subsurface interface or to measure the depth of layered materials. (Paragraph 43.)

b. Radar sensors, including standard pulsed radar sensors, provide information that can be used to calculate electrical properties of soil (paragraphs 45-51). Since correlations exist between the electrical properties of soil and soil moisture content (paragraphs 62-67), radar sensors are capable of providing information upon which to base estimates of soil moisture content.

c. Long wavelength radar waves (P-band) will reflect from a subsurface soil-metal interface. This indicates that it is feasible to measure depths of layered materials with a specially designed radar system operating at P-band frequencies (225 to 390 megacycles/sec). (Paragraphs 55-60.)

d. Insufficient data were produced by this program to show whether short wavelength radar waves (C-band or shorter) are as effective as long wavelength radar waves (P-band) for measuring the depth of layered materials. (Paragraphs 55-61.)

e. Radar signatures of a silt soil determined from Ka-, X-, and C-bands are more significantly altered by vegetation at various stages of growth than are P-band signatures for all angles of incidence. This suggests that short wavelength radar could be used to measure vegetation parameters (type, weight, density, moisture content, etc.) and that long wavelength radar could be used to investigate the soil beneath the vegetation either directly or with simple correction factors. (Paragraphs 68 and 69.)

Recommendations

76. Based on the findings of this study, it is recommended that:

a. Comprehensive tests be initiated to determine the basic electrical properties of soils at high radio frequencies and to establish correlations between these properties and soil moisture contents.

b. Field tests be conducted to determine if a variable-frequency radar set (such as that described in paragraphs 73-74) can detect and measure depths of layered materials, such as the depth to groundwater, depth of surface water, or ice thickness.

c. Tests be conducted to determine how much radar energy at various frequencies can penetrate vegetation of various types, heights, densities, and moisture contents and convey soil information.

LITERATURE CITED

1. U. S. Army Engineer Waterways Experiment Station, CE, Terrain Analysis by Electromagnetic Means; Laboratory Investigations in the 0.76- to 5.00-Micron Spectral Region, by B. R. Davis, E. B. Lipscomb, and S. J. Knight. Technical Report No. 3-693, Report 1, Vicksburg, Miss., October 1965.

2. _____, Feasibility Study of the Use of Radar to Detect Surface and Ground Water, by B. R. Davis, J. R. Lundien, and A. N. Williamson, Jr. Technical Report No. 3-727, Vicksburg, Miss., April 1966.

3. Cosgriff, R. L., Peake, W. H., and Taylor, R. C., Electromagnetic Reflection Properties of Natural Surfaces with Applications to Design of Radars and Other Sensors. Ohio State University Research Foundation, Department of Electrical Engineering, Report 694-9, Air Force Contract No. 33(616)3649, Task No. 41136, Columbus, Ohio, February 1959.

4. Von Hippel, A., Dielectrics and Waves. John Wiley and Sons, Inc., New York, N. Y., 1954.

5. Jordan, Edward C., Electromagnetic Waves and Radiating Systems. Prentice-Hall, Inc., Englewood Cliffs, N. J., 1950.

6. Beckmann, Petr, and Spizzichino, André, The Scattering of Electromagnetic Waves from Rough Surfaces. The McMillan Company, New York, N. Y., 1963, vol 4.

7. Dorsey, Noah Ernest, Properties of Ordinary Water-Substance in All Its Phases; Water-Vapor, Water, and All the Ices. Reinhold Publishing Corporation, New York, N. Y., 1940.

8. Barringer Research Limited, Scientific Reports No. 4 and 5, Contract No. AF 19(628)-2998, 145 Belfield Road, Rexdale, Ontario, Canada, dated 15 February and 15 April 1964.

9. Soil Conservation Service, U. S. Department of Agriculture, Soil Survey; Sharkey County, Mississippi. Series 1959, No. 3, February 1962. In cooperation with the Mississippi Agricultural Experiment Station.

10. _____, Soil Survey; Beaver County, Oklahoma. Series 1959, No. 11, August 1962. In cooperation with the Oklahoma Agricultural Experiment Station.

11. _____, Soil Survey; Boone County, Missouri. Series 1951, No. 12, December 1962. In cooperation with the Missouri Agricultural Experiment Station.

12. U. S. Geological Survey, Contributions to Economic Geology, 1955. Bulletin No. 1027, F-P, U. S. Government Printing Office, Washington, D. C., 1955.

Table 1

Calibration Data, P-, C-, X-, and Ka-Bands

Recorder Deflection in.	Receiver Attenuator db	Transmitter Attenuator db	Power Received dbm
		P-Band	
0.00	60.0	8.0	-42.5
0.15	60.0	7.0	-41.5
0.35	60.0	6.0	-40.5
0.55	60.0	5.0	-39.5
0.75	60.0	4.0	-38.5
1.05	60.0	3.0	-37.5
1.25	60.0	2.0	-36.5
1.45	60.0	1.0	-35.5
1.65	50.0	10.0	-34.5
1.85	50.0	9.0	-33.5
1.95	50.0	8.0	-32.5
2.20	50.0	7.0	-31.5
2.45	50.0	6.0	-30.5
2.60	50.0	5.0	-29.5
2.80	50.0	4.0	-28.5
3.00	50.0	3.0	-27.5
3.10	50.0	2.0	-26.5
3.35	50.0	1.0	-25.5
3.65	40.0	10.0	-24.5
3.85	40.0	9.0	-23.5
4.05	40.0	8.0	-22.5
4.20	40.0	7.0	-21.5
4.40	40.0	6.0	-20.5
4.55	40.0	5.0	-19.5
4.75	40.0	4.0	-18.5
4.95	40.0	3.0	-17.5
5.00	40.0	2.0	-16.5
5.15	40.0	1.0	-15.5
5.40	30.0	10.0	-14.5
5.55	30.0	9.0	-13.5
5.65	30.0	8.0	-12.5
5.85	30.0	7.0	-11.5
6.00	30.0	6.0	-10.5
6.10	30.0	5.0	-9.5
6.25	30.0	4.0	-8.5
6.40	30.0	3.0	-7.5
6.42	30.0	2.0	-6.5
6.52	30.0	1.0	-5.5
6.70	20.0	10.0	-4.5
6.75	20.0	9.0	-3.5
6.75	20.0	8.0	-2.5
6.75	20.0	7.0	-1.5
		C-Band	
0.00	36.2	36.0	-47.4
0.75	34.0	36.0	-45.2
1.40	34.0	33.7	-42.9
1.95	31.8	33.7	-40.7
2.40	31.8	31.4	-38.4
2.82	29.5	31.4	-36.1
3.22	29.5	29.2	-33.9
3.61	27.4	29.2	-31.8
3.95	27.4	27.1	-29.7
4.32	25.2	27.1	-27.5
4.62	25.2	25.1	-25.5
4.89	23.6	25.1	-23.9
5.14	23.6	23.2	-22.0
5.42	21.8	23.2	-20.2
5.65	21.8	21.4	-18.4
5.88	20.0	21.4	-16.6
6.08	20.0	19.7	-14.9
6.28	18.3	19.7	-13.2
6.44	18.3	18.0	-11.5
6.58	16.6	18.0	-9.8
6.70	16.6	16.3	-8.1
6.75	15.0	16.3	-6.5
6.78	15.0	14.8	-5.0
6.79	13.6	14.8	-3.6
6.80	13.6	13.3	-2.1
		X-Band	
0.00	42.4	41.8	-29.6
0.15	39.7	41.8	-26.9
0.70	39.7	39.2	-24.3
1.25	37.2	39.2	-21.8
1.85	37.2	36.6	-19.2
2.35	34.8	36.6	-16.8
2.90	34.8	34.2	-14.4
3.44	32.4	34.2	-12.0
3.99	32.4	31.9	-9.7
4.45	30.1	31.9	-7.4
4.90	30.1	29.6	-5.1
5.34	27.8	29.6	-2.8
5.73	27.8	27.4	-0.6
6.04	25.6	27.4	+1.6
6.30	25.6	25.2	+3.8
6.51	23.4	25.2	+6.0
6.64	23.4	23.2	+8.0
6.70	21.3	23.2	+10.1
6.75	21.3	21.2	+12.1
6.78	19.3	21.2	+14.1
6.80	19.3	19.2	+16.1
		Ka-Band	
0.00	36.3	32.3	-18.6
0.35	34.4	32.3	-16.7
0.50	34.4	30.7	-15.1
0.82	32.6	30.7	-13.3
1.10	32.6	29.1	-11.7
1.45	30.8	29.1	-9.9
1.75	30.8	27.6	-8.4
2.12	29.0	27.6	-6.6
2.45	29.0	26.0	-5.0
2.84	27.2	26.0	-3.2
3.17	27.2	24.0	-1.2
3.55	25.0	24.0	+1.0
3.90	25.0	22.8	+2.2
4.25	23.7	22.8	+3.5
4.60	23.7	21.2	+5.1
4.96	22.0	21.2	+6.8
5.31	22.0	19.6	+8.4
5.69	20.2	19.6	+10.2
6.00	20.2	18.0	+11.8
6.35	18.4	18.0	+13.6
6.57	18.4	16.3	+15.3
6.70	16.6	16.3	+17.1
6.75	16.6	14.6	+18.8
6.76	15.4	14.6	+20.0

Table 2

Electrical Properties of Soils and Perlite

Soil	Moisture Content %	Dry Density pcf	Radar Band	Test Results: Power Reflectance db	Apparent Relative Dielectric Constant	Wavelength in Soil in.	Attenuation Phase Constant Factor α m^{-1}	Attenuation Phase Constant Factor β m^{-1}	Relative Dielectric Constant	Conductivity mhos/m
Sharkey clay	9.7	75.8	Ka	-19.6	1.52	--	--	--	--	--
			X	-9.7	3.89	--	--	--	--	--
			C	-12.7	2.57	--	--	--	--	--
			P	--	9.08	13.2	2.19	18.70	8.76	0.0350
	20.8	82.5	Ka	-16.4	1.85	--	--	--	--	--
			X	-6.7	7.38	--	--	--	--	--
			C	-9.2	4.26	--	--	--	--	--
			P	--	12.60	11.2	4.45	22.10	12.10	0.0840
	36.5	82.5	Ka	-6.1	8.81	--	--	--	--	--
			X	-5.2	11.90	--	--	--	--	--
			C	-5.7	9.97	--	--	--	--	--
			P	--	36.40	6.6	4.48	37.50	36.00	0.1440
	51.4	68.1	Ka	-9.1	4.33	--	--	--	--	--
			X	-4.7	14.30	--	--	--	--	--
			C	-4.7	14.30	--	--	--	--	--
			P	--	44.00	6.0	4.81	41.20	43.90	0.1730
Richfield silt loam	8.3	76.7	Ka	-14.1	2.22	--	--	--	--	--
			X	-10.5	3.43	--	--	--	--	--
			C	-12.2	2.72	--	--	--	--	--
			P	--	7.03	15.0	2.99	16.50	6.78	0.0420
	24.1	92.9	Ka	-9.1	4.33	--	--	--	--	--
			X	-6.7	7.38	--	--	--	--	--
			C	-5.2	11.90	--	--	--	--	--
			P	--	24.70	8.0	4.49	30.90	24.20	0.1180
	27.9	92.1	Ka	-6.1	8.81	--	--	--	--	--
			X	-4.7	14.30	--	--	--	--	--
			C	-3.2	30.20	--	--	--	--	--
			P	--	28.10	7.5	4.62	33.00	27.60	0.1300
	35.8	81.8	Ka	-5.1	12.30	--	--	--	--	--
			X	-2.9	36.50	--	--	--	--	--
			C	-2.9	36.50	--	--	--	--	--
			P	--	41.20	6.2	4.43	38.80	38.50	0.1470
Putnam silt loam*	7.0	70.3	Ka	-16.3	1.85	--	--	--	--	--
			X	-9.7	3.89	--	--	--	--	--
			C	-9.5	4.03	--	--	--	--	--
			P	--	5.08	17.6	--	14.00	--	--
	35.7	79.9	Ka	-7.9	5.52	--	--	--	--	--
			X	-5.7	9.97	--	--	--	--	--
			C	-3.5	25.30	--	--	--	--	--
			P	--	41.10	6.2	--	39.80	--	--
Putnam clay	45.5	73.3	Ka	-6.9	7.02	--	--	--	--	--
			X	-3.7	22.60	--	--	--	--	--
			C	-2.5	49.00	--	--	--	--	--
			P	--	32.30	7.0	--	35.30	--	--
Perlite	0.0	10.0	Ka	-21.9	1.38	--	--	--	--	--
			X	-18.7**	1.59	--	--	--	--	--
			C	-5.0	NA†	--	--	--	--	--
			P	--	1.29	35.0	0.26	7.07	1.29	0.0016
	0.0	20.0	Ka	-19.9	1.50	--	--	--	--	--
			X	-12.7**	2.57	--	--	--	--	--
			C	-2.7	NA	--	--	--	--	--
			P	--	1.76	30.0	0.25	8.24	1.76	0.0017
	0.0	30.0	Ka	-16.9	1.78	--	--	--	--	--
			X	-15.7**	1.94	--	--	--	--	--
			C	-6.5	NA	--	--	--	--	--
			P	--	1.82	29.5	0.49	8.37	1.80	0.0035
	0.0	40.0	Ka	-14.9	2.07	--	--	--	--	--
			X	-14.7**	2.11	--	--	--	--	--
			C	-15.0††	2.06	--	--	--	--	--
			P	--	2.34	26.0	0.45	9.51	2.33	0.0037

* Putnam silt loam overlying Putnam clay. The depth of these samples was insufficient for analysis of the data by techniques used for the other samples. The parameters listed under P-band are therefore limited to those that could be derived by the wavelength method.

** X-band reflection from subsurface metal plate is larger than surface reflection for sample depths of approximately 1 ft or less.

† Not available. C-band reflection from subsurface metal plate is larger than surface reflection for entire cart.

†† C-band reflection from subsurface metal plate is larger than surface reflection for sample depths of approximately 20 in. or less.

Table 3

Depth-of-Penetration Data

Sharkey Clay

Soil Depth, in.	Normalized Echo Area, db Ka-Band	X-Band	C-Band	P-Band	Soil Depth, in.	Normalized Echo Area, db Ka-Band	X-Band	C-Band	P-Band	Soil Depth, in.	Normalized Echo Area, db Ka-Band	X-Band	C-Band	P-Band	Soil Depth, in.	Normalized Echo Area, db Ka-Band	X-Band	C-Band	P-Band
	Moisture Content 9.7 Percent				Moisture Content 20.8 Percent					Moisture Content 36.5 Percent					Moisture Content 51.4 Percent				
24-3/4	9.8	11.6	10.2	-6.5	24	-12.7	6.4	9.2	-3.7	23-1/2	21.5	14.8	20.2	-0.9	24	17.8	11.1	17.0	-0.6
24	0.3	10.9	10.6	-7.4	23-1/2	-4.4	11.4	13.5	-3.3	23	24.1	15.8	18.6	-1.2	23-1/2	13.5	14.6	20.5	-0.4
23-3/8	7.2	7.2	9.5	-6.6	23	-7.9	10.4	16.6	-4.0	22-1/2	19.7	12.0	19.0	-1.5	23	11.0	12.2	18.3	-0.5
23	-8.8	11.0	9.6	-6.8	22-1/2	-6.5	15.4	18.0	-3.4	22	14.5	16.4	23.3	0.0	22-1/2	-3.8	13.5	13.1	-1.3
22-1/2	-3.8	7.6	7.4	-6.5	22	-14.8	10.2	15.6	-2.9	21-1/2	22.8	13.2	25.5	-0.3	22	-0.6	11.8	14.2	-0.8
22	-6.2	8.5	7.6	-5.5	21-3/8	-22.7	4.8	11.7	-2.8	21	17.6	20.4	20.6	-1.6	21-1/2	-0.7	14.5	16.9	-0.8
21-1/2	12.1	12.9	6.2	-7.1	20-7/8	-10.7	13.7	15.1	-3.1	20-1/4	11.2	15.4	21.5	-0.4	21	12.5	16.3	19.7	-0.7
20-3/4	5.8	10.1	11.0	-2.7	20-5/16	-40.5	15.3	15.7	-4.1	19-3/4	16.6	11.9	18.6	0.0	20-1/2	5.6	14.5	15.4	-0.4
20	3.8	11.7	10.4	-3.0	19-3/4	-37.7	15.1	15.0	-3.9	19-1/8	7.7	12.6	18.0	-0.8	19-7/8	9.9	14.2	17.4	0.0
19-1/2	-2.5	8.8	9.2	-3.0	19-1/4	-6.1	15.5	17.2	-4.6	18-1/2	22.2	15.0	23.3	-0.9	19-3/8	10.1	13.1	12.1	0.0
19	1.0	7.9	8.4	-3.9	18-3/4	-5.5	14.1	7.7	-4.6	18	14.9	7.2	16.8	-0.4	18-3/4	14.9	15.7	21.8	0.3
18-1/2	6.4	11.7	10.9	-3.4	18-1/4	-15.5	10.9	13.6	-5.8	17-1/4	18.1	2.0	20.2	-0.3	18-1/4	10.7	15.3	17.3	-0.6
18	-6.1	10.7	10.2	-4.2	17-1/2	-9.1	15.3	17.2	-5.8	16-3/4	21.9	13.6	16.2	-0.3	17-7/8	5.9	12.0	19.4	-2.0
17-1/4	-0.9	8.0	10.1	-5.0	17	-5.5	14.1	14.7	-5.7	16-1/8	3.2	13.7	17.3	-0.5	17-1/4	7.6	17.3	19.3	-1.4
16-3/4	-4.0	9.6	10.5	-6.7	16-1/2	-15.9	12.8	11.4	-6.0	15-3/4	7.7	11.0	17.7	-2.5	16-7/8	16.5	17.7	22.6	-0.7
16-1/4	-8.3	9.2	8.2	-7.8	15-7/8	-30.2	9.8	11.6	-5.1	15	16.7	10.9	17.7	-1.2	16-1/4	-0.7	15.3	23.0	-0.5
15-3/4	4.3	9.4	9.8	-8.3	15-1/4	-19.4	13.7	14.3	-4.9	14-1/2	16.0	11.7	14.6	-1.9	15-5/8	0.8	16.2	18.5	-1.4
15	5.5	9.1	10.0	-5.9	14-3/4	-3.8	12.6	16.4	-4.7	14	20.9	15.2	17.0	-2.2	15	6.1	12.5	20.8	-0.1
14-1/2	-8.0	8.1	13.5	-4.9	14-1/4	-1.8	9.6	13.6	-5.3	13-1/2	13.2	16.8	21.9	-1.5	14-1/2	14.5	16.6	20.0	-0.4
14	-19.5	10.1	14.3	-2.5	13-3/4	4.0	11.9	14.2	-5.6	13	11.7	12.0	19.8	-0.2	14	-1.3	7.4	18.1	-1.0
13-1/2	-1.1	10.2	14.7	-2.2	13-1/4	-0.5	9.8	5.8	-5.6	12-1/2	4.2	13.3	21.8	-0.9	13-1/4	19.7	18.0	20.5	-0.8
13	-8.7	11.7	11.8	-1.7	12-3/4	-21.7	11.5	14.7	-5.0	11-3/4	13.1	15.6	17.7	-2.2	12-3/4	11.2	16.4	19.5	-1.1
12-1/2	-4.1	11.7	12.2	-1.9	12-3/8	-6.3	12.3	13.8	-4.4	11-1/4	15.4	7.9	21.4	-3.3	12	8.0	13.5	8.2	-1.1
12	-0.1	10.1	11.8	-2.1	11-7/8	-5.5	6.5	11.6	-5.6	10-3/4	10.4	16.5	18.1	-2.4	11-1/2	10.8	14.5	8.3	-1.3
11-1/2	-9.1	10.5	11.9	-2.7	11-1/2	-8.9	11.3	16.2	-5.1	10-1/8	16.2	16.9	20.3	-1.6	11	9.5	10.7	12.7	-1.7
11	-3.3	8.0	13.1	-4.1	11	-11.4	12.1	13.9	-4.6	9-1/2	19.3	13.1	18.0	-3.3	10	9.3	13.3	16.7	-1.6
10-1/4	-1.3	10.8	12.7	-6.7	10-5/8	-15.2	13.6	16.7	-4.5	8-7/8	0.3	13.5	13.1	-3.4	9-1/2	3.6	15.7	19.7	-1.6
9-5/8	5.5	11.9	13.6	-6.5	10-1/8	1.0	11.0	17.4	-5.6	8-3/8	10.5	13.3	19.1	-2.7	9	15.5	15.5	15.9	-2.1
9	-2.3	9.4	12.3	-3.9	9-1/2	-5.1	13.1	15.7	-5.6	7-3/4	5.2	15.0	16.6	-3.3	8-1/2	2.3	11.5	15.4	-2.1
8-1/2	-1.5	10.9	12.0	-1.6	9	-18.8	12.8	22.7	-6.6	7-1/4	10.4	14.3	17.5	-2.3	8	5.4	15.8	12.3	-2.6
7-7/8	-8.1	6.9	10.2	-0.5	8-1/2	-20.4	14.3	12.2	-4.9	6-3/4	12.9	15.4	17.2	-2.0	7-3/8	18.2	15.2	18.5	-0.8
7-3/8	-7.8	9.8	11.8	0.4	8	-13.9	14.8	17.4	-6.3	6-1/4	11.2	15.8	20.4	-0.4	6-3/4	11.4	17.1	20.3	0.0
6-7/8	-8.1	9.7	12.2	1.4	7-1/2	3.4	11.0	6.5	-4.6	5-3/4	6.3	15.3	20.7	-1.3	6-1/4	15.6	16.7	19.7	-0.5
6-1/4	-22.2	11.5	14.1	2.1	7	-2.5	15.5	16.0	-2.2	5	0.4	13.7	21.3	-1.0	5-3/4	6.2	10.5	8.0	0.1
5-3/4	-5.9	11.3	16.8	2.5	6-1/4	-6.8	17.0	14.6	-1.1	4-1/2	10.8	16.1	19.2	-0.9	5-1/4	13.1	14.1	20.0	0.5
4-7/8	3.5	12.4	16.8	2.8	5-3/4	-1.5	9.1	16.6	-0.6	4	4.2	15.0	17.8	0.0	4-5/8	8.3	5.5	18.1	-1.0
4-3/8	-4.0	10.6	16.1	1.7	5-1/4	-0.9	10.3	14.1	-0.6	3-1/2	20.9	17.9	20.2	1.2	4	8.4	18.6	19.8	-0.4
3-7/8	-0.1	11.5	14.2	-0.2	4-3/4	-16.2	12.9	11.6	-1.9	2-3/4	18.1	17.6	22.1	1.3	3-1/2	12.2	18.0	21.0	-0.1
3-3/8	1.7	12.2	15.2	-4.9	4-1/4	-2.6	12.9	7.2	-1.9	2-1/4	11.6	17.4	21.8	0.5	3	15.2	20.0	20.1	0.1
2-7/8	-5.6	12.9	12.3	-7.5	3-1/2	-21.8	11.3	14.6	-4.4	1-3/4	-0.6	14.7	12.1	-2.6	2-1/2	12.3	16.4	20.4	0.6
2-3/8	1.7	11.3	13.1	0.2	3	-3.4	17.1	15.6	-12.2	1	16.4	14.7	19.9	-5.1	2	15.3	19.8	23.6	-0.8
1-7/8	2.9	12.9	14.5	2.7	2-1/2	-3.1	16.4	16.4	-15.2	1/2	6.6	12.0	18.5	0.1	1-7/16	10.6	19.9	22.4	-6.7
1-1/4	5.7	9.3	13.1	3.1	2	-23.8	14.8	16.4	-1.8	Metal Plate	20.8	19.7	21.9	2.0	5/8	12.6	23.9	20.4	1.5
1/2	-5.9	4.3	17.1	3.1	1-3/4	-41.8	12.3	10.0	1.2						Metal Plate	19.1	20.0	23.4	1.5
Metal Plate	15.5	18.1	25.1	4.1	1-1/8	-9.9	8.4	-1.4	3.0										
					Metal Plate	6.4	23.2	24.2	3.2										

Table 4

Depth-of-Penetration Data

Richfield Silt Loam

Soil Depth, in.	Normalized Echo Area, db Ka-Band	X-Band	C-Band	P-Band	Soil Depth, in.	Normalized Echo Area, db Ka-Band	X-Band	C-Band	P-Band	Soil Depth, in.	Normalized Echo Area, db Ka-Band	X-Band	C-Band	P-Band	Soil Depth, in.	Normalized Echo Area, db Ka-Band	X-Band	C-Band	P-Band
	Moisture Content 8.3 Percent					Moisture Content 24.1 Percent					Moisture Content 27.9 Percent					Moisture Content 35.8 Percent			
25	2.7	1.2	8.4	-6.3	23-1/2	4.2	10.0	16.1	-1.1	25	11.1	14.8	19.5	-0.5	21-1/2	23.2	16.4	26.0	-0.2
24-3/4	-8.7	2.8	10.3	-7.0	23	16.4	12.6	13.6	-0.6	24-1/2	15.8	14.1	20.6	-0.3	20-3/4	21.3	18.4	26.2	0.1
24-1/8	2.9	3.9	13.7	-7.5	22-7/16	4.0	14.8	23.7	-0.2	24	8.6	17.3	19.6	0.0	20-1/4	16.1	15.4	24.4	-0.3
23-1/2	-0.3	2.6	11.2	-6.3	21-7/8	14.2	12.9	16.4	0.6	23-1/2	16.3	13.4	18.7	-0.6	20	19.1	15.7	24.8	0.0
23	1.9	-0.3	10.9	-5.7	21-3/8	7.9	14.4	20.2	0.7	22-7/8	16.9	18.4	25.3	-0.2	19-3/8	21.2	18.0	26.0	0.0
22-1/2	0.7	0.0	9.5	-5.5	20-3/4	9.7	12.5	15.6	0.2	22-1/4	8.9	15.8	21.5	0.2	18-3/4	13.1	17.3	24.4	0.1
21-3/4	4.8	2.8	12.2	-5.1	20-1/4	10.2	14.4	19.1	-0.8	21-3/4	16.5	14.1	21.0	0.6	18-1/4	16.3	15.6	22.6	0.0
21-1/4	1.3	-1.3	8.8	-4.7	19-7/8	-0.5	12.5	19.4	-1.5	21-1/4	9.1	14.4	22.1	0.3	17-1/2	15.4	16.1	23.8	-0.5
20-3/4	1.6	-2.2	8.7	-5.6	19-3/8	10.2	12.9	19.7	-1.2	20-3/4	11.7	15.1	22.1	0.2	17	21.9	14.5	21.9	-0.9
20-3/16	1.0	2.8	10.3	-5.3	18-3/4	11.8	8.5	18.6	-0.7	20-1/8	21.3	15.2	21.7	0.2	16-1/2	16.8	13.2	23.7	-0.9
19-9/16	0.7	-1.4	9.0	-6.9	17-7/8	4.8	3.4	20.9	-0.4	19-5/8	20.1	14.9	22.5	-0.4	16	6.9	14.5	22.8	-0.2
19-1/16	-4.7	0.4	10.2	-7.8	17-1/2	11.3	8.0	18.6	-0.5	19-1/8	15.5	13.7	22.5	0.0	15-1/2	8.5	14.7	22.2	-0.6
18-5/8	-5.3	0.6	11.0	-6.9	17-1/8	10.1	18.0	20.5	-1.2	18-1/2	17.6	16.5	21.5	-0.7	14-7/8	12.7	11.3	11.3	-0.3
18-1/16	-0.2	-0.6	9.3	-8.7	16-5/8	3.6	13.5	20.4	-0.8	18	18.9	17.7	21.2	-0.4	14-3/8	11.4	10.1	21.3	-0.2
17-1/2	1.4	2.2	10.1	-7.6	16	-1.3	9.6	20.2	-0.7	17-3/8	5.8	16.8	20.8	-0.3	13-7/8	10.8	11.7	22.7	0.1
16-3/4	3.4	-1.1	11.3	-6.2	15-1/2	1.1	12.6	17.3	-1.9	16-3/4	15.3	16.5	22.3	-0.2	13-1/4	12.7	10.8	23.4	-0.2
16-1/8	-1.0	-0.9	10.4	-6.2	14-7/8	6.3	13.3	16.2	-0.3	16-1/8	7.0	14.4	19.7	-0.4	12-7/8	14.4	13.9	22.8	-0.1
15-5/8	5.7	1.1	10.9	-5.6	14-1/4	8.0	6.7	14.7	-1.9	15-9/16	12.8	17.4	22.8	-0.6	12-1/4	15.5	10.4	17.5	-0.2
15-1/8	6.2	3.2	14.1	-5.1	13-3/4	-4.5	13.5	17.1	-1.7	15-1/8	12.4	14.9	18.3	-0.5	11-1/2	2.5	12.9	22.3	-1.2
14-1/2	6.4	-0.9	10.6	-5.0	13-1/4	14.5	13.0	17.0	-1.2	14-1/2	10.1	14.0	19.2	-1.2	11-1/8	10.5	10.8	23.4	-1.0
14	8.4	1.5	12.3	-5.0	12-3/4	7.1	12.2	19.1	-1.7	14	8.7	15.9	19.4	-1.7	10-1/2	7.9	12.5	21.5	-0.5
13-1/2	4.3	1.9	10.6	-6.5	12	5.4	8.2	19.1	-1.2	13-1/2	15.3	12.8	20.2	-1.5	10	10.6	12.0	20.7	-0.9
12-7/8	-4.1	-0.6	13.2	-4.6	11-1/2	12.6	12.2	17.0	-0.8	13	12.8	11.3	20.7	-1.2	9-1/2	16.3	12.8	23.0	0.1
12-3/8	-3.0	1.2	13.0	-6.3	11	5.0	13.6	16.9	-1.5	12-1/2	1.9	14.6	23.3	-1.3	9	11.9	15.3	24.4	-0.3
11-3/4	3.4	-7.3	9.9	-7.4	10-1/2	14.2	14.0	17.3	-1.8	12	20.5	15.5	22.2	-1.4	8-1/2	11.8	16.5	22.5	-0.5
11-1/4	7.1	-0.1	13.7	-8.9	10	2.4	12.3	17.1	-1.9	11-1/4	14.7	13.9	20.9	-1.6	7-7/8	4.5	13.6	23.7	0.1
10-3/4	-1.3	-0.2	11.8	-11.7	9-1/2	12.7	11.4	21.2	-1.9	10-3/4	14.2	15.4	22.4	-1.6	7-1/2	10.8	13.1	21.5	0.2
10-1/4	7.0	0.6	12.1	-10.6	9	5.2	17.1	21.3	-1.1	10-1/4	19.9	16.5	21.6	-2.6	6-7/8	8.7	14.8	24.7	0.9
9-5/8	6.3	1.0	11.9	-6.9	8-1/4	7.6	16.1	21.0	-0.1	9-3/4	3.9	14.2	19.3	-2.0	6-1/4	16.9	14.7	23.4	0.9
9-1/8	8.8	2.4	13.9	-4.4	7-3/4	6.7	14.5	19.0	-0.4	9	22.0	9.9	20.3	-1.0	5-3/4	16.3	13.3	24.6	1.1
8-1/2	4.3	-0.3	13.7	-2.1	7-1/4	13.1	16.8	13.1	-0.7	8-3/8	15.6	11.8	19.7	-0.5	5-1/4	14.5	12.3	21.7	0.0
8	4.2	2.7	12.6	-1.6	6-3/4	13.4	10.5	13.4	-1.2	7-7/8	11.1	9.4	19.1	-0.5	4-5/8	3.1	14.0	18.5	-0.6
7-3/8	6.1	2.2	13.6	-1.3	6-1/4	6.7	16.6	18.0	-1.8	7-1/2	4.8	3.8	14.8	-0.4	4-1/8	18.6	14.3	23.9	1.0
7	-0.5	1.2	11.6	-1.3	5-3/4	3.8	12.7	18.1	-6.2	7	12.3	15.3	21.8	0.2	3-9/16	17.0	14.7	24.3	2.5
6-1/2	6.9	2.5	8.7	-1.0	5-1/4	14.2	14.2	22.1	-3.0	6-1/4	17.4	15.0	23.0	0.4	3-1/16	18.8	16.2	24.2	2.6
5-3/4	5.5	1.2	11.9	-1.0	4-1/2	15.6	12.5	18.9	-3.4	5-3/4	7.9	12.2	17.8	1.1	2-5/8	16.9	18.0	25.9	2.5
5-1/8	4.5	2.8	13.2	-1.9	4	7.9	12.8	20.7	1.0	5	14.7	16.7	23.1	0.6	2	15.6	17.0	23.5	-0.6
4-1/2	4.3	3.1	14.2	-3.7	3-1/2	6.6	10.7	20.5	1.3	4-1/2	14.6	12.4	17.8	0.9	1-1/2	15.4	19.0	23.6	-1.2
4	9.9	3.0	12.3	-5.1	3	15.3	12.7	20.5	-0.2	3-7/8	13.5	11.0	19.1	1.5	1/2	18.6	17.5	25.2	2.9
3-3/8	3.3	2.2	13.6	-9.5	2-1/2	8.9	11.2	19.1	-0.6	3-1/4	3.7	11.8	17.2	1.9	Metal Plate	20.2	17.4	26.7	3.9
2-3/4	7.4	1.2	12.8	-5.7	2	11.3	12.6	18.8	-12.9	2-3/4	3.6	8.2	15.3	1.8					
2-1/4	7.1	1.3	12.5	-4.8	1-7/16	10.7	11.3	20.2	-1.0	2-1/4	6.3	12.6	19.8	1.1					
1-3/4	3.3	0.7	15.0	1.2	1	10.6	14.5	18.5	2.1	1-3/4	10.5	12.5	18.9	-2.8					
1	6.2	1.4	9.7	1.6	1/2	10.9	11.6	17.2	3.5	1	9.3	15.9	25.5	0.2					
1/2	1.2	1.1	16.5	2.1	Metal Plate	17.3	20.3	24.3	3.7	1/2	13.8	13.7	22.1	1.9					
Metal Plate	15.9	11.5	22.2	1.8						Metal Plate	22.7	18.2	24.7	3.0					

Table 5

Depth-of-Penetration Data

Perlite

Depth of Material in.	Normalized Echo Area, db				Depth of Material in.	Normalized Echo Area, db				Depth of Material in.	Normalized Echo Area, db				Depth of Material in.	Normalized Echo Area, db			
	Ka-Band	X-Band	C-Band	P-Band		Ka-Band	X-Band	C-Band	P-Band		Ka-Band	X-Band	C-Band	P-Band		Ka-Band	X-Band	C-Band	P-Band
	Dry Density 10 pcf					Dry Density 20 pcf					Dry Density 30 pcf					Dry Density 40 pcf			
24	-12.7	4.1	19.4	2.2	23-1/4	-21.4	6.5	11.2	-0.4	24-1/8	5.9	7.6	11.8	0.1	24-1/8	3.9	6.5	1.3	2.0
23-1/2	-22.4	6.5	17.3	-1.8	22-3/4	-0.3	4.1	12.6	-0.5	23-1/2	3.4	3.8	11.6	0.3	23-9/16	4.0	5.0	1.5	1.6
23	-23.6	5.3	17.8	-2.0	22-1/8	-1.1	2.4	16.0	-1.8	23	1.4	1.4	6.9	0.0	23-1/16	1.6	7.0	-1.2	1.5
22-1/2	-13.5	1.8	16.5	-2.0	21-1/2	4.1	7.7	14.7	-2.5	22-1/2	-3.4	2.1	11.7	-0.8	22-9/16	7.9	7.2	-0.9	1.4
22	-12.5	-7.3	19.1	-1.3	21	-0.4	6.4	13.5	-2.0	22	-11.2	-3.2	14.2	0.3	22	6.6	7.3	1.5	1.6
21-1/2	-24.1	-2.7	18.2	-1.1	20-1/2	-1.5	6.9	17.4	-1.5	21-1/2	2.4	3.5	8.4	0.0	21-1/2	1.9	6.8	3.5	1.0
21	-6.3	-7.3	19.7	-0.6	20	-1.8	8.8	9.1	-2.6	21	2.0	1.6	12.9	-0.4	21	4.6	2.5	-7.0	1.2
20-3/8	-4.2	-0.8	19.1	-0.2	19-3/8	1.7	8.2	9.3	-2.9	20-3/8	-0.7	-1.5	13.1	-0.8	20-1/2	2.2	3.6	6.9	-0.2
19-3/4	-8.1	0.8	16.7	-1.0	19	-5.9	6.4	12.0	-2.3	19-5/8	-2.0	4.5	8.1	-1.3	20	2.3	5.7	3.9	-0.1
19-1/4	-9.5	1.1	20.1	0.5	18-1/2	4.8	7.3	10.8	-1.7	19-1/4	4.1	7.3	6.0	-1.5	19-1/2	-0.7	5.2	3.1	-1.9
18-3/4	-7.3	5.5	18.1	0.5	17-3/4	1.5	8.2	15.0	-2.1	18-3/4	-2.1	6.2	13.3	-1.6	19	3.7	5.5	-11.8	-2.3
18-1/4	-5.1	9.1	19.6	1.1	17-1/4	-0.1	12.4	16.6	-2.5	18-1/4	3.6	3.3	8.8	-1.9	18-1/2	0.5	6.1	8.3	-2.6
17-3/4	-2.6	10.8	20.2	1.9	16-3/4	-2.3	12.9	13.9	-2.1	17-5/8	1.8	6.7	10.0	-1.8	17-3/4	4.3	5.1	5.6	-2.6
17-1/4	-11.0	8.7	18.5	1.9	16-3/16	-15.3	8.7	16.6	-1.6	17-1/4	-2.1	7.1	14.6	-1.9	17-1/4	5.5	2.3	-9.0	-3.1
16-7/8	-0.4	8.1	20.4	2.3	15-3/4	0.1	11.5	15.8	-1.6	16-9/16	-2.5	3.9	14.2	-0.8	16-3/4	2.1	6.2	6.2	-4.0
16-1/16	2.2	6.1	20.2	1.3	15-1/8	4.3	12.3	15.5	-0.8	16	-3.0	2.0	11.1	-0.6	16-1/4	5.4	9.6	10.1	-5.1
15-5/8	-0.8	7.1	20.9	2.3	14-5/8	-3.1	12.7	14.8	-0.6	15-1/2	3.1	10.3	12.0	-0.9	15-3/4	2.5	8.9	-0.2	-3.7
15-1/8	0.6	10.3	21.2	2.9	14-1/8	-7.7	13.0	15.5	-0.7	15	3.8	11.8	12.5	0.3	15	6.0	7.3	4.9	-3.2
14-5/8	-7.9	10.8	21.7	3.4	13-5/8	0.0	13.0	18.4	0.2	14-7/16	2.8	12.0	1.4	0.0	14-1/2	5.2	4.1	12.7	-2.4
14-1/8	-4.4	11.2	21.9	2.7	13-3/8	2.9	15.7	18.8	1.1	14	3.8	11.8	0.0	0.3	14	5.9	-3.4	14.8	-1.7
13-5/8	-2.1	12.6	21.6	2.7	12-1/4	2.5	19.3	18.7	1.2	13-1/2	2.4	10.9	7.2	0.8	13-1/2	4.3	4.8	11.9	-2.0
13-1/8	-0.9	12.8	21.8	3.0	11-3/4	4.5	19.3	19.5	1.8	13	3.6	13.3	6.0	1.0	13	8.2	2.4	9.6	-1.1
12-1/4	-1.3	12.6	21.9	3.5	11-1/4	-9.6	18.3	18.8	2.5	12-1/4	5.3	12.7	14.9	2.0	12-9/16	8.1	9.9	2.5	0.2
11-5/8	-1.0	14.8	21.5	2.3	10-3/4	-6.7	18.3	18.6	2.0	11-3/4	3.4	12.8	7.8	2.2	12-1/16	4.1	7.7	11.5	0.3
11	-1.1	13.1	22.1	3.5	10-1/4	-4.1	19.8	20.9	1.8	11-1/4	-3.9	13.4	17.4	2.9	11-7/16	5.3	7.9	15.4	0.5
10-1/2	-4.7	14.8	21.9	3.6	9-3/4	-4.4	20.7	20.5	2.2	10-1/2	-0.8	13.8	17.8	3.4	11-1/16	7.4	6.4	14.1	0.5
10	-4.5	12.0	22.2	3.3	9-1/4	-6.3	20.4	21.3	2.0	10	2.1	12.6	19.2	2.6	10-7/16	5.7	-0.8	11.9	1.0
9-1/2	-4.0	12.5	22.0	3.6	8-1/4	-18.3	20.1	20.0	1.6	9-1/2	3.7	12.2	18.1	1.8	10	-1.5	13.8	15.2	0.3
9	-3.8	15.6	21.4	2.9	7-3/4	-5.9	20.1	18.8	1.7	9	4.3	8.9	18.5	2.4	9-9/16	1.8	13.6	17.4	0.8
8-3/8	1.3	16.7	22.6	2.3	7-1/4	-6.5	19.0	18.3	0.6	8-1/2	-1.8	15.9	20.4	1.7	8-6/16	6.1	14.1	15.8	1.0
8	2.1	14.0	22.0	1.8	6-3/4	-8.2	20.6	18.1	-0.5	8	0.7	16.0	20.2	1.9	8	5.5	9.0	14.2	1.3
7-1/2	5.6	16.2	22.8	1.9	6-1/4	-2.1	20.8	19.0	0.0	7-1/2	0.4	15.9	22.4	2.2	7-1/2	1.7	9.4	12.0	0.7
6-3/4	5.9	18.1	23.0	1.3	5-3/4	-7.6	21.8	16.5	1.6	7	-3.6	15.1	21.2	0.4	6-7/8	5.6	13.0	12.1	0.5
6-1/4	0.4	17.6	22.2	1.2	5-1/4	-17.1	21.5	16.4	1.7	6-1/2	-1.8	15.5	20.1	0.8	6-5/16	3.5	10.9	13.1	1.7
5-3/4	2.7	18.0	22.6	0.5	4-1/2	-6.2	19.6	14.9	-1.8	5-7/8	3.8	17.5	19.8	0.2	5-3/4	5.6	11.3	15.2	1.0
5-1/4	3.1	18.1	22.3	1.6	4	-16.9	22.3	16.9	-1.9	5-5/16	-0.5	19.9	21.3	0.1	5-1/4	6.0	13.3	11.6	0.2
4-1/2	4.6	17.2	22.4	0.6	3-1/2	-4.1	21.4	16.4	-2.3	4-11/16	-4.7	20.9	21.2	0.4	4-1/2	3.9	7.4	13.6	-0.1
4	4.5	17.4	22.3	1.1	3	-2.6	22.8	16.4	-0.6	4-1/8	3.6	21.1	20.9	-0.3	4	1.0	10.8	14.5	-0.6
3-1/2	10.5	18.6	22.3	1.0	2-1/2	0.0	23.2	17.2	-1.2	3-9/16	1.3	20.7	21.5	-0.5	3-1/2	4.6	13.6	18.0	-0.8
3	12.9	18.6	22.3	1.0	2	4.4	23.5	15.8	-0.3	3-1/16	5.7	21.1	20.3	-0.2	3	8.0	12.6	13.2	-0.7
2-1/2	12.7	18.2	22.6	0.9	1-1/2	6.8	21.3	15.9	-1.2	2-9/16	7.8	22.3	18.1	0.2	2-1/2	5.9	12.8	10.7	-0.8
2	13.6	19.9	22.4	2.3	1	4.9	21.5	15.9	0.4	2	8.2	21.9	17.6	-0.4	2	4.6	18.7	8.5	-1.0
1-1/2	15.5	19.2	22.6	2.6	1/2	10.6	20.1	17.0	1.3	1-1/2	12.4	25.6	18.9	0.2	1-1/2	4.8	19.2	13.4	0.2
1	7.2	18.4	23.0	2.7	Metal Plate	4.0	20.5	15.2	1.3	1	15.2	21.7	17.0	1.4	1	6.5	19.2	14.0	0.7
1/2	14.1	19.7	23.1	3.0						1/2	17.1	19.9	17.1	1.9	1/2	14.7	19.8	17.5	1.0
Metal Plate	15.1	18.1	23.0	3.8						Metal Plate	17.8	19.6	16.5	3.7	Metal Plate	16.9	20.9	17.5	1.1

Table 6

Depth-of-Penetration Data

Putnam Silt Loam Overlying Putnam Clay

Soil Depth, in.	Normalized Echo Area, db Ka-Band	X-Band	C-Band	P-Band	Soil Depth, in.	Normalized Echo Area, db Ka-Band	X-Band	C-Band	P-Band	Soil Depth, in.	Normalized Echo Area, db Ka-Band	X-Band	C-Band	P-Band
Silt Loam at 7.0 Percent Moisture Content					Silt Loam at 35.7 Percent Moisture Content					Clay at 45.5 Percent Moisture Content				
25	0.1	7.0	5.0	-12.2	25	3.1	3.9	13.3	-2.8	13-1/2	12.9	17.3	14.7	-3.7
24-1/2	4.6	10.4	6.9	-10.9	24-1/2	12.6	19.9	13.4	-3.1	13	8.8	11.5	11.2	-2.6
24	3.4	10.3	8.0	-8.1	24	9.4	7.7	13.8	-3.2	12-1/2	-2.4	12.5	11.7	-2.9
23-1/2	6.1	10.0	8.8	-7.3	23-1/2	8.2	16.3	15.0	-1.9	12	11.8	19.1	12.4	-3.9
23	5.6	9.6	8.4	-7.0	23	8.8	13.0	13.2	-0.9	11-1/2	6.4	15.8	13.8	-2.6
22-1/2	6.2	10.7	7.8	-6.1	22-1/2	5.2	14.5	12.3	-1.8	11	13.0	14.6	13.7	-3.2
22	5.9	8.7	8.5	-5.3	22	3.1	15.4	14.8	-0.5	10-1/2	-3.3	17.4	15.1	-3.1
21-1/2	6.6	9.3	7.6	-4.1	21-1/2	6.6	15.7	14.7	-1.1	9-1/2	12.5	11.4	13.8	-1.9
20-3/4	5.6	9.6	5.1	-4.2	20-3/4	7.2	15.2	13.8	-0.7	9	17.2	20.1	17.9	-2.1
20-1/4	6.0	10.5	4.9	-5.1	20-1/4	13.5	16.8	15.3	-0.6	8-1/2	12.1	18.8	15.4	-2.2
19-3/4	6.0	9.9	3.3	-5.5	19-3/4	15.3	17.3	14.7	-1.3	8	14.8	17.3	15.8	-2.3
19-1/4	5.8	10.2	5.5	-6.7	19-1/4	8.5	17.2	15.0	-0.6	7-3/8	16.6	17.2	15.6	-1.9
18-3/4	6.3	10.2	6.1	-8.4	18	11.9	9.5	6.7	-1.0	7	9.8	18.7	15.6	-1.4
18-1/4	4.7	9.7	5.2	-12.2	17-1/2	10.0	20.1	15.7	-1.4	6-1/2	10.1	20.2	16.2	-1.7
17-3/4	6.3	10.7	5.5	-19.6	17	3.0	18.7	15.6	-2.3	5-3/4	13.8	17.7	15.9	-1.4
16-3/4	6.7	11.0	6.8	-23.8	16-1/2	17.0	17.0	15.8	-2.7	5	14.3	17.0	15.4	-1.4
16	9.1	10.6	6.0	-13.0	15-7/8	9.8	18.2	15.4	-2.1	4-1/2	8.3	16.2	13.1	-1.7
15-1/2	5.4	10.4	6.4	-10.2	15-1/4	14.7	16.8	16.5	-3.8	3-7/8	16.6	17.8	16.3	-2.4
15	6.7	11.2	6.5	-8.3	14-3/4	2.9	12.3	9.9	-3.5	3-3/8	13.7	18.4	15.9	-2.5
14-1/2	7.1	8.6	5.1	-6.5	14-1/4	17.7	19.6	16.6	-3.7	2-7/8	2.0	16.1	13.0	-0.7
14-1/4	3.6	12.5	11.5	-5.1						2-3/8	16.1	19.1	17.2	-1.0
										1-3/4	7.8	16.9	15.2	-2.1
										1	9.6	19.0	13.9	-4.4
										1/2	10.1	18.7	16.0	-0.1
										Metal Plate	18.2	20.8	17.0	+1.0

Table 7

Vegetation (Wheat) Signature Test Data

Angle of Incidence, deg	Normalized Echo Area, db			
	Ka-Band	X-Band	C-Band	P-Band
	Height 3-1/2 in.			
0	-21.6	-1.9	+0.5	-0.9
10	-25.7	-16.6	-16.8	-11.2
20	-27.2	-15.8	-19.1	-15.8
30	-28.3	-17.7	-21.5	-15.4
40	-26.9	-15.1	-22.5	-13.5
50	-27.2	-15.8	-24.0	-17.0
60	-27.0	-14.8	-23.5	-13.5
	Height 14 in.			
0	-10.5	-1.4	+1.2	-2.4
10	-17.5	-6.6	-11.2	-13.3
20	-19.6	-9.8	-16.2	-16.5
30	-17.6	-11.6	-15.6	-17.9
40	-16.5	-12.5	-16.2	-13.2
50	-16.9	-8.9	-15.7	-16.0
60	-15.1	-12.1	-18.5	-10.1
	Height 29 in.			
0	-19.4	-15.6	-15.5	-4.7
10	-16.8	-14.2	-16.9	-15.5
20	-19.7	-17.4	-18.9	-14.8
30	-21.0	-16.2	-16.3	-15.6
40	-23.9	-16.6	-19.0	-13.4
50	-20.4	-16.3	-21.8	-19.4
60	-22.8	-11.3	-17.5	-15.1

Note: Horizontal polarization.

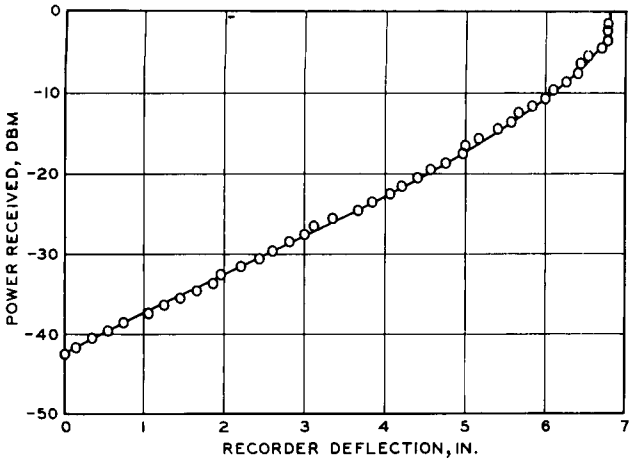

a. P-BAND

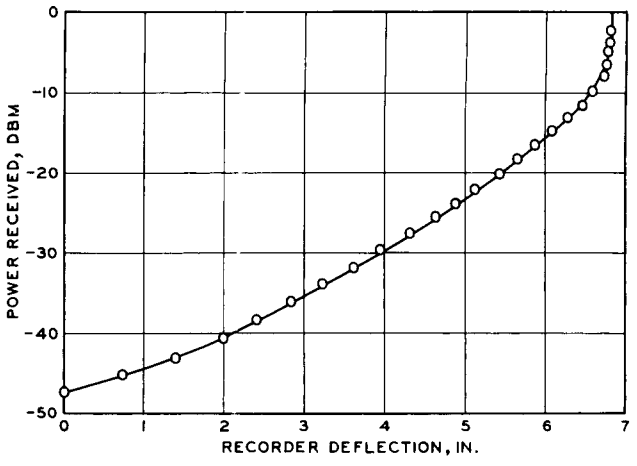

b. C-BAND

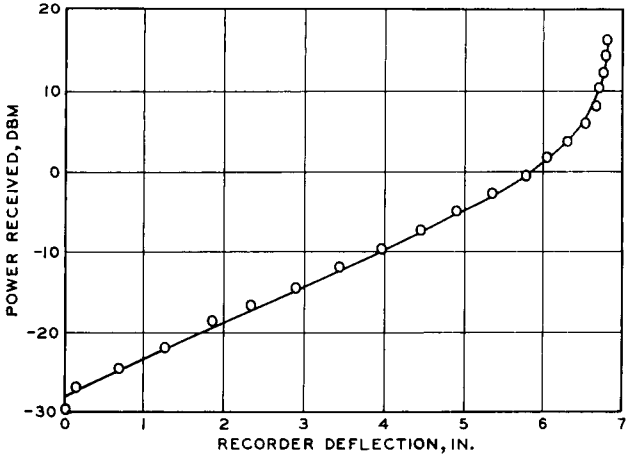

c. X-BAND

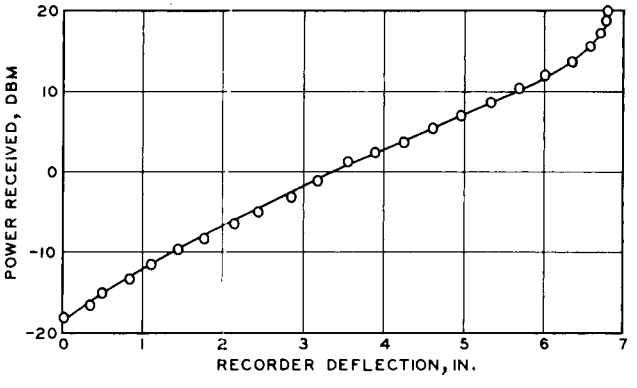

d. Ka-BAND

CALIBRATION CURVES

RECORDER DEFLECTION
VS POWER RECEIVED

PLATE I

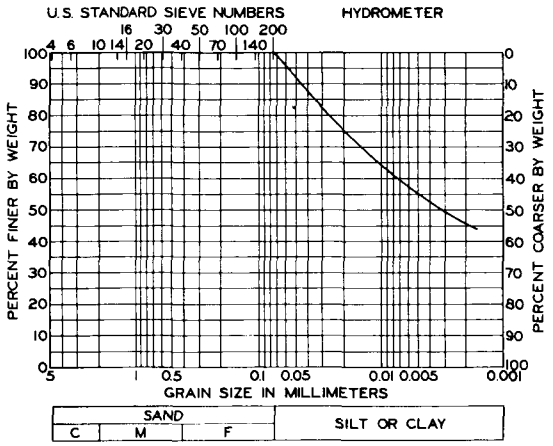

a. SHARKEY CLAY

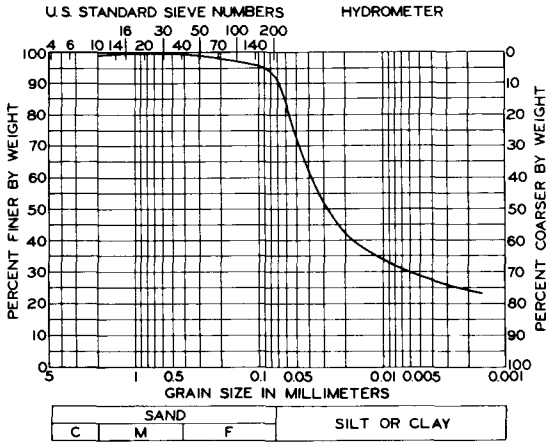

b. RICHFIELD SILT LOAM

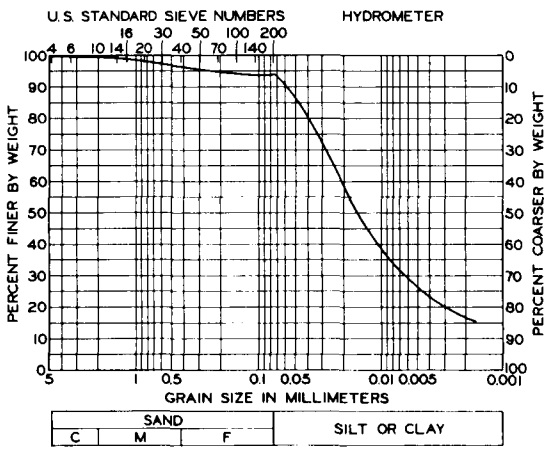

c. PUTNAM SILT LOAM (TOPSOIL)

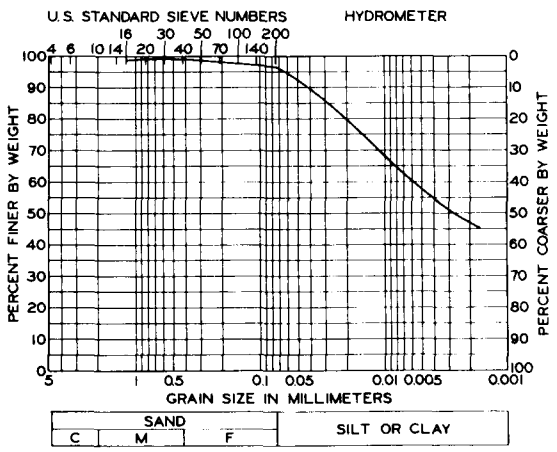

d. PUTNAM CLAY (SUBSOIL)

FIG.	DEPTH	Gs	L.L.	P.L.	P.I.	CLASSIFICATION		SOURCE
						USCS	USDA	
a.	6- TO 18"	2.66	72	26	46	CLAY (CH)	SiC	SHARKEY COUNTY, MISS.
b.	0- TO 12"	2.67	38	20	18	CLAY (CL)	SiL	GARDEN CITY, KANS.
c.	0- TO 12"	2.61	38	26	12	SILT (ML)	SiL	MEXICO, MO.
d.	12- TO 18"	2.67	86	29	57	CLAY (CH)	C	MEXICO, MO.

SOIL CLASSIFICATION DATA

PLATE 2

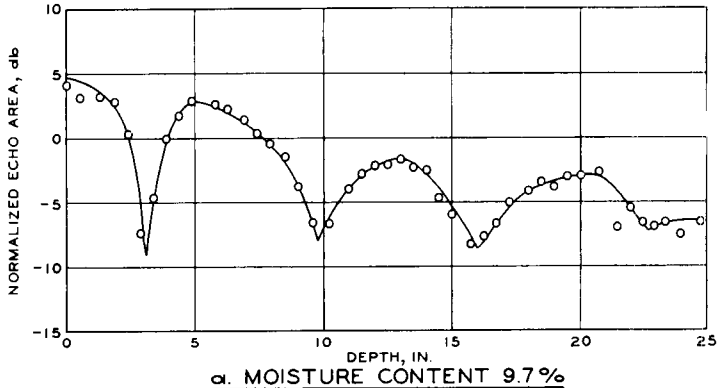

a. MOISTURE CONTENT 9.7%

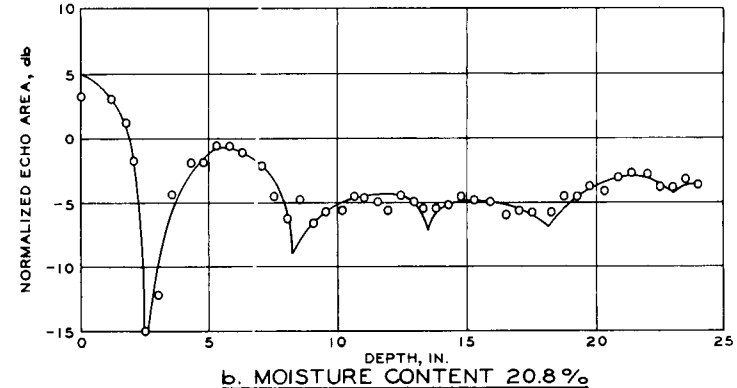

b. MOISTURE CONTENT 20.8%

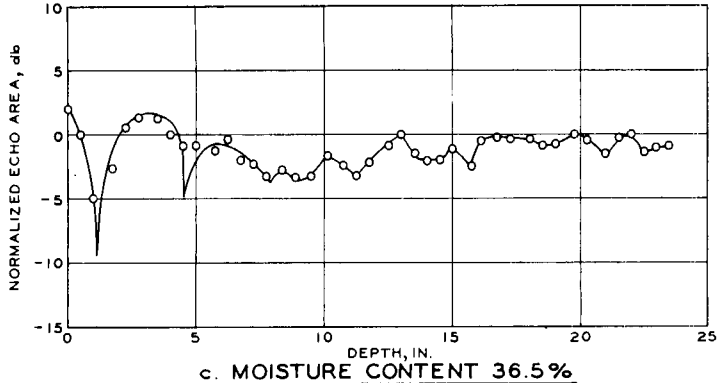

c. MOISTURE CONTENT 36.5%

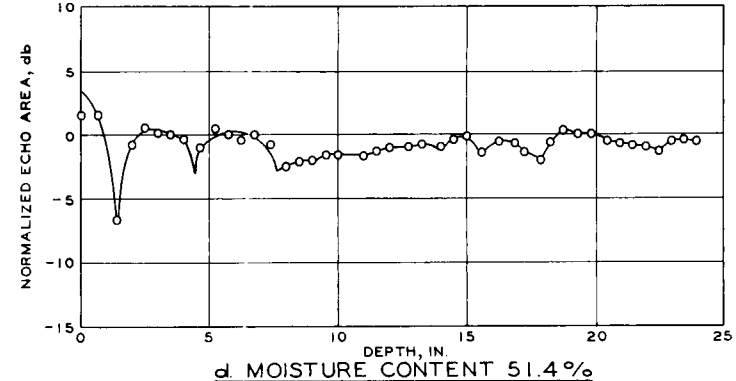

d. MOISTURE CONTENT 51.4%

NORMALIZED ECHO AREA
VS MATERIAL DEPTH

DEPTH OF PENETRATION TEST

SHARKEY CLAY
P - BAND

PLATE 3

PLATE 4

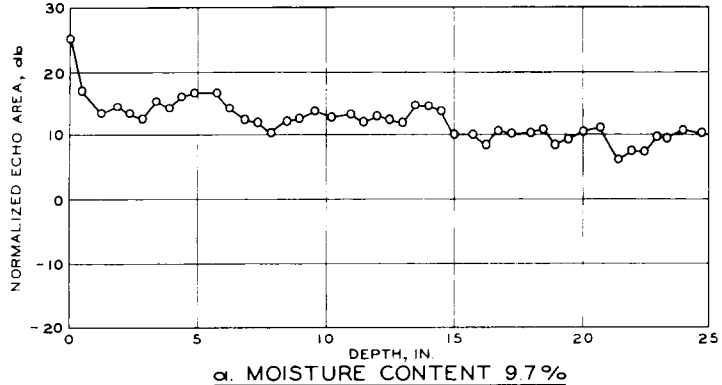

a. MOISTURE CONTENT 9.7%

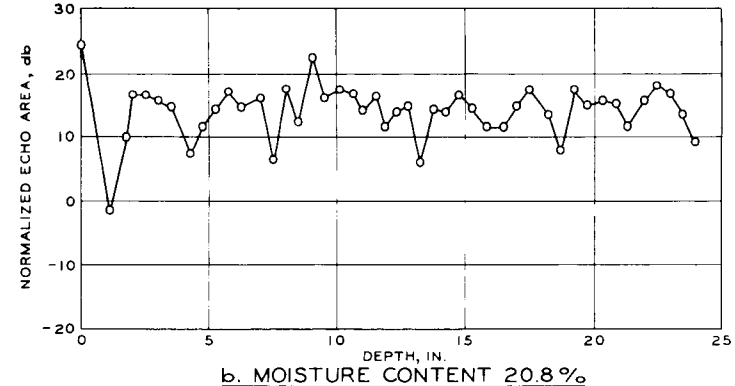

b. MOISTURE CONTENT 20.8%

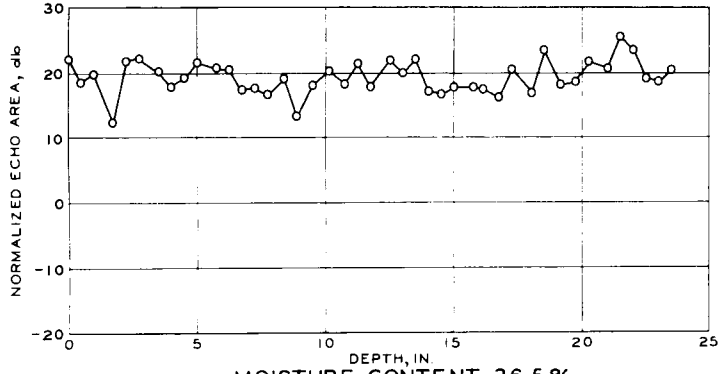

c. MOISTURE CONTENT 36.5%

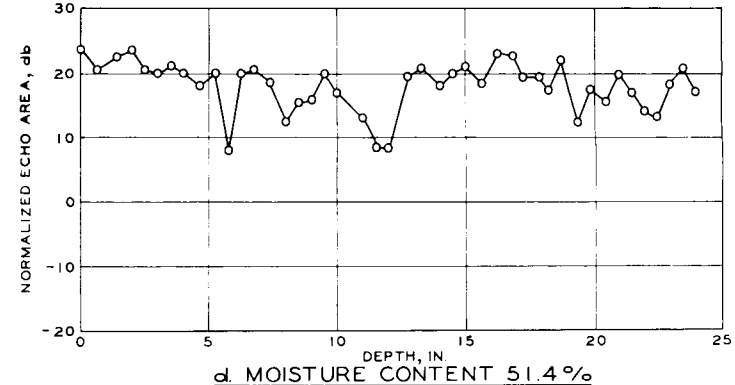

d. MOISTURE CONTENT 51.4%

NORMALIZED ECHO AREA
VS MATERIAL DEPTH

DEPTH OF PENETRATION TEST

SHARKEY CLAY
C-BAND

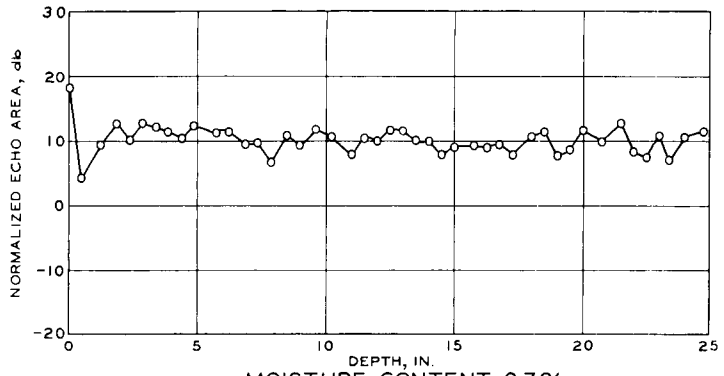

a. MOISTURE CONTENT 9.7%

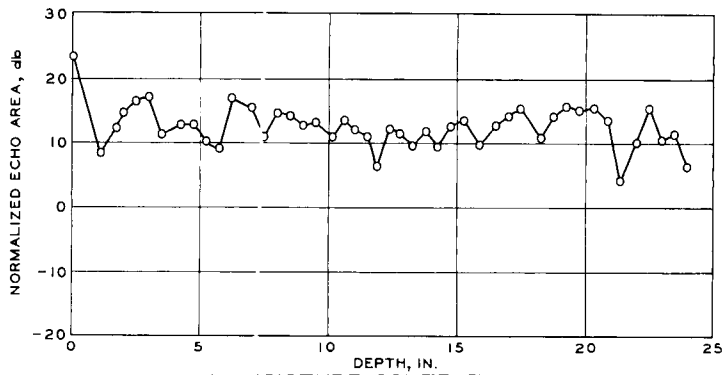

b. MOISTURE CONTENT 20.8%

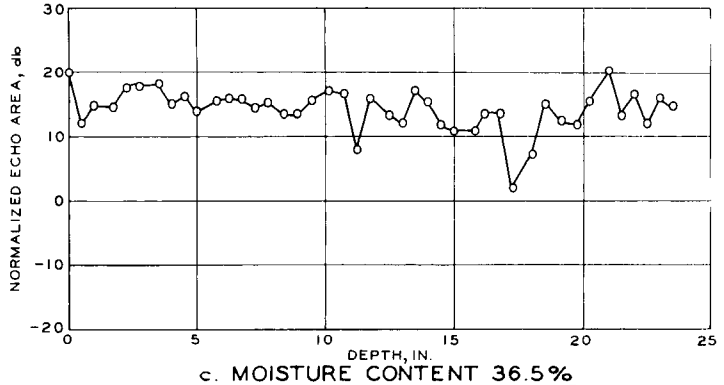

c. MOISTURE CONTENT 36.5%

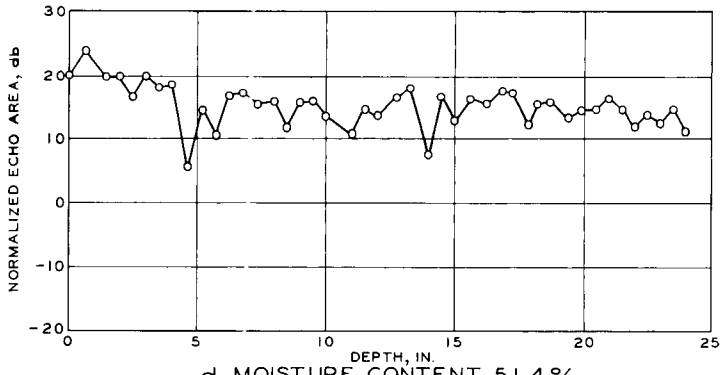

d. MOISTURE CONTENT 51.4%

NORMALIZED ECHO AREA
VS MATERIAL DEPTH

DEPTH OF PENETRATION TEST

SHARKEY CLAY
X-BAND

PLATE 5

PLATE 6

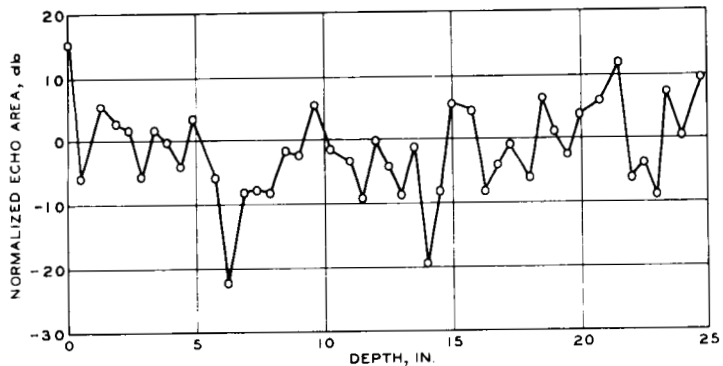

a. MOISTURE CONTENT 9.7%

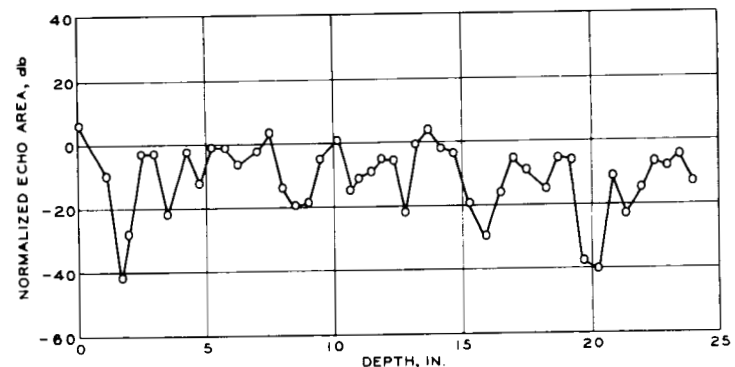

b. MOISTURE CONTENT 20.8%

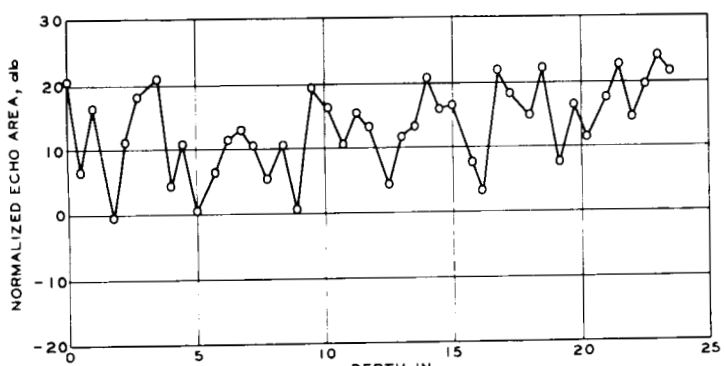

c. MOISTURE CONTENT 36.5%

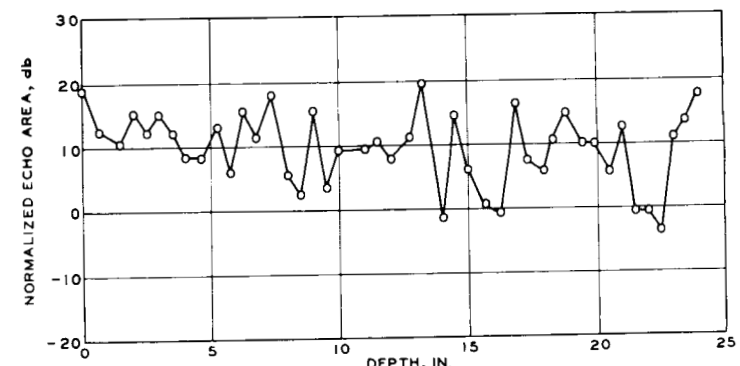

d. MOISTURE CONTENT 51.4%

NORMALIZED ECHO AREA
VS MATERIAL DEPTH

DEPTH OF PENETRATION TEST

SHARKEY CLAY
Ka - BAND

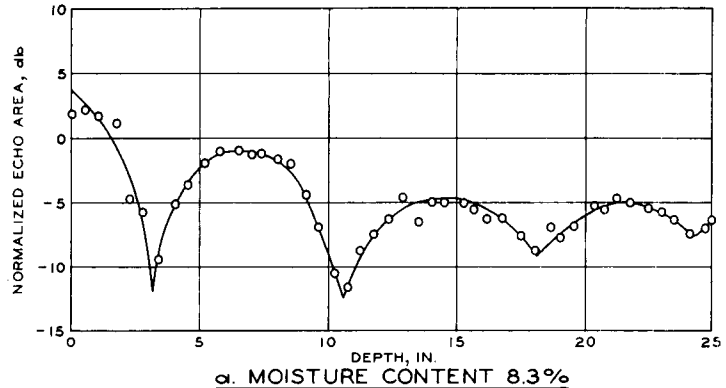

a. MOISTURE CONTENT 8.3%

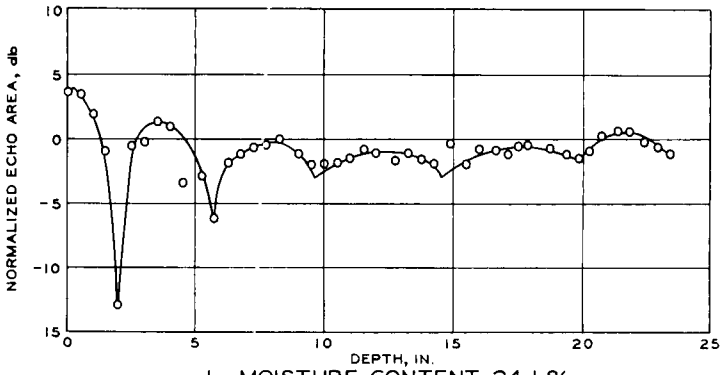

b. MOISTURE CONTENT 24.1 %

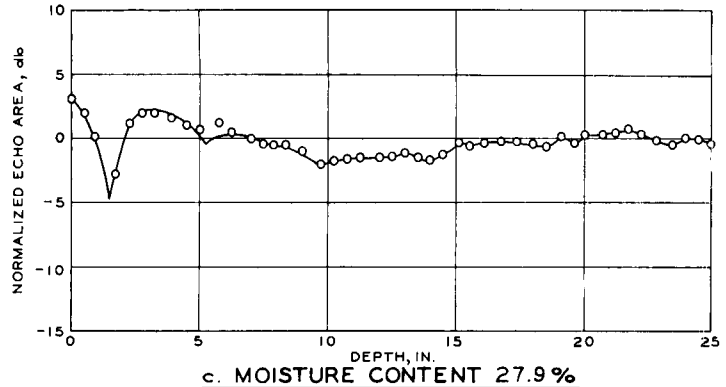

c. MOISTURE CONTENT 27.9%

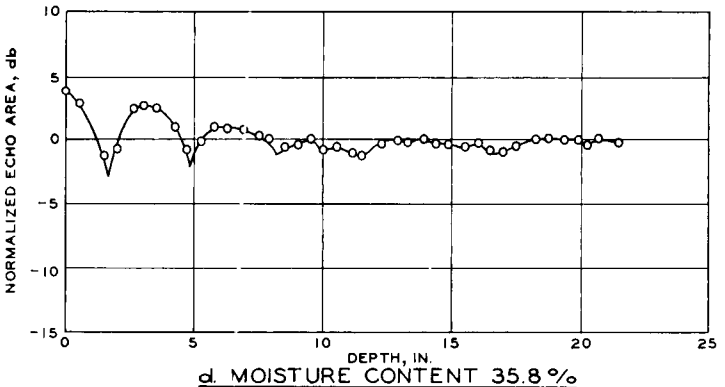

d. MOISTURE CONTENT 35.8 %

NORMALIZED ECHO AREA
VS MATERIAL DEPTH

DEPTH OF PENETRATION TEST

RICHFIELD SILT LOAM
P - BAND

PLATE 7

PLATE 8

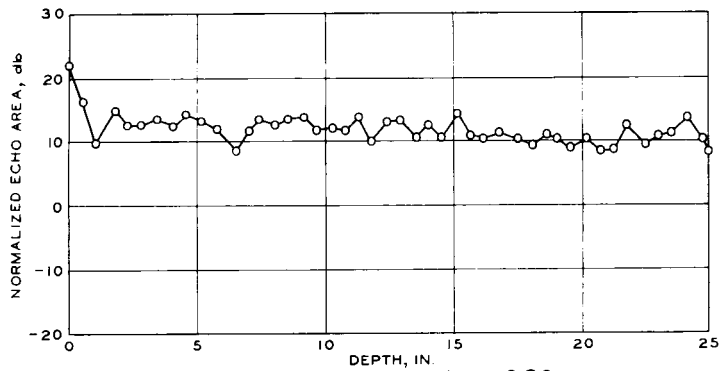

a. MOISTURE CONTENT 8.3%

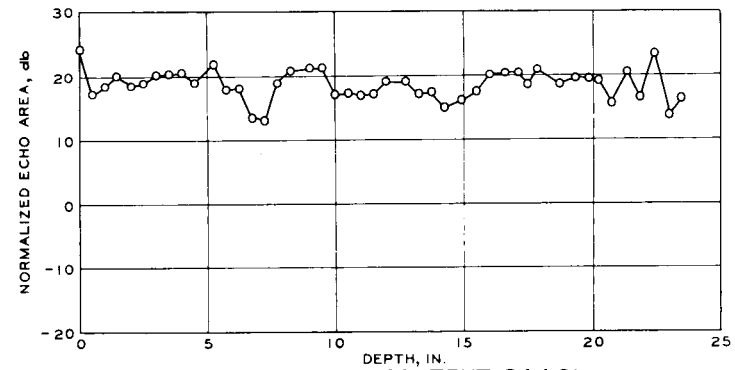

b. MOISTURE CONTENT 24.1 %

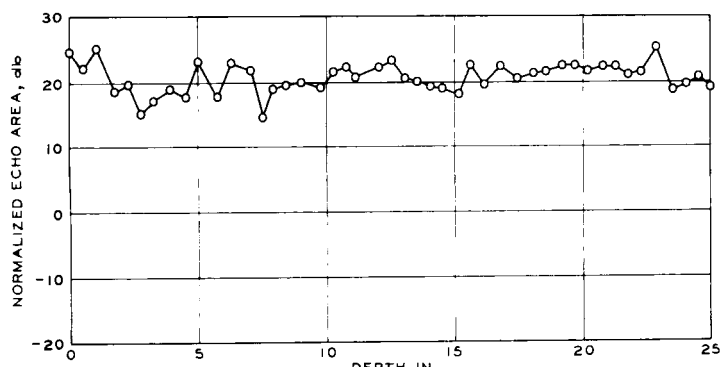

c. MOISTURE CONTENT 27.9 %

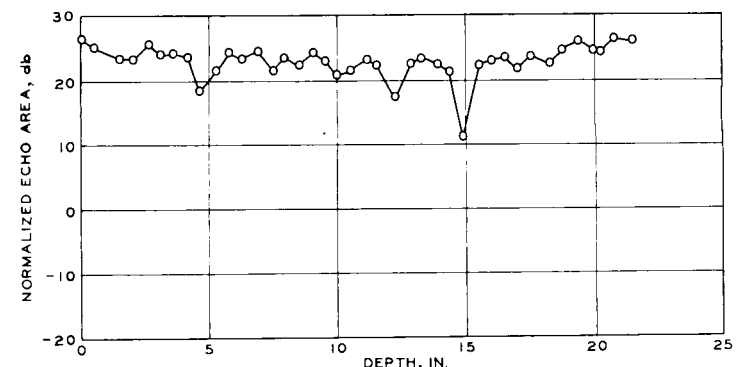

d. MOISTURE CONTENT 35.8 %

NORMALIZED ECHO AREA
VS MATERIAL DEPTH

DEPTH OF PENETRATION TEST

RICHFIELD SILT LOAM
C-BAND

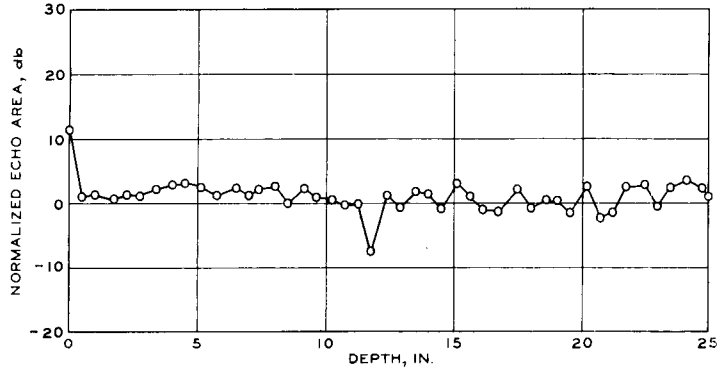

a. MOISTURE CONTENT 8.3%

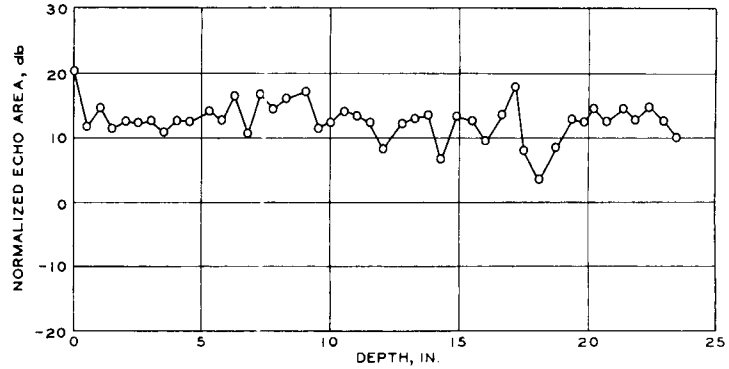

b. MOISTURE CONTENT 24.1%

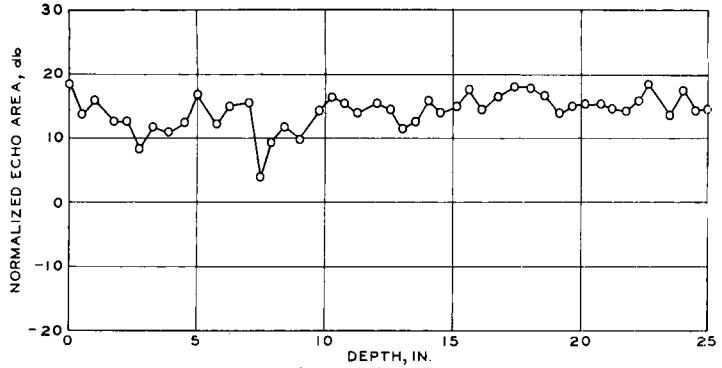

c. MOISTURE CONTENT 27.9%

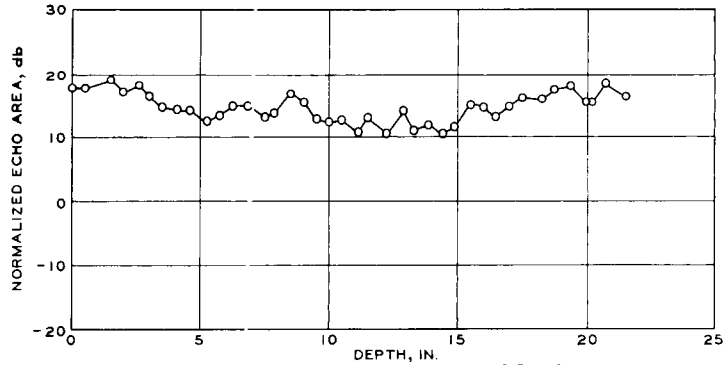

d. MOISTURE CONTENT 35.8%

NORMALIZED ECHO AREA
VS MATERIAL DEPTH

DEPTH OF PENETRATION TEST

RICHFIELD SILT LOAM
X-BAND

PLATE 9

PLATE 10

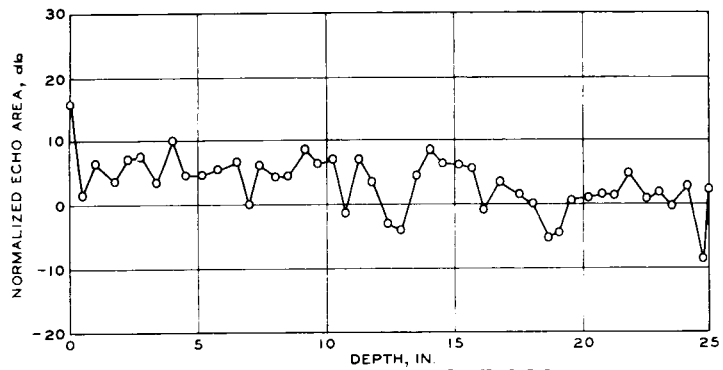

a. MOISTURE CONTENT 8.3%

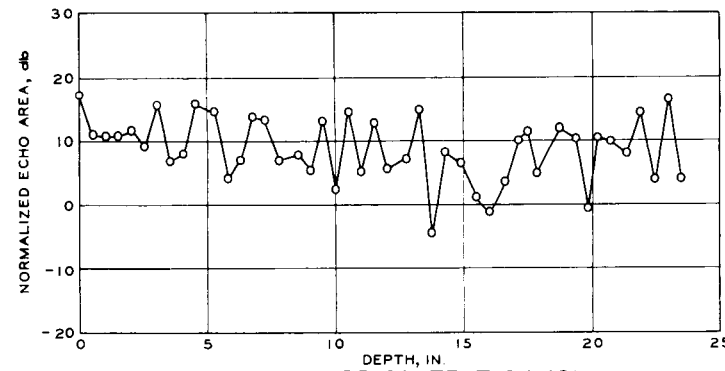

b. MOISTURE CONTENT 24.1%

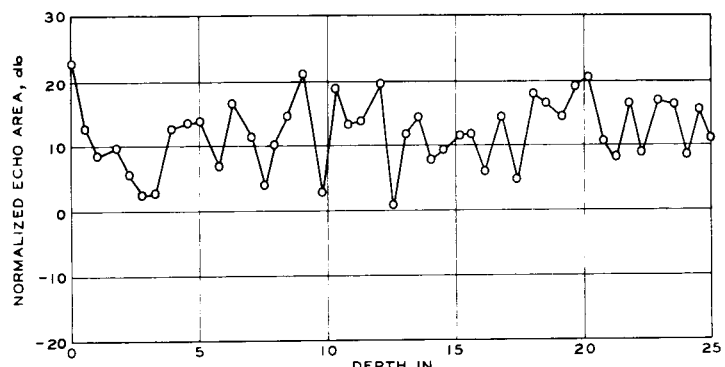

c. MOISTURE CONTENT 27.9%

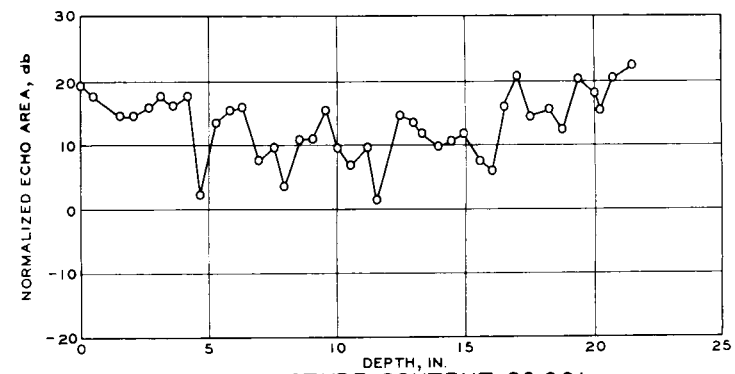

d. MOISTURE CONTENT 35.8%

NORMALIZED ECHO AREA
VS MATERIAL DEPTH

DEPTH OF PENETRATION TEST

RICHFIELD SILT LOAM
Ka-BAND

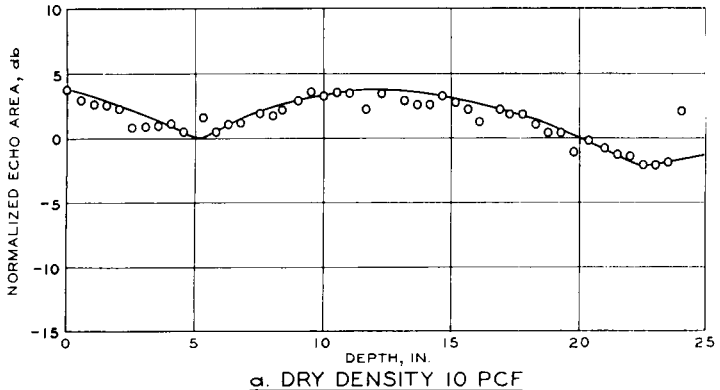

a. DRY DENSITY 10 PCF

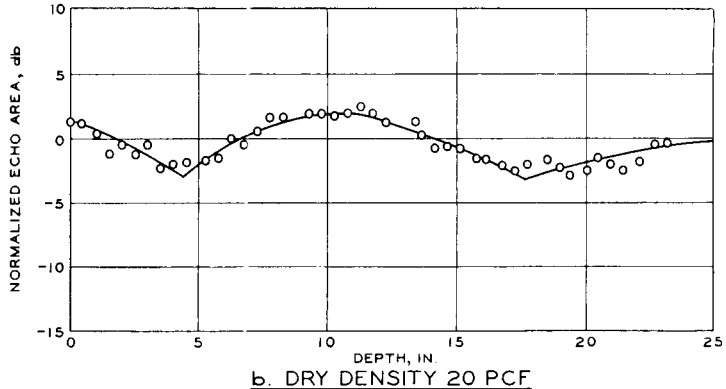

b. DRY DENSITY 20 PCF

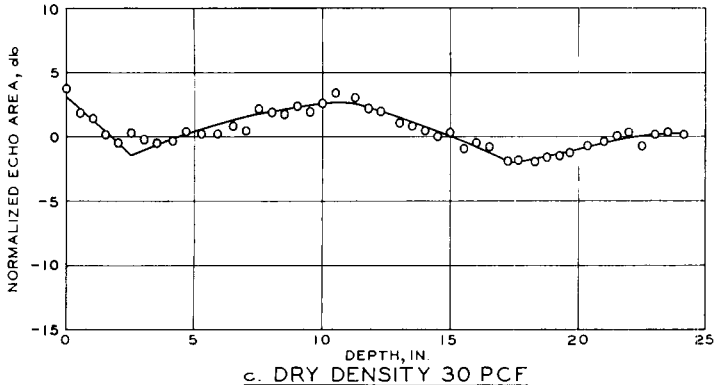

c. DRY DENSITY 30 PCF

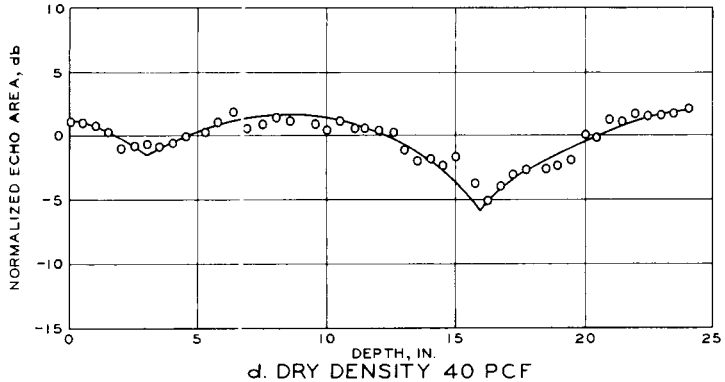

d. DRY DENSITY 40 PCF

NORMALIZED ECHO AREA
VS MATERIAL DEPTH

DEPTH OF PENETRATION TEST

PERLITE
P - BAND

PLATE 11

PLATE 12

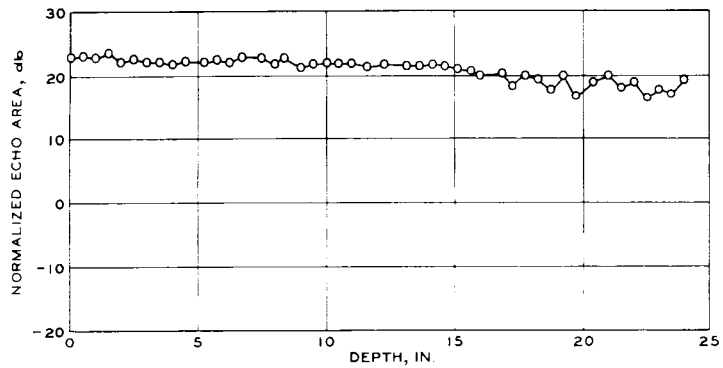

a. DRY DENSITY 10 PCF

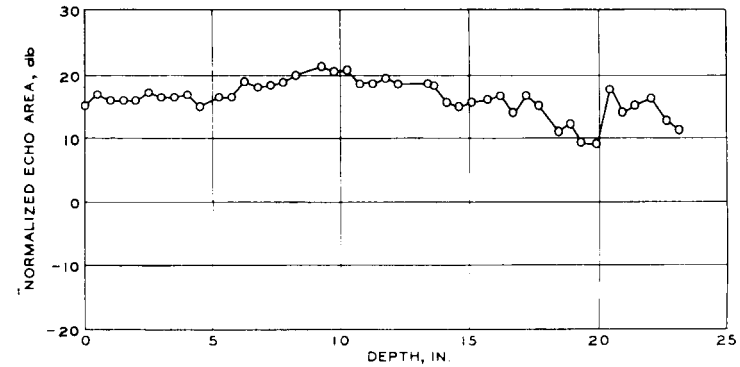

b. DRY DENSITY 20 PCF

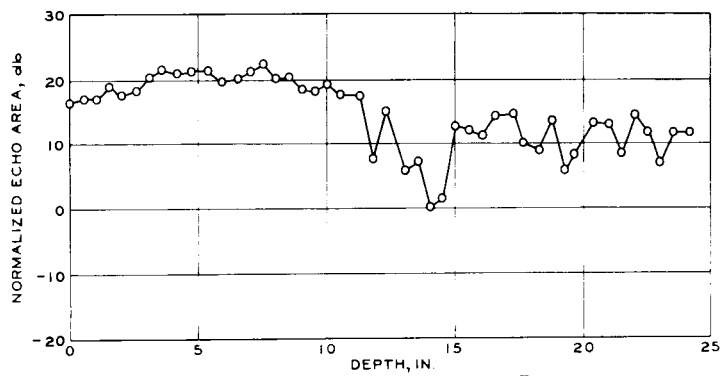

c. DRY DENSITY 30 PCF

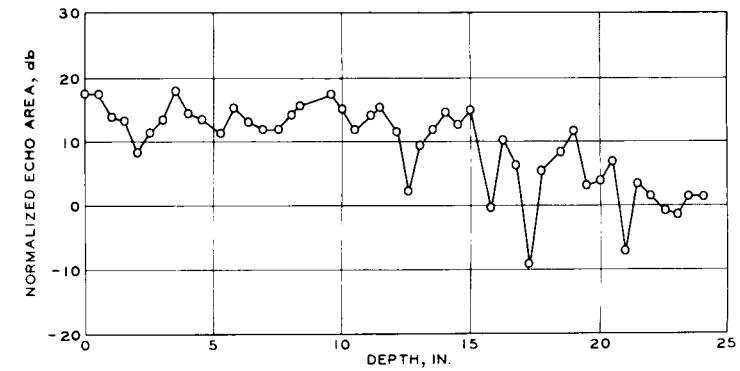

d. DRY DENSITY 40 PCF

NORMALIZED ECHO AREA
VS MATERIAL DEPTH

DEPTH OF PENETRATION TEST

PERLITE
C - BAND

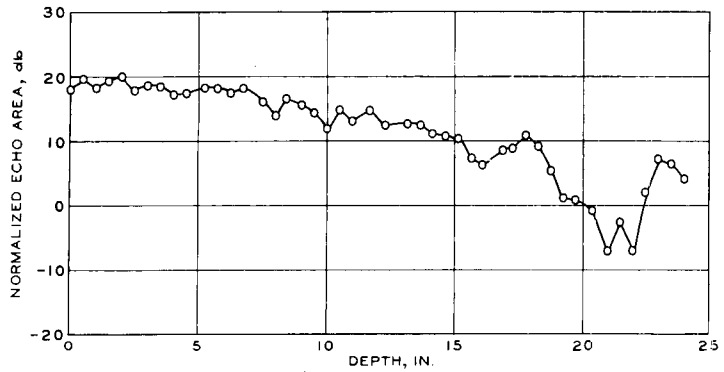

a. DRY DENSITY 10 PCF

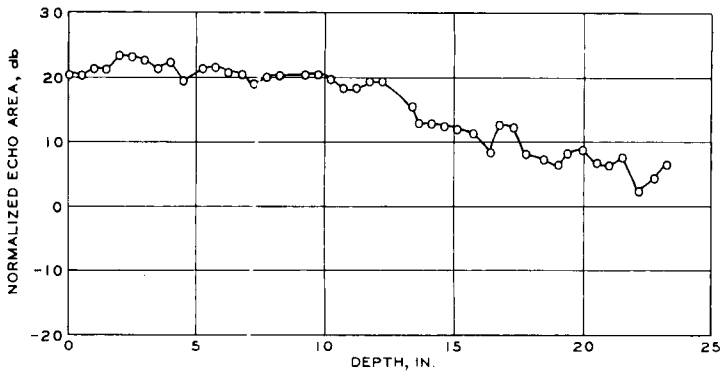

b. DRY DENSITY 20 PCF

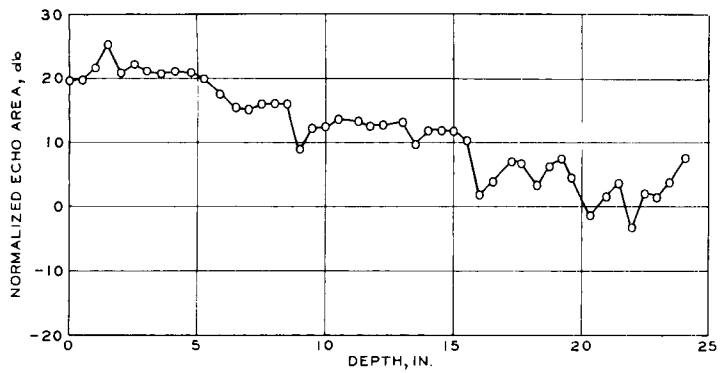

c. DRY DENSITY 30 PCF

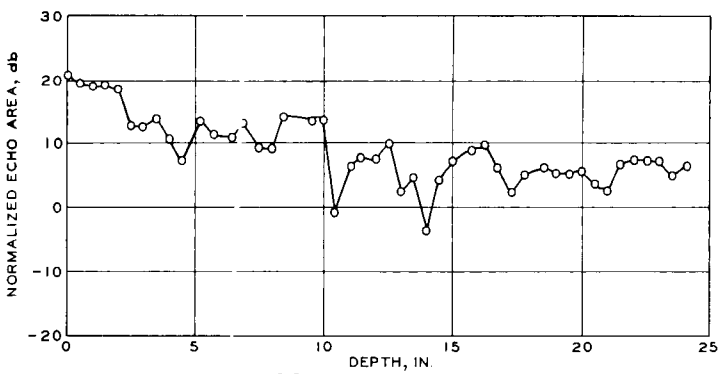

d. DRY DENSITY 40 PCF

NORMALIZED ECHO AREA
VS MATERIAL DEPTH

DEPTH OF PENETRATION TEST

PERLITE
X-BAND

PLATE 13

PLATE 14

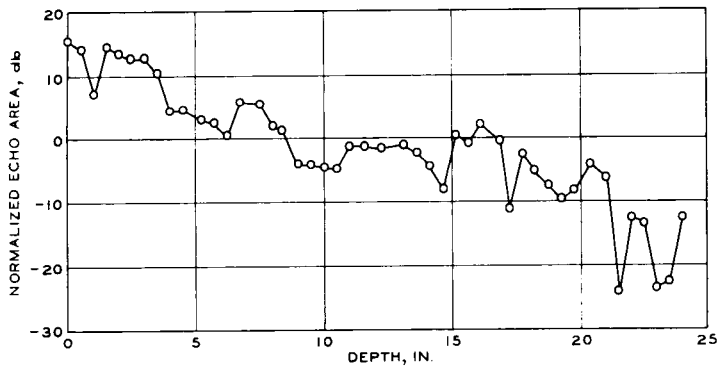

a. DRY DENSITY 10 PCF

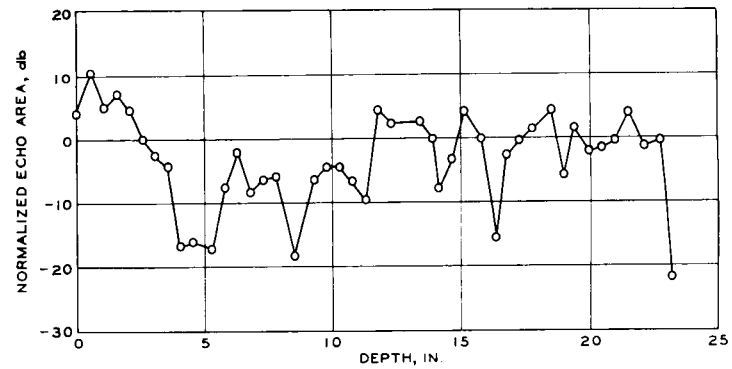

b. DRY DENSITY 20 PCF

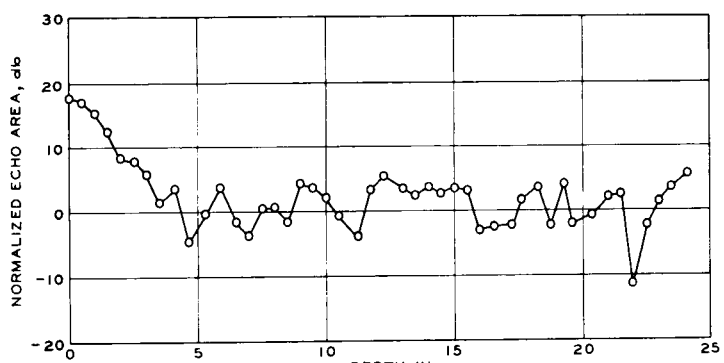

c. DRY DENSITY 30 PCF

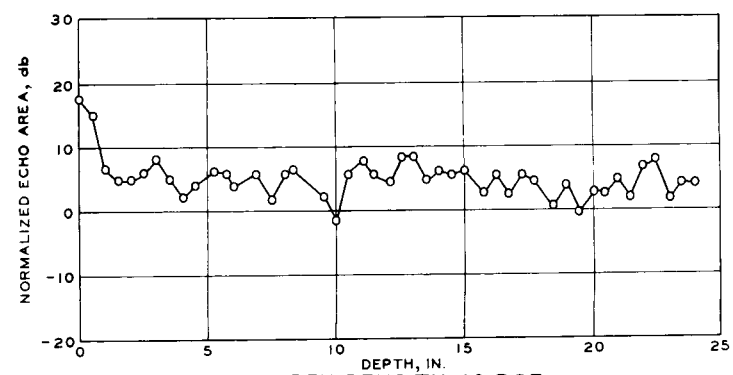

d. DRY DENSITY 40 PCF

NORMALIZED ECHO AREA
VS MATERIAL DEPTH

DEPTH OF PENETRATION TEST

PERLITE
Ka-BAND

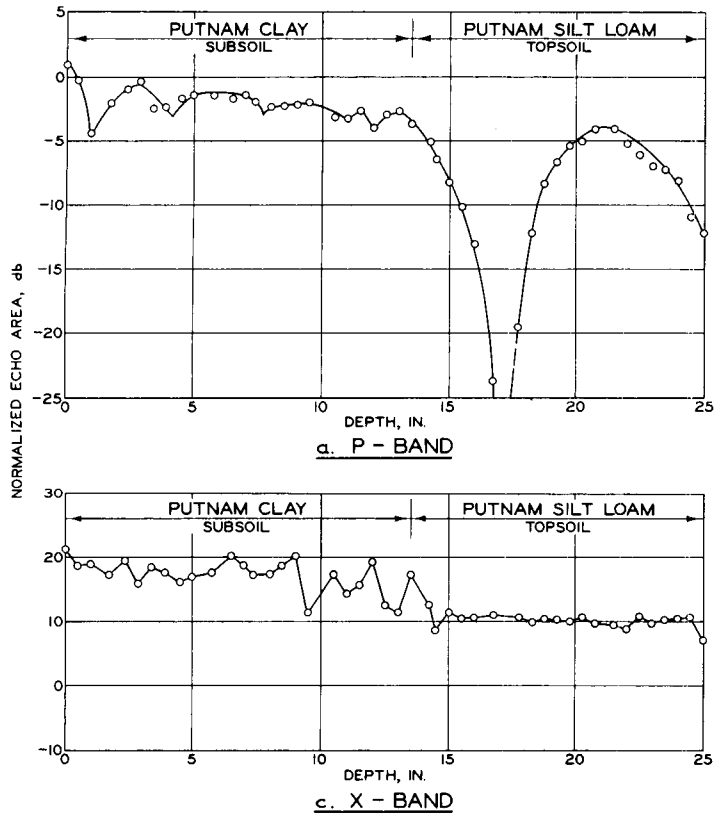

NOTE: DATA FOR THE PUTNAM CLAY SUBSOIL WERE OBTAINED AFTER THE TEST WITH PUTNAM SILT LOAM TOPSOIL AT A MOISTURE CONTENT OF 35.7%.

NORMALIZED ECHO AREA
VS MATERIAL DEPTH

DEPTH OF PENETRATION TEST

PUTNAM SILT LOAM TOPSOIL,
MOISTURE CONTENT 7%

PUTNAM CLAY SUBSOIL,
MOISTURE CONTENT 45.5%

PLATE 15

PLATE 16

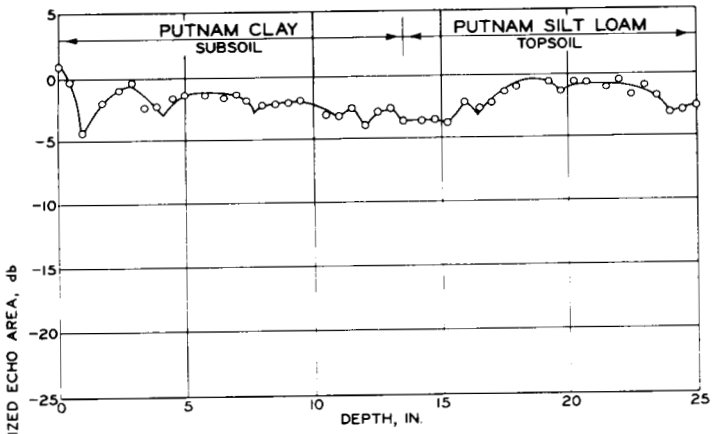

a. P - BAND

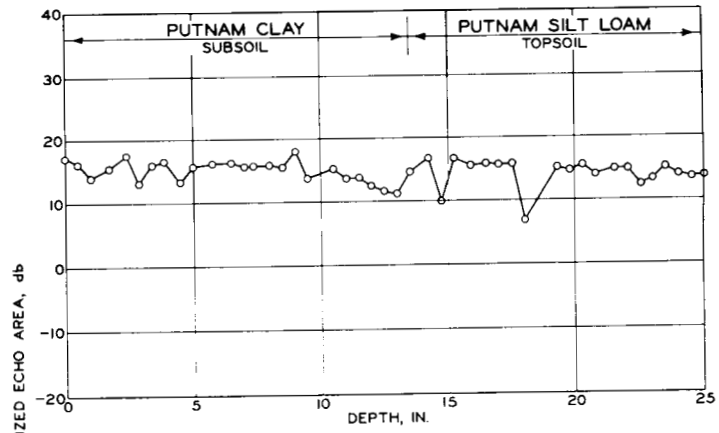

b. C - BAND

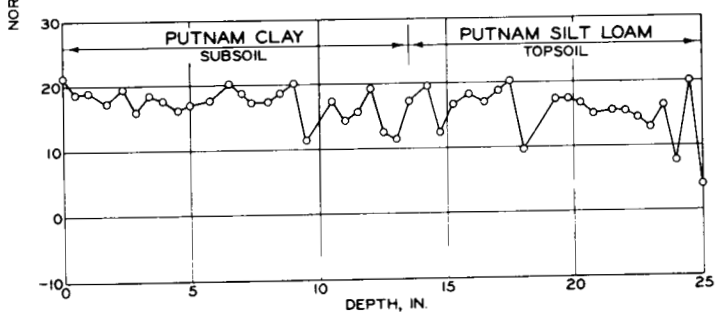

c. X - BAND

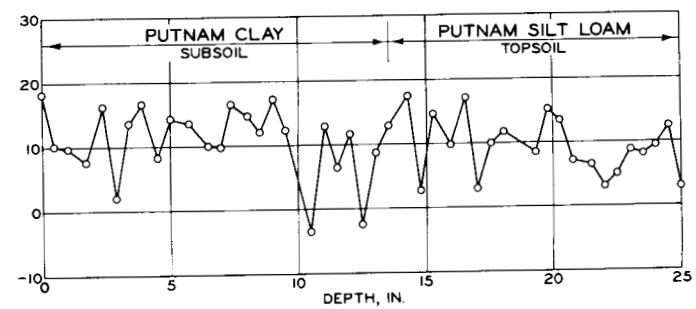

d. Ka - BAND

NORMALIZED ECHO AREA
VS MATERIAL DEPTH

DEPTH OF PENETRATION TEST

PUTNAM SILT LOAM TOPSOIL,
MOISTURE CONTENT 35.7%

PUTNAM CLAY SUBSOIL,
MOISTURE CONTENT 45.5%

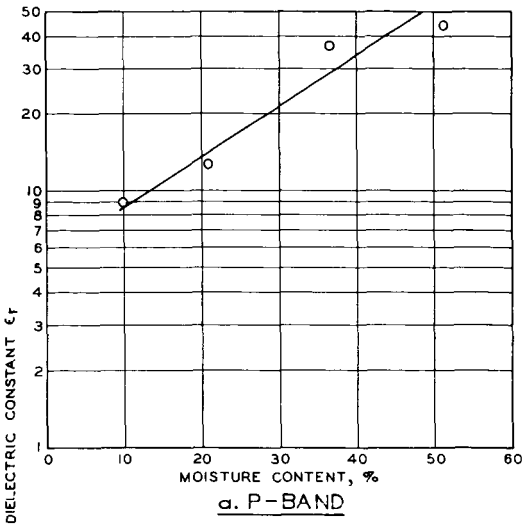

a. P-BAND

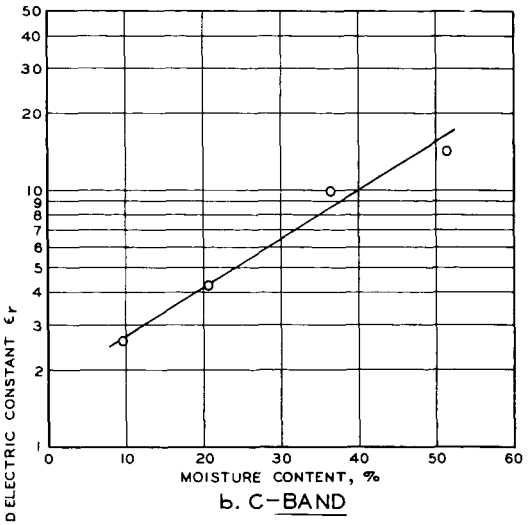

b. C-BAND

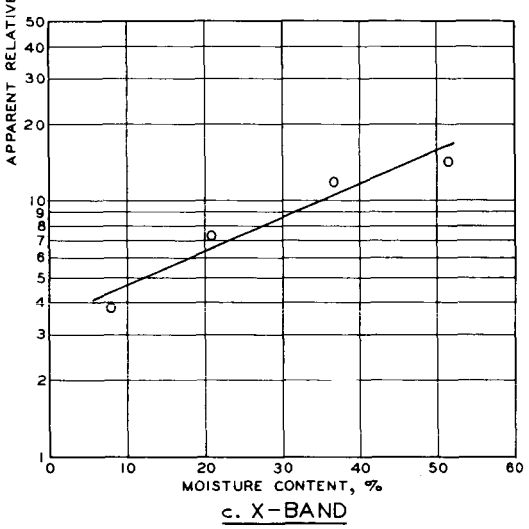

c. X-BAND

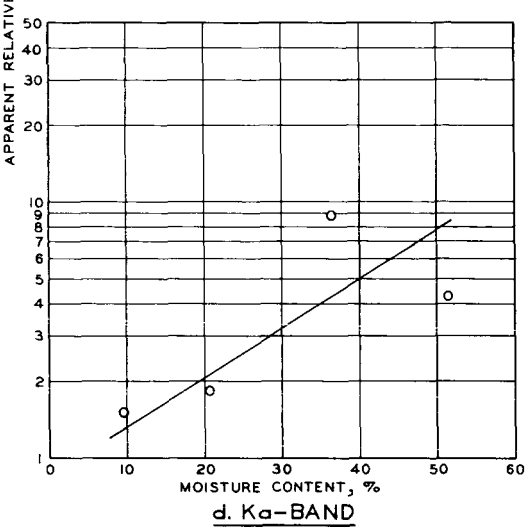

d. Ka-BAND

APPARENT RELATIVE DIELECTRIC CONSTANT VS MOISTURE CONTENT

SHARKEY CLAY

PLATE 17

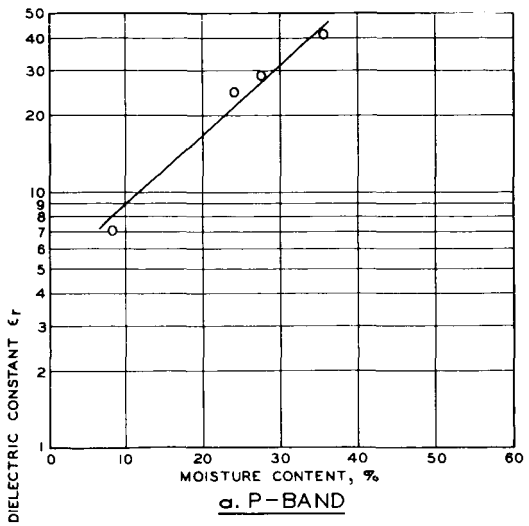

a. P-BAND

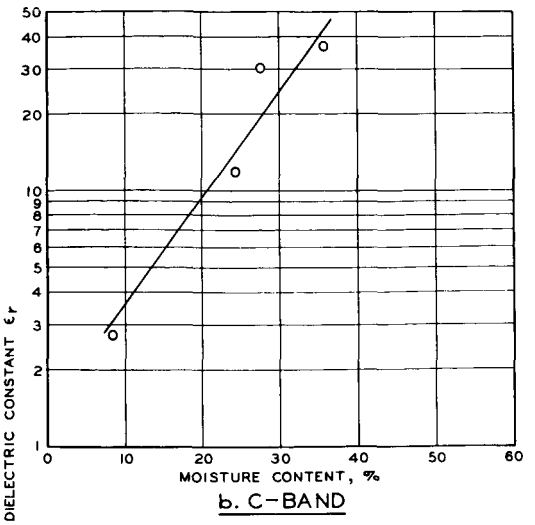

b. C-BAND

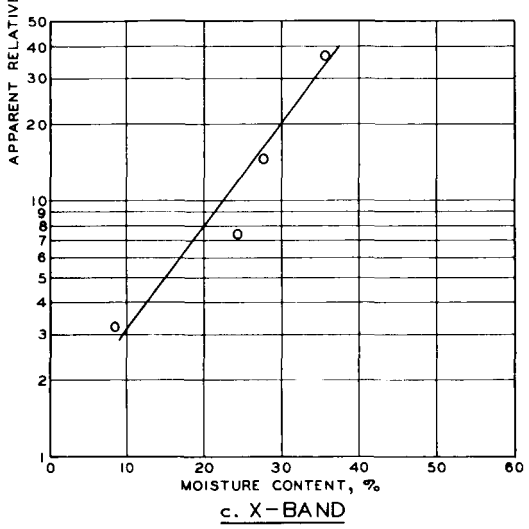

c. X-BAND

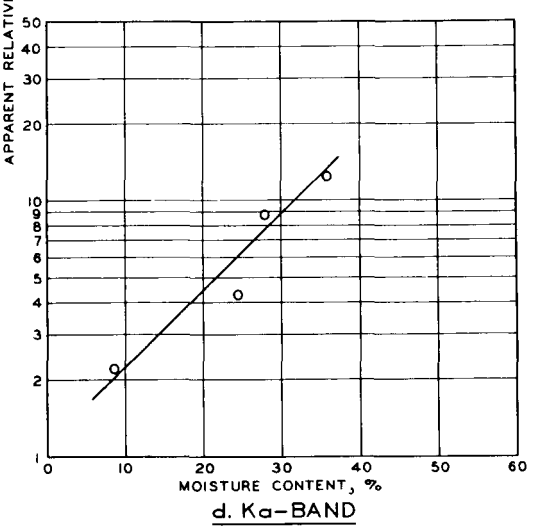

d. Ka-BAND

APPARENT RELATIVE DIELECTRIC CONSTANT VS MOISTURE CONTENT

RICHFIELD SILT LOAM

PLATE 18

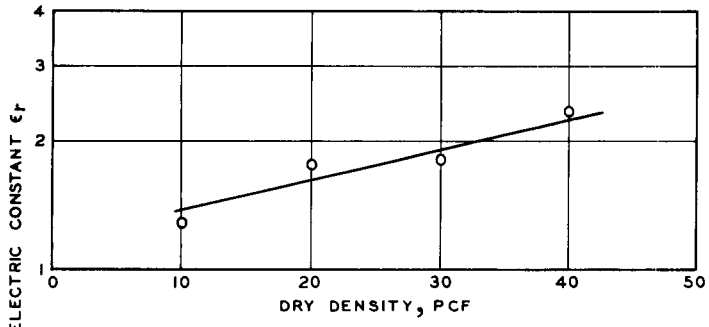

a. P-BAND

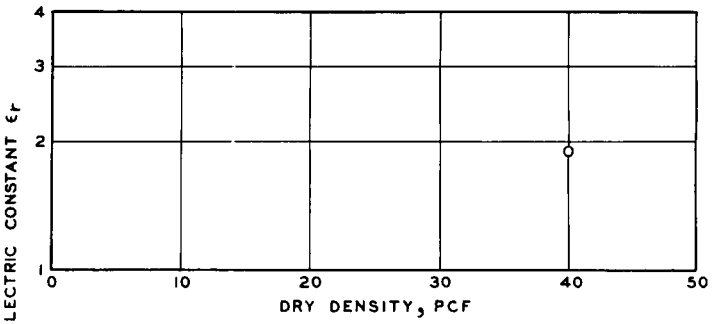

b. C-BAND

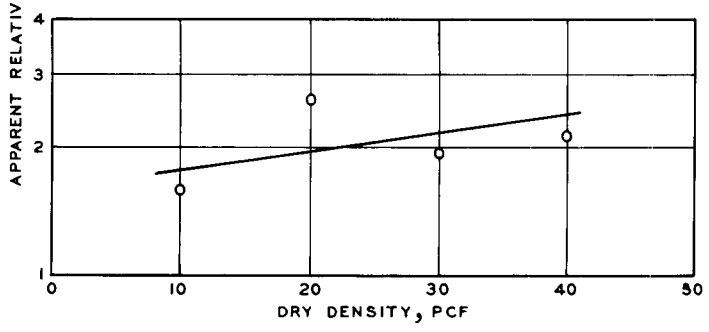

c. X-BAND

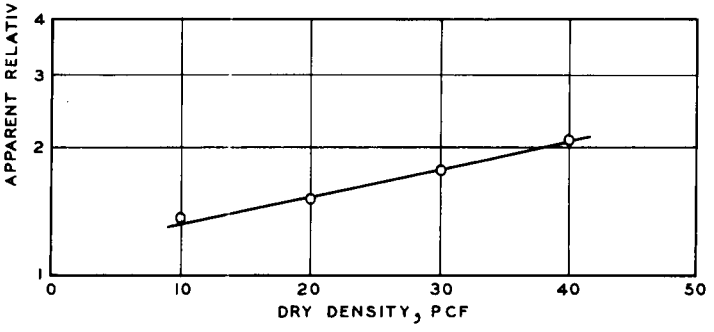

d. Ka-BAND

APPARENT RELATIVE DIELECTRIC CONSTANT VS DRY DENSITY

PERLITE

PLATE 19

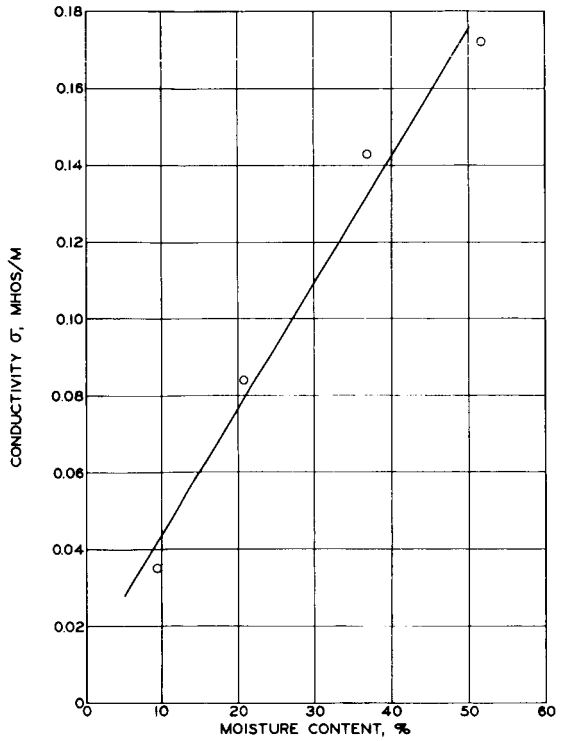

a. SHARKEY CLAY

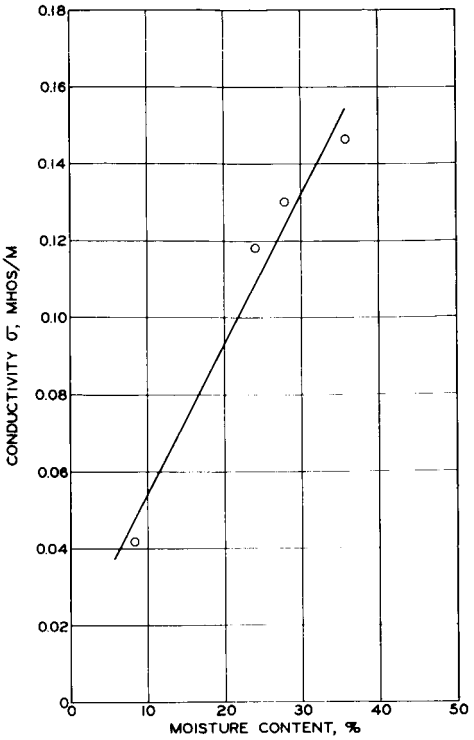

b. RICHFIELD SILT LOAM

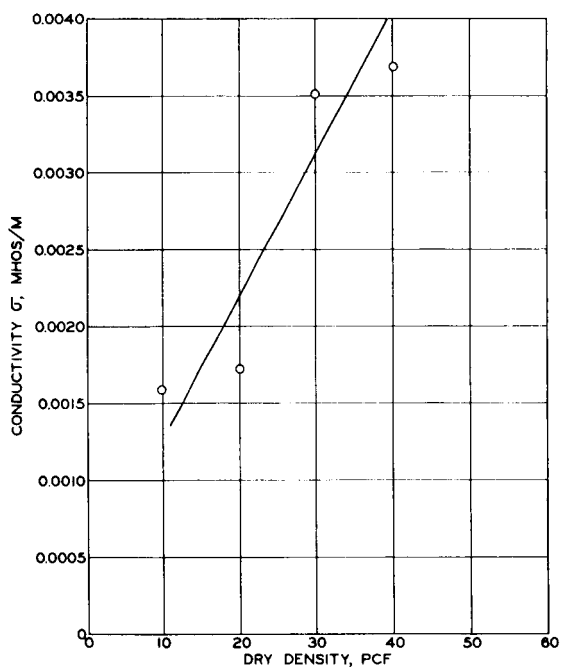

c. PERLITE

NOTE: DATA FROM P-BAND DEPTH-OF-PENETRATION TESTS.

CONDUCTIVITY VS MOISTURE CONTENT AND DENSITY

PLATE 20

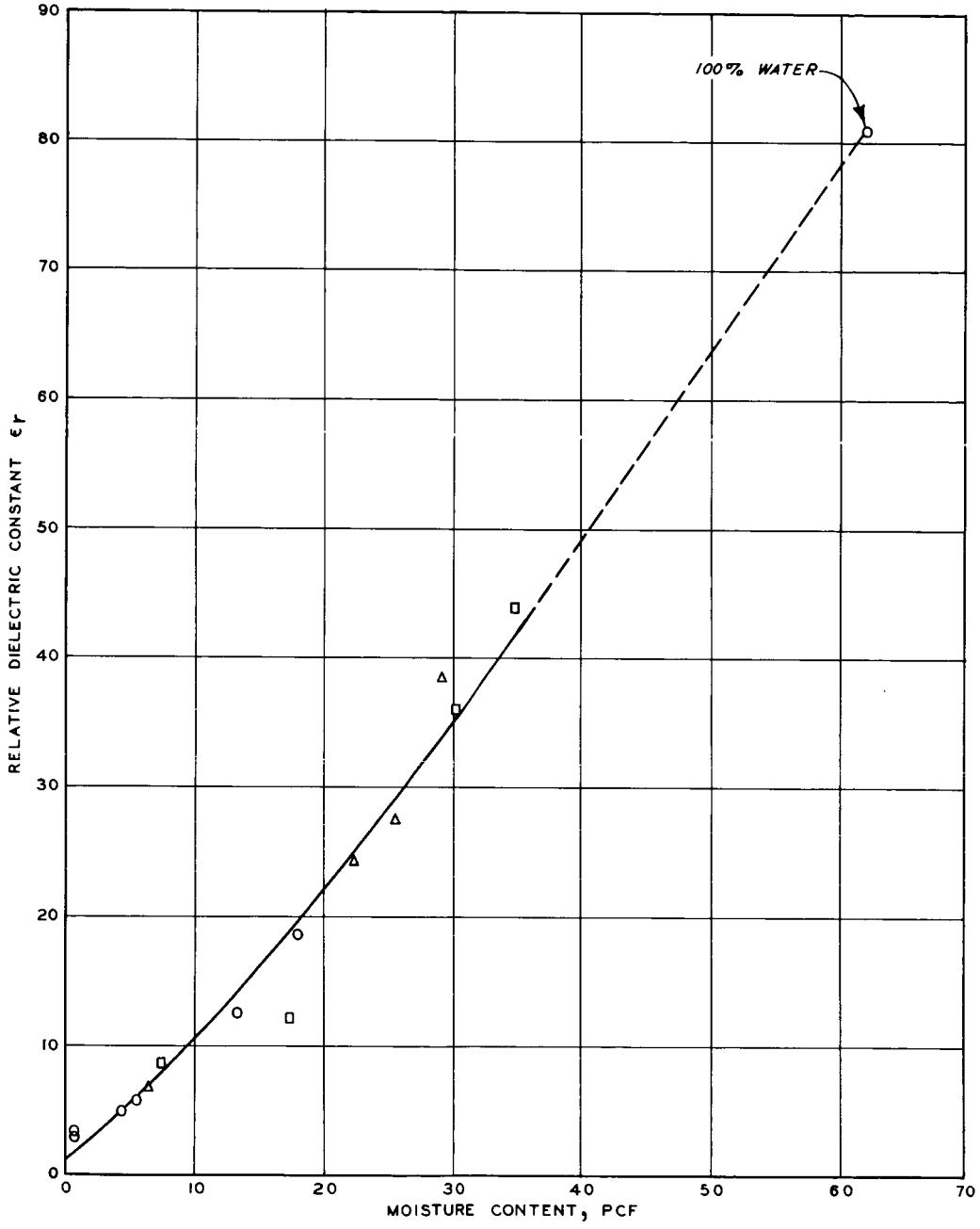

LEGEND

- ○ YUMA SAND
- △ RICHFIELD SILT LOAM
- □ SHARKEY CLAY

RELATIVE DIELECTRIC CONSTANT VS MOISTURE CONTENT

P-BAND

PLATE 21

PLATE 22

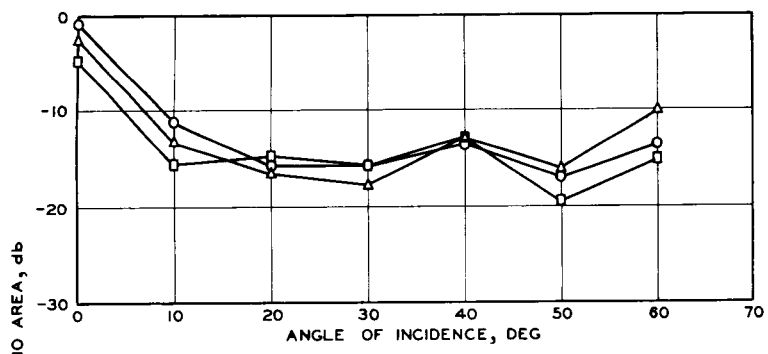

a. P-BAND

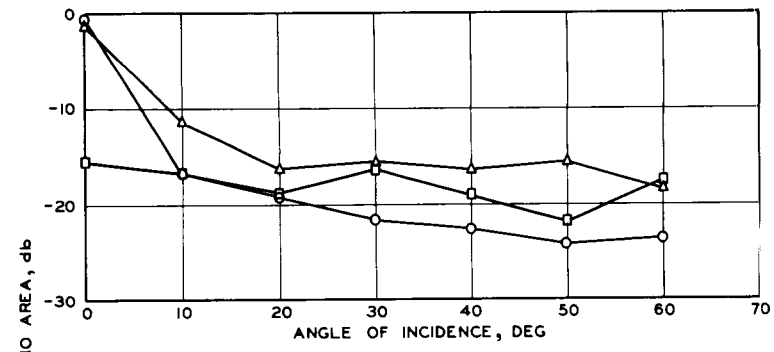

b. C-BAND

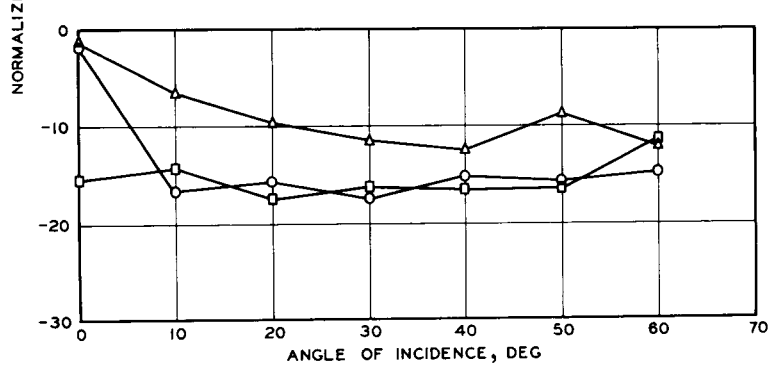

c. X-BAND

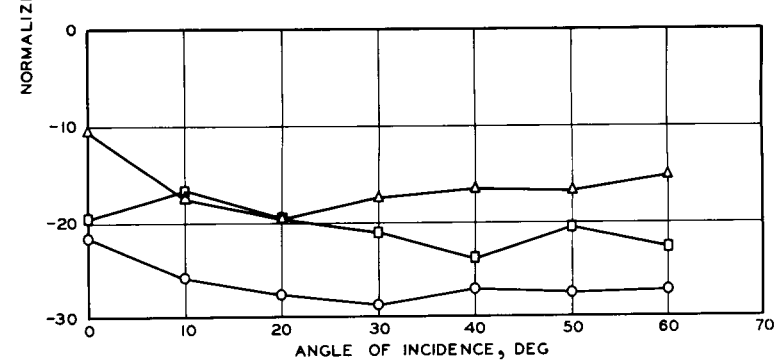

d. Ka-BAND

LEGEND

- ○ $3\frac{1}{2}$-IN. VEGETATION HEIGHT
- △ 14-IN. VEGETATION HEIGHT
- □ 29-IN. VEGETATION HEIGHT

NOTE: HORIZONTAL POLARIZATION.

VEGETATION SIGNATURE TEST
NORMALIZED ECHO AREA
VS ANGLE OF INCIDENCE

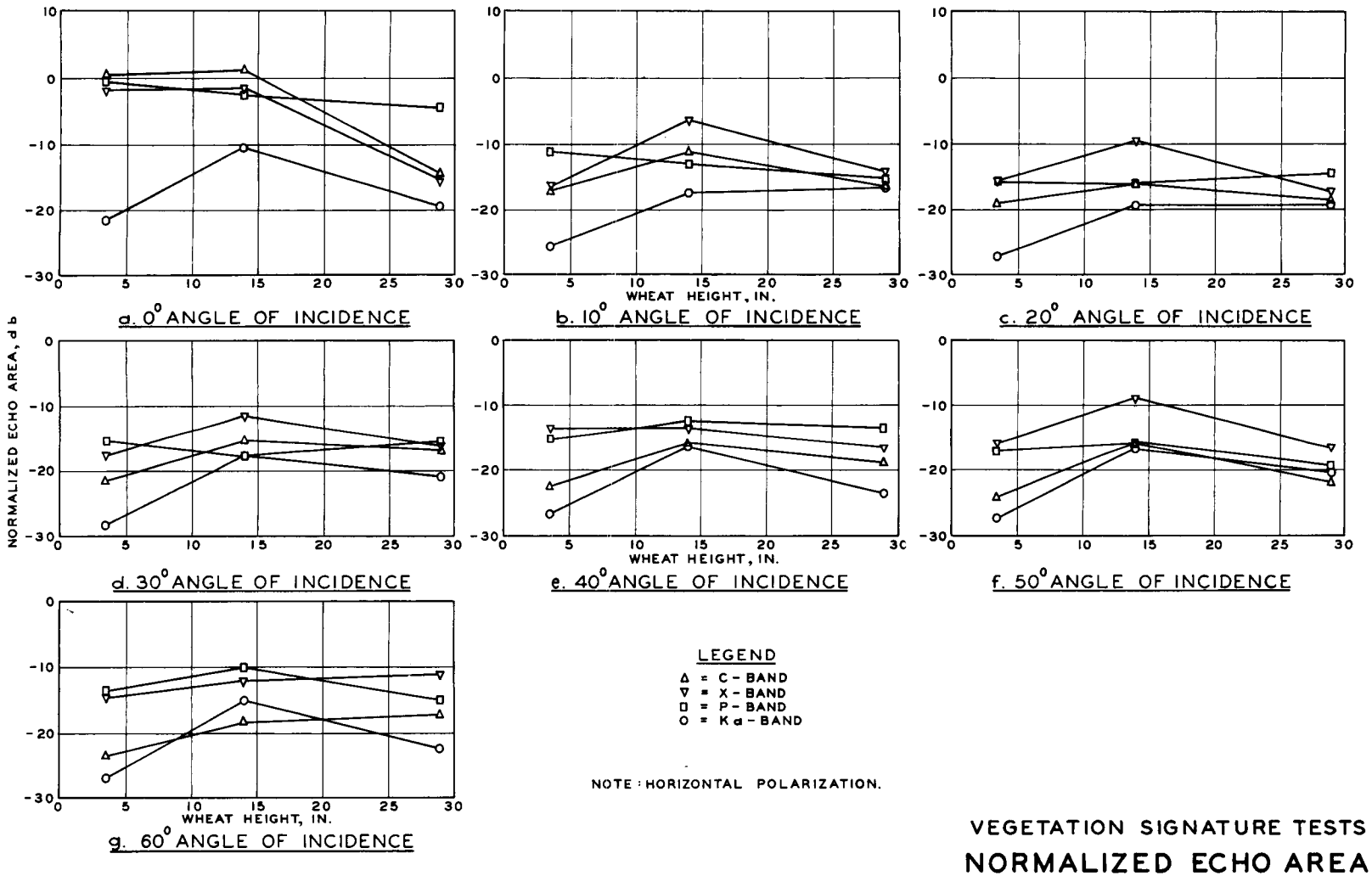

VEGETATION SIGNATURE TESTS

NORMALIZED ECHO AREA VS WHEAT HEIGHT

PLATE 23

APPENDIX A: DESCRIPTION OF MATERIALS

Sharkey Clay[9*]

1. The Sharkey clay is representative of the group of poorly drained, clayey soils that form in fine-textured sediments in slack-water areas along the Mississippi River. The soil contains a large percentage of clay minerals, chiefly illitic varieties. When dry, such soils shrink and form cracks that may be from 1 to 5 in. wide and several feet deep. When wet, the soil expands and the cracks fill. The soils reaction in the pH test is medium acid to neutral.

Richfield Silt Loam[10]

2. The Richfield silt loam is derived from calcareous fine-textured loess and is quite uniform chemically over large regions. The soil occurs on smooth, nearly level to moderately sloping uplands in the high plains region.

Putnam Silt Loam and Clay[11]

3. Putnam silt loam and clay are planosols formed from loess. In nature the silt loam surface layer is about 12 to 18 in. thick. It overlies very plastic clay subsoil that prevents rapid drainage of rainwater downward through the soil profile. The surface soil layer usually is either very wet or very dry.

Perlite[12]

4. In commercial usage the term "perlite" refers to any naturally occurring glass of igneous origin that will expand when heated to 1500 to 2000 F to yield a frothy, lightweight product. The name refers to the

---

* Raised number refer to similarly numbered items in Literature Cited which follows the main text of this report.

expanded product as well as to the unexpanded raw material, and both types were used in the construction of radar samples. In strict petrological usage, the term "perlite" is restricted to a single variety of volcanic glass in which strain incident to cooling has yielded a concentric or "onion" structure of fracturing which may be visible to the naked eye or may be observed only under the microscope.

5. Perlite is an aluminum silicate commonly containing small amounts of other compounds. The silica content of the ore ranges from 55 to 72 percent, and the aluminum content from 10 to 15 percent. The water content of raw perlite is commonly 3 to 4 percent by weight and it is chemically bound. The expanded perlite product is a white, rough, vesicular, granular aggregate that may vary in weight, according to the degree of expansion, from less than 3 to more than 15 pcf.

6. The perlite used in the tests described in this report was obtained from the J. J. Brouk Company, St. Louis, Mo. The two grades of this material obtained were as follows:

a. Expanded perlite aggregate, grade No. 77-40, with a weight of approximately 10 pcf. Approximately 90 percent of the material had a grain size between 0.1 and 2.0 mm.

b. Crushed unexpanded perlite, grade No. 77, with a weight of approximately 61 pcf. Approximately 90 percent of the material had a grain size between 0.2 and 4.0 mm.

APPENDIX B: CALCULATION OF NORMALIZED ECHO AREA

1. The normalized echo area γ of a material is determined by means of the following equation:

$$P_R = \frac{P_T G^2 \lambda^2 A_i \gamma}{(4\pi)^3 R^4} \tag{B1}$$

where

P_R = power received, watt

P_T = power transmitted, watt

G = antenna gain, dimensionless

λ = wavelength, m

A_i = cross-sectional area of radar beam at a distance equal to R , sq m

γ = normalized echo area, dimensionless

R = range, m

Equation B1 can be written in a more convenient form by dividing P_R and P_T by 10^{-3} watts, taking ten times the logarithm of both sides of the equation, and solving for $10 \log \gamma$.

$$10 \log \gamma = 10 \log \frac{P_R}{10^{-3}} - \left\{ 10 \log \frac{P_T}{10^{-3}} + 2(10 \log G) + 10 \log \left[\frac{\lambda^2 A_i}{(4\pi)^3 R^4} \right] \right\} \tag{B2}$$

where

$10 \log \gamma$ = normalized echo area γ_{db} , db

$10 \log \frac{P_R}{10^{-3}}$ = power received, dbm

$10 \log \frac{P_T}{10^{-3}}$ = power transmitted, dbm

The values for the terms in equation B2 were established as described in the following paragraphs.

Power Received P_R

2. Values of recorder deflection were converted to power received by the radar receiver through the use of the appropriate calibration curve shown in plate 1 of the main text. The receiver attenuation (see data in upper right corner of fig. 9 of main report) was added to the values obtained from the calibration curve to calculate the power actually reaching the receiving antenna.

Power Transmitted P_T

3. The quantity of power transmitted was recorded as average pulse power transmitted on each signature (as shown in upper right corner of fig. 9 of main report, the average pulse power transmitted for C-band is 46.6 dbm).

Antenna Gain G

4. The gain of the antenna was calculated by the following equation:

$$10 \log G = 10 \log \frac{4\pi A_a k}{\lambda^2} \qquad \text{(B3)}$$

where

$k = 0.6$ (constant for a parabolic antenna)

λ = wavelength, m

A_a = antenna aperture area, sq m, $= \pi \left(\frac{d}{2}\right)^2$, where d is the diameter of the antenna, m

The following table gives the antenna gain and the values used to calculate the gain for each radar system.

Radar Band	λ meter	d meter	A_a sq meter	10 log G
Ka	0.0087	0.228	0.0408	36.1
X	0.0321	0.456	0.163	30.8
C	0.051	0.71	0.292	29.3
P	1.01	2.438	4.66	15.4

Range R

5. R is fixed by the design of the radar facility and has a value of 13.7 m. This is equal to the radius of the arch (50 ft) minus the distance that the antenna carriage and antennas are mounted in from the outer edge of the arch.

Cross-sectional area of radar beam A_i

6. A_i at vertical incidence was calculated using the following equation:

$$A_i = \pi \left(R \tan \frac{\theta}{2} \right)^2 \tag{B4}$$

where

θ = antenna beam width for each radar band as follows:

Radar Band	θ, deg
Ka	2.66
X	4.93
C	5.86
P	29.00

Substituting these beam width values in equation B4 yields the following cross-sectional areas:

Radar Band	A_i, sq m
Ka	0.3
X	1.1
C	1.6
P	4.0

7. Using the above values established for the variables in equation B2, the following sample calculation was made for the C-band soil signature shown in fig. 9.

$$10 \log \gamma = 10 \log \frac{P_R}{10^{-3}} - \left\{ 10 \log \frac{P_T}{10^{-3}} + 2(10 \log G) + 10 \log \left[\frac{\lambda^2 A_i}{(4\pi)^3 R^4} \right] \right\}$$

or

$$\gamma_{db} = 10 \log \frac{P_R}{10^{-3}} - \left\{ 46.6 + 2(29.3) + 10 \log \left[\frac{(0.051)^2 (1.6)}{(4\pi)^3 (13.7)^4} \right] \right\}$$

$$\gamma_{db} = 10 \log \frac{P_R}{10^{-3}} - 2.9 \qquad \text{(B5)}$$

One inch of deflection on the X-Y recorder corresponds to a power received value of -44.5 dbm (plate 1b). Correcting this value of power received by the amount of attenuation in the receiver at the time of the test, 14.1 db (see receiver attenuation listed in upper right corner of fig. 9), yields the following value of γ_{db} for a deflection of 1 in.

$$\gamma_{db} = (-44.5 + 14.1) - 2.9$$

$$\gamma_{db} = -33.3 \text{ db}$$

8. Similar calculations for recorder deflections of 0, 2.0, 3.0, 4.0, 5.0, 6.0, and 6.8 in. yield the following values of corrected power received and γ_{db} :

Recorder Deflection in.	Corrected Power Received, dbm	γ_{db}, db
0.0	-33.2	-36.1
1.0	-30.4	-33.3
2.0	-26.2	-29.1
3.0	-21.2	-24.1
4.0	-15.5	-18.4
5.0	-9.0	-11.9
6.0	-1.4	-4.3
6.8	+11.1	+8.2

Unclassified
Security Classification

DOCUMENT CONTROL DATA - R&D

(Security classification of title, body of abstract and indexing annotation must be entered when the overall report is classified)

1. ORIGINATING ACTIVITY *(Corporate author)*
U. S. Army Engineer Waterways Experiment Station
Vicksburg, Mississippi

2a. REPORT SECURITY CLASSIFICATION
Unclassified

2b GROUP

3. REPORT TITLE
TERRAIN ANALYSIS BY ELECTROMAGNETIC MEANS; RADAR RESPONSES TO LABORATORY PREPARED SOIL SAMPLES

4. DESCRIPTIVE NOTES *(Type of report and inclusive dates)*
Report 2 of series

5. AUTHOR(S) *(Last name, first name, initial)*
Lundien, Jerry R.

6. REPORT DATE	7a. TOTAL NO. OF PAGES	7b. NO. OF REFS
September 1966	99	12

8a. CONTRACT OR GRANT NO.	9a. ORIGINATOR'S REPORT NUMBER(S)
b. PROJECT NO.	Technical Report No. 3-693, Report 2
c.	9b. OTHER REPORT NO(S) *(Any other numbers that may be assigned this report)*
d.	

10. AVAILABILITY/LIMITATION NOTICES
This document is subject to special export controls and each transmittal to foreign governments or foreign nationals may be made only with prior approval of U. S. Army Engineer Waterways Experiment Station.

11. SUPPLEMENTARY NOTES	12. SPONSORING MILITARY ACTIVITY
Service Agency: U. S. Army Materiel Command Washington, D. C.	National Aeronautics and Space Administration, Washington, D. C.

13. ABSTRACT Laboratory tests were conducted with radar sensors to detect the presence of and measure the depth to subsurface interfaces when the surface was bare, and to determine the influence of vegetation at various stages of growth on radar responses. A secondary purpose was to continue earlier studies to relate radar returns and the electrical constants that they provided to moisture content and density of samples. Large laboratory samples were prepared at various moisture contents and densities and with various depths to a subsurface metal plate. Standard pulsed radar sensors operating with frequencies of 297, 5870, 9375, and 34,543 megacycles/sec and directed at various angles of incidence to the surface were employed. The results of this laboratory study indicate that the standard pulsed radar sensors can provide information that will permit an estimate of the moisture content of deep, homogeneous soil samples and the detection of surface vegetation of various heights. Radar signatures of vegetation-covered soil were more significantly altered at Ka-, X-, and C-band frequencies than at P-band frequencies. However, standard pulsed radar sensors used monochromatically cannot provide information for predicting depth to subsurface interfaces or for directly indicating the presence of a subsurface interface. The systematic manner in which soil depths were varied in this study permitted an analytical solution to the problem of measuring depths of layers and led to the conclusion that properly designed radar systems could measure depths to subsurface interfaces. Three such systems are proposed.

DD FORM 1 JAN 64 1473

Unclassified
Security Classification

14. KEY WORDS	LINK A		LINK B		LINK C	
	ROLE	WT	ROLE	WT	ROLE	WT
Radar						
Soils--sampling						
Terrain analysis						
Dielectric constant						
Electrical conductivity						

INSTRUCTIONS

1. ORIGINATING ACTIVITY: Enter the name and address of the contractor, subcontractor, grantee, Department of Defense activity or other organization *(corporate author)* issuing the report.

2*a*. REPORT SECURITY CLASSIFICATION: Enter the overall security classification of the report. Indicate whether "Restricted Data" is included. Marking is to be in accordance with appropriate security regulations.

2*b*. GROUP: Automatic downgrading is specified in DoD Directive 5200.10 and Armed Forces Industrial Manual. Enter the group number. Also, when applicable, show that optional markings have been used for Group 3 and Group 4 as authorized.

3. REPORT TITLE: Enter the complete report title in all capital letters. Titles in all cases should be unclassified. If a meaningful title cannot be selected without classification, show title classification in all capitals in parenthesis immediately following the title.

4. DESCRIPTIVE NOTES: If appropriate, enter the type of report, e.g., interim, progress, summary, annual, or final. Give the inclusive dates when a specific reporting period is covered.

5. AUTHOR(S): Enter the name(s) of author(s) as shown on or in the report. Enter last name, first name, middle initial. If military, show rank and branch of service. The name of the principal author is an absolute minimum requirement.

6. REPORT DATE: Enter the date of the report as day, month, year; or month, year. If more than one date appears on the report, use date of publication.

7*a*. TOTAL NUMBER OF PAGES: The total page count should follow normal pagination procedures, i.e., enter the number of pages containing information.

7*b*. NUMBER OF REFERENCES: Enter the total number of references cited in the report.

8*a*. CONTRACT OR GRANT NUMBER: If appropriate, enter the applicable number of the contract or grant under which the report was written.

8*b*, 8*c*, & 8*d*. PROJECT NUMBER: Enter the appropriate military department identification, such as project number, subproject number, system numbers, task number, etc.

9*a*. ORIGINATOR'S REPORT NUMBER(S): Enter the official report number by which the document will be identified and controlled by the originating activity. This number must be unique to this report.

9*b*. OTHER REPORT NUMBER(S): If the report has been assigned any other report numbers *(either by the originator or by the sponsor)*, also enter this number(s).

10. AVAILABILITY/LIMITATION NOTICES: Enter any limitations on further dissemination of the report, other than those imposed by security classification, using standard statements such as:

(1) "Qualified requesters may obtain copies of this report from DDC."

(2) "Foreign announcement and dissemination of this report by DDC is not authorized."

(3) "U. S. Government agencies may obtain copies of this report directly from DDC. Other qualified DDC users shall request through _____."

(4) "U. S. military agencies may obtain copies of this report directly from DDC. Other qualified users shall request through _____."

(5) "All distribution of this report is controlled. Qualified DDC users shall request through _____."

If the report has been furnished to the Office of Technical Services, Department of Commerce, for sale to the public, indicate this fact and enter the price, if known.

11. SUPPLEMENTARY NOTES: Use for additional explanatory notes.

12. SPONSORING MILITARY ACTIVITY: Enter the name of the departmental project office or laboratory sponsoring *(paying for)* the research and development. Include address.

13. ABSTRACT: Enter an abstract giving a brief and factual summary of the document indicative of the report, even though it may also appear elsewhere in the body of the technical report. If additional space is required, a continuation sheet shall be attached.

It is highly desirable that the abstract of classified reports be unclassified. Each paragraph of the abstract shall end with an indication of the military security classification of the information in the paragraph, represented as *(TS), (S), (C), or (U)*.

There is no limitation on the length of the abstract. However, the suggested length is from 150 to 225 words.

14. KEY WORDS: Key words are technically meaningful terms or short phrases that characterize a report and may be used as index entries for cataloging the report. Key words must be selected so that no security classification is required. Identifiers, such as equipment model designation, trade name, military project code name, geographic location, may be used as key words but will be followed by an indication of technical context. The assignment of links, rules, and weights is optional.

DISTRIBUTION LIST A

(For Distribution of TR's and MP's on Trafficability and Mobility Studies and Related Investigations)

Address	No. of Copies
Commanding General, U. S. Army Materiel Command ATTN: AMCRD-DM ATTN: AMCRD-RV-E Washington, D. C.	1 2
Commanding Officer, USACRREL ATTN: Library Hanover, N. H.	1
Commanding Officer, USA Engineer Research and Development Laboratories ATTN: Technical Document Center Fort Belvoir, Va.	2
Commanding Officer, USA Electronics Research and Development Activity, Ariz. ATTN: SELHU-M Fort Huachuca, Ariz.	1
Commanding Officer, USA Electronics Research and Development Laboratories ATTN: SELRA/ADT Fort Monmouth, N. J.	1
Chief of Research and Development ATTN: Chief, Combat Materiel Division Department of the Army Washington, D. C.	1
Chief of Research and Development ATTN: CRD/M, Department of the Army Washington, D. C.	1
Chief of Research and Development Headquarters, Department of the Army ATTN: Director of Army Technical Information Washington, D. C.	3 copies of Form 1473
Defense Intelligence Agency ATTN: DIAAP-1E2 Washington, D. C.	1

Address	No. of Copies
Commanding Officer, U. S. Army Tropic Test Center Fort Clayton, Canal Zone	1
Commanding Officer, U. S. Army Arctic Test Center APO Seattle, Wash.	1
Chief of Engineers	
ATTN: ENGTE-E	1
ATTN: ENGAS-I	2
ATTN: ENGMC-ER Department of the Army Washington, D. C.	2
OCE (ENGTE) (for Engineer Standardization Program)	4
War Plans Division, Engineer Strategic Studies Group Office, Chief of Engineers, U. S. Army Erskine Hall, Army Map Service Washington, D. C.	1
Commander, U. S. Army Combat Development Command ENGINEER AGENCY ATTN: CAGEN-SC Fort Belvoir, Va.	1
The Librarian, U. S. Army Engineer School Library Thayer Hall Fort Belvoir, Va.	2
USA Engr School ATTN: Heavy Construction Section, Department of Engineering Pavements and Materials Group Fort Belvoir, Va.	1
Commanding General, XVIII Airborne Corps ATTN: Corps Engineer Fort Bragg, N. C.	2
Commanding Officer 326th Engineer Battalion Fort Campbell, Ky.	1

Address	No. of Copies
Senior Engineer Instructor Office of Military Instruction, United States Corps of Cadets West Point, N. Y.	1
President U. S. Army Armor Board Fort Knox, Ky.	1
President U. S. Army Artillery Board Fort Sill, Okla.	1
President U. S. Army Infantry Board Fort Benning, Ga.	1
Commanding General, U. S. Army Weapons Command ATTN: AMSWE-RDR Rock Island, Ill.	1
Commanding General, U. S. Army Tank-Automotive Command ATTN: SMOTA-RCL Warren, Mich.	1
Commander, U. S. Army Forces Southern Command ATTN: Engineer Fort Amador, Canal Zone	1
Commanding General, U. S. Continental Army Command Engineer Division, DCSLOG ATTN: ATLOG-E-MB Fort Monroe, Va.	2
Commanding General, U. S. Continental Army Command ATTN: ATUTR-AVN Fort Monroe, Va.	1
Commandant, Command and General Staff College ATTN: Archives Fort Leavenworth, Kans.	1

Address	No. of Copies
Commanding Officer, U. S. Army Rock Island Arsenal ATTN: SWERI-RDD-RA Rock Island, Ill.	1
Commander, U. S. Army Picatinny Arsenal ATTN: SMUPA-VC1, Mr. D. Sen Dover, N. J.	1
Commanding Officer, Yuma Proving Ground ATTN: STEYT-TGM Yuma, Ariz.	1
Technical Library, Branch No. 4 U. S. Army Limited War Laboratory Aberdeen Proving Ground, Md.	1
Automotive Engineering Laboratory ATTN: STEAP-DP-LU Aberdeen Proving Ground, Md.	1
Commanding General, USA Test and Evaluation Command ATTN: Director, USA Development and Proof Services (Automotive Division) Aberdeen Proving Ground, Md.	1
Commanding Officer ATTN: Tech Library, Bldg 313 Aberdeen Proving Ground, Md.	2
Commanding Officer, U. S. Army General Equipment Test Activity Fort Lee, Va.	1
Chief, Crops Division U. S. Army Biological Laboratories Fort Detrick, Md.	1
Commanding Officer, U. S. Army Combat Developments Command Transportation Agency ATTN: Mr. Earl S. Brown Fort Eustis, Va.	1

Address	No. of Copies
Asst. Chief of Staff for Force Development Hqs, Department of the Army, ATTN: FOR DS SSS Washington, D. C.	1
United States Army Attaché, American Embassy U. S. Navy 100, Box 36 Fleet Post Office New York, N. Y.	2
Office of Naval Research ATTN: Geography Branch Department of the Navy Washington, D. C.	1
Office of Naval Research, Navy Department ATTN: Mr. Irv. Schiff (Code 493) Washington, D. C.	1
Commanding Officer, PHIBCB Two U. S. Naval Amphibious Base Little Creek, Norfolk, Va.	1
Commanding Officer, PHIBCB One U. S. Naval Amphibious Base Coronado, San Diego, Calif.	1
Commanding Officer and Director Naval Civil Engineering Laboratory Port Hueneme, Calif.	1
Director, Naval Warfare Research Center Stanford Research Institute Menlo Park, Calif.	1
Chief, Bureau of Yards and Docks ATTN: Code 42, Department of the Navy Washington, D. C.	2
Commanding Officer, U. S. Naval Photographic Interpretation Center Washington, D. C.	1

Address	No. of Copies
Chief, Combat Service Support Division Marine Corps Landing Force Development Center Marine Corps Schools Quantico, Va.	1
Commander, 3800th AB Wing, AU ATTN: BDCE-ED Maxwell AFB, Ala.	1
Headquarters, USAF (AFRSTC) Astronautics Division DCS/Research and Development Washington, D. C.	1
Commander, U. S. Strike Command ATTN: J4-E McDill AFB, Fla.	1
Commander, Air Proving Ground Command ATTN: PGBPS-12 Eglin AFB, Fla.	1
Headquarters, Tactical Air Command ATTN: DEDSA Langley AFB, Va.	2
Headquarters, U. S. Air Force Director of Civil Engineering (AFOCE-KA) Washington, D. C.	2
Headquarters, USAF Base Structures Branch, Directorate of Civil Engineering ATTN: AFOCE-GC Washington, D. C.	1
Commander, Hqs, Military Air Transport Service ATTN: MAMCE/FS Scott AFB, Ill.	1
Commander SEG (SEHB) Wright-Patterson AFB, Ohio	1
Systems Engineering Group, Deputy for Systems Engineering Directorate of Technical Publications and Specifications (SEPRR) Wright-Patterson AFB, Ohio	1

Address	No. of Copies
Air Force Weapons Laboratory ATTN: Civil Engineering Branch Kirtland AFB, N. Mex.	1
Terrestrial Sciences Lab (CRJT) Air Force Cambridge Res Lab, L. G. Hanscom Field Bedford, Mass.	1
Library, Division of Public Documents U. S. Government Printing Office Washington, D. C.	1
Library of Congress Documents Expediting Project Washington, D. C.	3
Defense Documentation Center, ATTN: Mr. Myer Kahn Cameron Station Alexandria, Va.	20
National Tillage Machinery Laboratory U. S. Department of Agriculture Auburn, Ala.	1
Mr. A. C. Orvedal, Chief, World Soil Geography Unit Soil Conservation Service Hyattsville, Md.	1
Chief, Crops Protection Branch Crops Research Division, Agricultural Research Service Beltsville, Md.	1
Director, Pacific Southwest Forest and Range Experiment Station, ATTN: Henry W. Anderson Berkeley, Calif.	1
U. S. Geological Survey Chief, Source Material Unit, Branch of Military Geology Washington, D. C.	2
Coastal Studies Institute Louisiana State University Baton Rouge, La.	1

Address	No. of Copies
New York University, School of Engineering and Science Research Division, University Heights New York, N. Y.	1
Ohio University Engineering Experiment Station ATTN: Mr. Seth Bonder Columbus, Ohio	1
Professor L. C. Stuart University of Michigan Ann Arbor, Mich.	1
University of Arkansas, College of Engineering ATTN: Mr. Henry H. Hicks, Jr. Fayetteville, Ark.	1
Dr. Clark N. Crain, Director Project DUTY Department of Geography, University of Denver Denver, Colo.	1
Stanford Research Institute ATTN: Mr. Gordon S. Wiley Menlo Park, Calif.	1
Engineering Societies Library New York, N. Y.	1
Highway Research Board Washington, D. C.	1
Research Analysis Corporation ATTN: Library McLean, Va. 22101	1
Davidson Laboratory, Stevens Institute of Technology ATTN: Dr. I. R. Ehrlich Hoboken, N. J.	1

Address	No. of Copies
Wilson, Nuttall, Raimond Engineers, Inc. ATTN: Library Chestertown, Md.	1
Battelle Memorial Institute, ATTN: RACIC Columbus, Ohio	1
Miss Winnie M. Morgan, Technical Reports Officer Grants and Research Contract Division Office of Space Science and Applications National Aeronautics and Space Administration Washington, D. C. 20546	25
Dr. R. K. Moore University of Kansas Center for Research Lawrence, Kans.	3

Consultants

Dr. A. R. Barringer	1
Dr. F. C. Bates	1
Dr. R. N. Colwell	1
Dr. Allen Martin Feder	1
Dr. L. H. Lattman	1
Mr. J. O. Morgan	1